8-16-2021 10:30 AM

Urban Heat Mitigation for Current and Future Conditions: A case study for downtown London ON

Maryam Shams, *The University of Western University*

Supervisor: Peerhossaini, Hassan, *The University of Western Ontario*
Co-Supervisor: Voogt, James, *The University of Western Ontario*
Co-Supervisor: DeGroot, C.T., *The University of Western Ontario*
A thesis submitted in partial fulfillment of the requirements for the Master of Engineering Science degree in Civil and Environmental Engineering
© Maryam Shams 2021

Abstract:

The urban heat island is a phenomenon wherein urban areas experience warmer temperatures than their surrounding rural areas. Techniques to reduce excess heat in urban environments are known as heat mitigation or heat island mitigation solutions, with the intent that they reduce urban temperatures. This research presents an investigation on the impacts and effectiveness of urban heat mitigation techniques on improving the outdoor thermal conditions of downtown London, Ontario. The impact of increasing vegetated areas and applying higher albedo materials for road pavements is assessed with ENVI-Met software for current and future summer weather. Furthermore, investigations were conducted for current and future winter weather scenarios to explore the effects of these heat mitigation techniques on other seasons' outdoor conditions. Finally, the effects of heat mitigation strategies on building energy consumption were simulated by HAP Carrier software. Results show that increasing vegetation and trees reduce the air temperature and mean radiant temperature during both day and night periods. A higher air temperature reduction is detected for the greenery model with a higher percentage of trees relative to grasslands. The average air temperature at 17h is reduced up to 0.56°C and 0.66°C for respectively, for increasing trees and high albedo materials scenarios. Furthermore, results showed an increase in the mean radiant temperature value for the scenario with increasing albedo of the road materials. The results further demonstrated a reduction in the cooling load of buildings with increasing trees in the building neighborhoods.

Keywords:

Summary for lay audience:

Urban areas are hotter than their non-developed surrounding areas. According to projections, the urban areas will be warmer over the 21st century due to global climate change and urban development. Urban heat island is an urban area with a significantly warmer temperature than its surrounding rural neighborhoods. The increasing urbanization process in cities, increasing paved areas, and decreasing green areas are the reasons for urban heat island generation. Extremely hot weather events are becoming more frequent and intense as a result of climate change. Urban heat islands, during the hot seasons, can lead to adverse impacts on the health of citizens and increasing energy consumption. Several solutions are proposed to reduce the urban heat island in cities namely, increasing vegetation and increasing the heat reflectance of the road or building materials. This study assesses the impacts of increasing green areas and increasing the reflectance of road materials on the air temperature for a study area in downtown London, Ontario. The heat reduction potential of these solutions for current and future weather conditions subjected to climate change is analyzed by the simulation software ENVI-Met. In addition, to better understanding the impacts of these heat mitigations on other seasons, further assessments were conducted for the cold season, winter. Finally, the building energy consumption in the context of these heat mitigation strategies is analyzed by simulation. Results show that areas with low thermal comfortable conditions correspond to large flat paved areas and parking spaces without shading facilities. Increasing trees and vegetated spaces on the site can improve the outdoor thermal condition for pedestrians. Assessment of the impact of high reflectance materials on air temperature indicates that while applying these materials reduces the surface air temperature, they can cause a negative effect on the thermal comfort

of the pedestrian. Adding trees in the neighborhood of buildings can reduce the energy consumption of building for cooling.

Acknowledgments:

I would first like to thank my supervisor, Dr. Hassan Peerhossaini, who gave me the opportunity to work under his guidance. His support and guidance helped me and motivated me during this research and writing my thesis. Also, I would like to express my thankfulness to my other supervisor Dr. James Voogt, whose guidance and immense knowledge was invaluable throughout the way of completing this research. I would also like to thank Dr. Christopher DeGroot for his practical advice and encouragement throughout this research. It was an incredible journey, and I have learned so much from every one of you in my research.

Finally, I would like to thank my family and friends who supported me throughout the course of this research: To my mother Farzaneh Karimi and father Mehrdad Shams, thank you for your unconditional support and love; to my sister Mandana Shams, who always inspires and encourages me to try my best. It would not be possible without you.

Table of Contents

List of Tables:

List of Figures:

List of Appendices

Chapter 1: Thesis Overview

1.1. Background

Urban Climate around the world is subjected to change as a result of increasing urbanization and population growth. The consequence of these changes is increasing the anthropogenic heat in the urbanized area (Rosheidat, 2014). Anthropogenic heat, changing the fabric of the cities, and reducing the natural landscape, are the primary reasons for experiencing higher ambient temperature during the evening and nighttime in cities rather than a rural area. This phenomenon is urban heat island and has investigated by several studies. The generation of urban heat islands is attributed to the effect of anthropogenic activities, change in urban surface energy balance, thermal properties of the material, drastic change in energy consumption(Rizwan et al., 2008; Oke, T.R., 1987; Kikegawa et al., 2006).

A recent investigation that characterized the urban heat island in the London, Ontario (MLHU report, 2015) during a summer heat wave period showed evidence of urban heat islands in surface and air temperatures exist in London. According to this report, which applied modelled outputs from the Environment and Climate Change Canada (ECCC) GEM-SURF numerical model, the calculated London surface temperature UHI is highly variable within the city by day with a spatially averaged daily maximum of between 3°C-6°C. At night, the spatially averaged surface temperature UHI is still positive with a nocturnal minimum generally between 0°C-1°C and with low intra-urban variability.

Furthermore, the report is indicated a low canopy layer urban heat island during the selected hot weather events.

Studies have indicated increased health risks in urban populations compared with rural or suburban populations in hot weather and a disproportionate impact on more vulnerable social groups (Heaviside et al., 2017). Increased ambient temperatures cause a significant impact on the cooling energy consumption, heat-related mortality, urban environmental quality, and thermal comfort. Furthermore, synergies between urban heat islands and heat waves increase urban overheating impacts (Santamouris, 2020).

Many studies have been highlighted the impact of increasing the urban vegetation as the most effective strategy to accomplish UHI mitigation (McPherson et al. 1994; Akbari et al. 1995; Taha et al. 1997; Rosheidat 2014). Akbari et al. (2001) reported that urban tree planting, combined with increasing the surface albedo citywide, has the potential of modifying the entire City's energy balance.

There is no comprehensive investigation on the potential of urban heat island mitigation strategies in London. Moreover, downtown core of London stands out as prone to high potential of outdoor thermal discomfort, and high UHI effects would be expected (MLHU, 2015). This study assesses the impact of urban heat island mitigation solutions on the outdoor microclimate conditions and pedestrian thermal comfort.

1.2. Research Objectives

The overall objective of this study is to evaluate the impacts of urban heat mitigation techniques on the outdoor microclimate condition of downtown London. Other objectives of the study are listed below:

- Assess the local microclimate conditions and thermal comfort of the current conditions of the study area

- Evaluate the impact of increasing vegetation and trees, "green scenario" on the site microclimate conditions for different seasons (summer and winter) and different time scopes (present and future climates)

- Investigate the microclimate mitigation potential of increasing the albedo of road material for different time scopes (present and future climates)

- Assess the impact of "green scenario" and green walls on the building thermal energy performance

1.3. Research Questions

The questions that will be addressed in this study:

1- What is the most efficient urban heat mitigation strategy that could be applied to the existing urban canyon regarding the pedestrian's thermal comfort?

2- What is the impact of mitigation strategies on other seasons (winter) and future weather conditions?

3- What are potential changes in the cooling energy loads of buildings due to the addition of street trees?

1.4. Summary of Chapters

This thesis consists of 6 chapters. After an overview in Chapter one, the background literature is presented in Chapter 2. It provides a review on previous studies regarding the urban heat island and strategies that applied to reduce the effect of heat island and discomfort thermal conditions.

Chapter 3 presents a review of the ENVI-Met software. The characteristics of ENVI-met, models and sub-models of software are described. Finally, previous studies that have used ENVI-met software to assess urban heat mitigation strategies are reviewed.

Chapter 4 presents an investigation on the outdoor thermal condition of the study area in downtown London, Ontario. This chapter explains the results of an assessment of the microclimate cooling potential of increasing green areas and increasing albedo of road materials. For this purpose, mitigation scenarios using the ENVI-met model simulated, and the results are explained in this chapter.

Chapter 5 presents an evaluation of the impacts of microclimate mitigation solutions on the thermal energy performance of buildings. Furthermore, it describes modeling with HAP Carrier software and represents the results of simulation with this software.

Chapter 6 summarizes the primary findings shown in Chapters 4 and 5. It provides a conclusion with final remarks.

1.5. References

Akbari, H. (1995). Validation of an algorithm to disaggregate whole-building hourly electrical load into end uses. Energy, 20(12), 1291-1301.

Akbari, H., Pomerantz, M., & Taha, H. (2001). Cool surfaces and shade trees to reduce energy use and improve air quality in urban areas. Solar energy, 70(3), 295-310.

Dyce D.R., Voogt J.A. (2015). Characterizing the Urban Health Island Effect in Middlesex-London. Middlesex-London Health Unit (MLHU).

Heaviside, C., Macintyre, H., & Vardoulakis, S. (2017). The urban heat island: implications for health in a changing environment. Current environmental health reports, 4(3), 296-305.

U.S. Environmental Protection Agency. 2012. "Cool Pavements." In: Reducing Urban Heat Islands: Compendium of Strategies. Draft. https://www.epa.gov/heat-islands/heat-island-compendium.

Kikegawa, Y., Genchi, Y., Kondo, H., & Hanaki, K. (2006). Impacts of city-block-scale countermeasures against urban heat-island phenomena upon a building's energy-consumption for air-conditioning. Applied Energy, 83(6), 649-668.

McPherson, E. G. (1994). Chicago's urban forest ecosystem: results of the Chicago Urban Forest Climate Project (Vol. 186). US Department of Agriculture, Forest Service, Northeastern Forest Experiment Station.

Oke, T. R., & Cleugh, H. A. (1987). Urban heat storage derived as energy balance residuals. Boundary-Layer Meteorology, 39(3), 233-245.

Rizwan, A. M., Dennis, L. Y., & Chunho, L. I. U. (2008). A review on the generation, determination and mitigation of Urban Heat Island. Journal of environmental sciences, 20(1), 120-128.

Rosheidat, A. (2014). Optimizing the effect of vegetation for pedestrian thermal comfort and urban heat Island mitigation in a hot arid urban environment. Arizona State University.

Santamouris, M. (2020). Recent progress on urban overheating and heat island research. Integrated assessment of the energy, environmental, vulnerability and health impact. Synergies with the global climate change. Energy and Buildings, 207, 109482.

Taha, H. (1997). Urban climates and heat islands: albedo, evapotranspiration, and anthropogenic heat. Energy and buildings, 25(2), 99-103.

Chapter 2: Background Literature

It is now well established that climate change posses serious risks to the health of Canadians and people around the world (Health Canada, 2011). One of the key issues health risks from extreme heat events is an emerging public health concern. The 2003 extreme heat event in Europe that resulted in 70,000 deaths (Watts et al., 2017) and the 2010 event in Russia that resulted in an estimated 55,000 deaths (Barriopedro et al., 2011) indicate the significant toll on health that such events can have (Schnall et al., 2017). Extreme heat is a health concern in Canada as well; research shows that in Toronto alone an average of 120 people died from extreme heat annually between 1954 and 2000. In 2005, Toronto experienced 41 extremely hot days exceeding 30°C(86°F) during which health officials called a total of 26 heat alert days to warn the public of the hazardous conditions. In British Columbia, an extreme heat event from July 27 to August 3 in 2009 resulted in 156 excess deaths as temperatures reached 34.4°C(93.9°F) (Health Canada, 2011; Cheng et al, 2005; Environment Canada, 2010). More recently, Quebec experienced a heatwave in 2018 that contributed to 86 deaths. In late June 2021, the BC Corners Service (2021) reported 219 excess deaths due to a heat wave in British Columbia with additional deaths in other countries western Canadian provinces expected. Heat-related deaths are preventable, and assessments of individual and community vulnerability can help to reduce mortality associated with extreme heat events (Health Canada, 2011). The Intergovernmental Panel on Climate Change (IPCC) defines "vulnerability to climate change as the degree to which a system is susceptible to, and unable to cope with, adverse impacts of climate variability" (IPCC, 2007, P. 48). Current and future factors influencing

health outcomes, including potential risks and protective measures, are investigated when assessing heat-health vulnerability.

2.1. Urban Heat Island

Many urban and suburban areas experience higher temperatures in comparison to their rural surroundings This phenomenon, called the urban heat island (UHI), is one of the most documented phenomenon of local climate change in cities (Santamouris, 2015). The annual mean air temperature of a city with one million or more population can be 1 to 3°C warmer than its surroundings, and on a clear, calm night, this temperature difference can be as much as 12°C (U.S. Environmental Protection Agency, EPA 2008). There exists a relationship between the size of a village, town or city, and the magnitude of the urban heat island it produces (Oke, 1973). Even smaller cities and towns will produce heat islands, though the effect often decreases as city size decreases (Akbari et al,2009).

While the temperatures of an UHI are relatively straightforward to measure, there are several types of UHI each of which is temporally and spatially dynamic which makes it methodologically complex to study. These different types exist in different scales and have various causative thermal process (Oke et al., 2017).

- Subsurface urban heat island (UHI_{Sub}) is the difference between temperatures in the ground and groundwater under the city, including urban soils and the subterranean built fabric, and those in the surrounding rural ground.

- Surface urban heat island (UHI_{Surf}) is defined by temperature differences at the interface of the outdoor atmosphere with the solid materials of the city and equivalent rural ground surface.

- Canopy layer urban heat island (UHI_{UCL}) is the difference between the temperature of the air contained in the urban canopy layer, the layer between the urban surface and roof level, and the corresponding height in the near-surface layer of the countryside. The urban canopy layer (UCL) is the layer of the air extending from the ground up to the mean height of the elements (buildings, trees) that make up the urban surface.

- Boundary layer urban heat island (UHI_{UBL}), the difference between the temperature of the air in the layer between the top of the UCL and the top of the urban boundary layer, and that at similar elevations in the atmospheric boundary layer of the surrounding rural region.
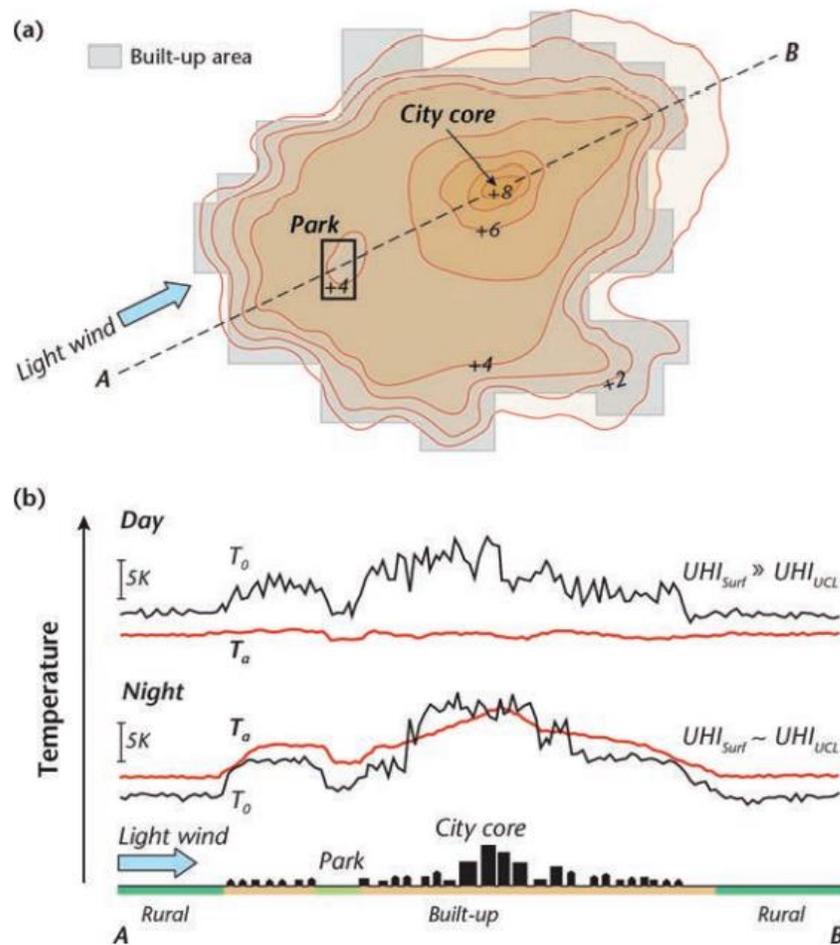
Figure 2-1. Schematic depiction of a typical UHI$_{UCL}$ at night in calm and clear conditions in a city on relatively level terrain. (a) Isotherm map illustrating typical features of the UHI and their correspondence with the degree of urban development. (b) 2D cross-section of both surface and screen-level air temperature in a traverse along the line A–B shown in (a) From Oke et al. (2017). Reproduced with permission of the Licensor through PLSclear

Figure 2-1 shows a schematic depiction of a typical UHI urban canopy layer (UCL) at night in calm and clear conditions in a city on relatively level terrain presented by Oke et al., (2017).

The development of the UHI is influenced by several factors, synoptic weather conditions in the area, the local morphological and structural parameters of the city, the thermal properties of the materials used, the magnitude of the anthropogenic heat released, and the presence of heat sources and sinks in the cities (Santamouris et al., 2016). In 1833, Luke Howard hypothesized that the excess heat in cities during summer was due to greater absorption of solar radiation by the vertical surfaces of a city and the lack of available humidity for evaporation (Lima Alves, 2017).

In the daytime, urban horizontal and vertical surfaces are exposed to solar radiation; variation in the climate of a surface is driven by the surface energy balance, which describes the net result of energy exchanges by radiation, convection and conduction between a facet, an element or a land surface and the atmosphere (Oke et al., 2017).

In an extensive, homogenous and flat non-urban land surface where all heat flux densities are restricted to the vertical direction and essentially one-dimensional in the first approximation, the surface energy balance equation is :

$$Q^* = Q_H + Q_E + Q_G \quad (\text{W m}^{-2}) \tag{2-1}$$

where Q^* is the net all wave radiation, Q_H is the sensible heat flux density, Q_E is the latent heat flux density, and Q_G is the ground heat flux density that transfers sensible heat by conduction to the substrate(Oke et al., 2017).

For an urban building-soil-air control volume that includes multiple facets (roof, wall, road, ground), facets are coupled via radiation, wind, and turbulence to each other and cause

changes in their energy balance. Therefore, the energy balance for such a control volume reads:

$$Q^* + Q_F = Q_H + Q_E + \Delta Q_S + \Delta Q_A \quad (\text{W m}^{-2}) \qquad (2\text{-}2)$$

where Q_F is the heat released inside the control volume due to the human activities associated with living, work and travel, often called anthropogenic heat flux density. ΔQ_S is the net heat storage change by the fabric of the city, and ΔQ_A is the net energy added to, or subtracted to the control volume by advection (Oke et al., 2017).

Five surface properties control the surface energy equation; 1. geometric, 2. radiative, 3. thermal, 4. moisture, and 5. aerodynamic. Surface geometry properties include orientation and openness to the sun and sky. Radiative properties control the reflectance ability of a surface. For example, facets with high albedo reduce shortwave gain and lead to a cooler temperature. Thermal properties of materials consist of their thermal conductivity and heat capacity. Facets made of materials with low thermal conductivity and heat capacity concentrate heat in a thin surface layer instead of transferring heat into the substrate. This resistance leads to a higher temperature of these surfaces and layers near to the surface. Moisture properties correspond to the availability of surface and near-surface soil and plant water moisture to evaporate. Evaporation provides a cooler temperature and a lower diurnal temperature range. Finally, aerodynamic properties, especially roughness length and exposure to wind influence temperature. Variabilities between these properties in urban and rural areas generate different urban and rural temperatures as well as large intra-urban temperature differences (Oke et al., 2017).

Climate warming can affect human health by influencing the surrounding environment and natural and social ecosystems; it is important to describe the generation mechanism of climatic variations on regional to local scales. Cities contain more than half of the world's population, and it is estimated that 70% of the global population will live in cities by 2050. Therefore, city warming and heat waves due to the UHI effect can have a significant impact on the lives, well-being, and human health of urban residents (Grimm et al., 2018; Patz et al., 2005; United Nations Population Division, 2007; Douglas, 2012; Huang and Lu, 2015).

2.2. Urban Outdoor Thermal Comfort

Thermal comfort is related to the thermal balance between heat gains due to the metabolism of the body and heat losses from the body to the environment (Baker, 2003).

Human thermal comfort is a function of air temperature, and five other, less obvious parameters: mean radiant temperature, relative air velocity, humidity, activity level, and clothing thermal resistance. Most of the causes of discomfort can be explained by a long-term imbalance of losses and metabolic gains or extreme values of one of the environmental parameters (Olesen, 1982). In an urban landscape, a complex radiation environment exists that affects urban residents' thermal comfort (Oke et al., 2017).

It can sense different thermal sensations among people, even in the same environment. Even though temperature sensors render the same results regardless of the geographical position where a measurement is being taken, this is not the case for persons (Djongyang et al., 2010). The human body experiences different temperature distributions during cool and warm conditions. In cool conditions, the warmest temperature is confined to the head,

while in warm conditions, the warm core temperature is found over much of the whole body (Mount, 1979; Oke et al. 2017).

The PMV (Predicted Mean Vote) index is suggested by Fanger. The index predicted the mean response of a large group of people according to the ASHRAE thermal sensation scale. Subjects exposed to climate chambers are asked to give their opinions according to the ASHRAE seven-point thermal sensation scale. A mean vote (MV) is derived for a given condition by finding the mean value of the feeling given by all the subjects for that condition. Fanger related PMV to the imbalance between the actual heat flow from a human body in a given environment and the heat flow required for optimum comfort at a specified activity (Lin et al., 2008; Djongyang et al., 2010; Fanger, 1967).

In an urban setting, the total radiation is one of the most effective gain/loss factors on the human energy balance. Energy exchanges at the surface of the human body include direct shortwave radiation, diffuse shortwave radiation from the sky, diffuse longwave radiation that is emitted from the sky and from the ground, emitted longwave radiation which is a function of the surface temperature, convective heat losses by sensible and latent heat exchange with the ambient air that is partly a function of wind speed and conductive heat exchange with the ground through physical contacts (Oke et al. 2017).

Air temperature is considered by most people as the leading indicator of comfort. The way that the human body feels in outdoor spaces is controlled by the interaction of various weather parameters. Mean radiant temperature controls outdoor thermal comfort in the exposed surfaces on a summer day (Höppe, 1999). Mean radiant temperature is the equivalent temperature of the environment that a person is exposed which generates the same radiation gain to the body as longwave and net shortwave receipt from the natural

environment (Oke et al., 2017). Spatial variation of mean radiant temperature during the day is governed by shadow patterns generated by obstructing objects such as trees, buildings, general topography, thermal and radiative properties of surrounding surface materials (Lindberg and Grimmond 2011b; Lindberg et al., 2013). The mean radiant temperature is calculated according to the sum of all shortwave and longwave radiation fluxes exposed by a human body (Thorsson et al., 2007).

There are various thermal comfort indexes, as illustrated in Figure 2-6. Thermal comfort indexes can be divided into two main types, rational or empirical. The rational indices

PMV	Thermal perception	Grade of physiological stress
-3.5	Very cold	Extreme cold stress
-2.5	Cold	Strong cold stress
	Cool	Moderate cold stress
-1.5	Slightly cool	Slight cold stress
-0.5		
	Comfortable	No thermal stress
0.5		
1.5	Slightly warm	Slight heat stress
	Warm	Moderate heat stress
2.5	Hot	Strong heat stress
3.5		
	Very hot	Extreme heat stress

Figure 2-2. Ranges of the thermal indexes Predicted Mean Vote (PMV) for different grades of thermal perception by human beings and physiological stress on human beings (Modified after: Matzarakis et al., 1999 and Oke et al. 2017).

include the PPD (percent people dissatisfied), Effective Temperature, the PMV (predicted mean vote), the Standard Effective Temperature (SET), and the empirical indices include RT (resultant temperature), HOP (humid operative temperature), OP(operative temperature) (Toudert, 2005).

2.3. Urban Heat Island Mitigation

This section presents a review of the literature related to heat mitigation methods and impacts on urban climate. These studies employed field observation method and numerical models to investigate the impacts, from the street scale to the larger (city) scale.

Assessing the impacts of buildings and the surrounding outdoor environment on the urban climate and outdoor thermal comfort control, as well as mitigation of the UHI effect is a multidisciplinary task that involves subjects in landscaping, urban planning, architecture, and building materials, and many others (Berkovic et al. 2012; Makaremi et al. 2012; Taleb and Taleb 2014; Taleghani et al. 2015; Wang et al. 2016). Given the negative effects of UHI, many studies have focused on techniques to reduce UHI by modeling single neighbors in the last two decades (Krayenhoff et al., 2003; Bosselmann et al., 1995; Baklanov and Nuterman 2009; Sailor, 2014; Wang and Akbari, 2014; Wang et al., 2016). Preliminary findings indicate that urban design has a significant impact on the microclimate of outdoor areas and urban canopy layers (Ghaffarianhoseini and Berardi, 2015; Tian et al., 2017; Yang et al., 2013; Wang et al., 2016). In addition, some detailed urban planning methods, such as green roofs or urban vegetation, have been indicated to have beneficial effects (Berardi and Ghaffarianhoseini, 2014; Wang and Zacharias, 2015; Wang et al., 2016).

Asphalt and concrete constitute up to 40% of Canadian urban surface area (Williamson et al., 2009). Krayenhoff et al., 2003, surveyed the land covers in Toronto, they found, in average, asphalt area constitutes 16.2% and concrete area almost 13.7% of the total land

cover (Krayenhoff et al. 2003). Obviously, these average values are higher for downtown zones. Asphalt and concrete materials are classified as urban surface covers that contribute to the urban heat island formation. Low albedo materials such as asphalt and concrete enhance the absorption of sunlight and increase temperatures (Dyce and Voogt, 2015). As a strategy for mitigating the UHI, surface materials with high albedo and emissivity have been proposed worldwide since they remain cooler when exposed to solar radiation (Akbari et a., 2001; Akbari and Konopacki 2004; Synnefa et al., 2007; Pisello and Cotana 2014; Wang et al., 2016).

Cool pavement and materials with high albedo absorb less sunlight and remain cooler than low albedo material. Due to the higher heat capacity of high albedo materials, the daytime maximum surface temperature occurs later; however, it contributes to a higher surface temperature at night. Furthermore, as a result of evaporation below porous pavements, road surface temperature can reduce. According to the results of Taleghani and Berardi research on the impact of pavement albedo on pedestrian thermal comfort, increasing the albedo of pavement from 0.1 to 0.3 and 0.5, can be reduced the air temperature 0.5 to 1 ℃ (Taleghani and Berardi, 2018).

In urban areas, the fraction of the ground that is covered by trees and vegetation is smaller and contains less biomass than nonurban areas (Wang et al., 2016; Oke, 1988). Akbari (2009) classified the effect of trees on urban climate into two categories: direct and indirect. Shading and reducing wind speed have a direct impact on urban climate and modify the interaction between a building and its surroundings. Trees in full leaf can be highly efficient in blocking solar radiation and reducing cooling loads. Furthermore, with evapotranspiration, trees influence the surrounding urban environment. Plants release

moisture in the form of water vapour through evapotranspiration, which absorbs energy from solar radiation or heated air. When solar energy is used for evapotranspiration rather than directly heating the air, the daytime temperatures will be lowered (Akbari, 2009). Air temperature reduction due to vegetation, including green roofs and ground-level vegetations such as grass, varies widely between 1 °C to 10 °C (Krayenhoff et al., 2021). In summer, the amount of solar radiation through a tree canopy is as low as 10 – 30% of the available solar energy reaching the surface of the tree canopy (US EPA, 2008; Hulley, 2012). Although winter benefits are less pronounced, they still warrant some considerations. For example, deciduous trees provide shade in summer and increase solar heating during winter (Hulley, 2012). Santamouris et al. indicated that street trees inside urban areas might lead to maximum air temperature reduction ranging between 0.1 °C and 5.0 °C with a median maximum temperature drop close to 1.5 °C (Santamouris et al., 2017).

Parking lots paved with asphalt, a low-albedo material, contribute to the urban heat island effect (Rosenzweig et al., 2005). In order to reduce the heat stored in the asphalt surfaces and in the cars parked there, it is recommended that vegetation be planted around the perimeter of (vegetation strips) and within (vegetation medians) parking lots (Giguere, 2009). The objective is to create shade on paved surfaces. The shade from trees can also protect the pavement from significant thermal variations and extend its lifespan (McPherson and Muchnick, 2005). A study by McPherson et al. (2001) reported that the temperature of a car shaded by vegetation is approximately 7°C lower than a car parked in the sun, while shaded asphalt pavement will be 2°C to 4°C cooler.

2.4. Urban Microclimate Models, ENVI-met:

After reviewing the beneficial aspects of urban climate numerical models, this section presents an exploration of the literature that used ENVI-met software for simulation of urban microclimate. The dynamic variability of weather conditions, complex geometry of urban design and different configurations of cities all over the world impose limitations on the empirical study of urban microclimate. Understanding and solving problems in complex environmental designs can be attained by simulation modelling. Numerical simulation is well suited to dealing with the complexities and non-linearities of the urban climate system; it has been widely used in urban climate study and continues to grow in popularity (Nik et al., 2020). Microclimate models evaluate a wide range of urban configurations for a specific purpose or to answer explicit urban planning and design questions (Roth and Lim, 2017).

Many researchers use ENVI-met software to assess the urban heat island and evaluate its mitigation techniques. Huttner et al. (2008) investigated the effects of global warming on heat stress using ENVI-met in central European cities. They recommended that green spaces be considered an important factor to improve human thermal comfort. Hedquist et al. (2009) used ENVI-met as well as CFD modeling in a Central Business District, Phoenix, to interpret the local flow modifications due to the UHI diurnal cycle. Results from this study explained the dynamics of the UHI within the built environment, and also suggested solutions to mitigate heat and increase outdoor thermal comfort in hot, arid cities. A study presented by Maleki and Mahdavi (2016) used ENVI-met to simulate microclimate conditions in a part of the city of Vienna. This study focused on investigating the effects of the variation of physical and geometrical properties of the urban area (cool roofs, green

lands, and perviousness of paving materials) on the urban micro-climate and outdoor thermal comfort. The results suggested that modifications within the urban canopy were more effective in influencing the microclimate conditions than those implemented to the roof levels. Increasing vegetation and permeable pavements can cool the air temperature down by up to 3 K. Several researchers studied cool materials' application on urban open spaces and their positive effect on the human thermal comfort with ENVI-met (Makropoulou, 2017; Wang et al., 2017; Salata et al., 2017; Taleghani et al., 2016; Yang et al., 2016). In all those cited studies, the contribution of cool materials to ambient temperature reduction was confirmed.

There are several investigations on the impact of street trees and vegetation on urban heat island mitigation with ENVI-met(Shahidan et al., 2012; Taleghani et al., 2016; Chow and Brazel, 2012; Alchapar and Correa, 2016; Yang and Lin, 2016; Wang et al., 2016; Skelhorn et al., 2014; Lee et al., 2016b). Most of the studies yielded decreased canopy layer air temperature on a summer afternoon by increasing the number of trees (Krayenhoff et al., 2021).

2.5. References

Akbari, H. (2009). Cooling our communities. A guidebook on tree planting and light-colored surfacing.

Akbari, H., & Konopacki, S. (2004). Energy effects of heat-island reduction strategies in Toronto, Canada. Energy, 29(2), 191-210.

Akbari, H., Pomerantz, M., & Taha, H. (2001). Cool surfaces and shade trees to reduce energy use and improve air quality in urban areas. Solar energy, 70(3), 295-310.

Alchapar, N. L., & Correa, E. N. (2016). The use of reflective materials as a strategy for urban cooling in an arid "OASIS" city. Sustainable Cities and Society, 27, 1-14.

Baker, N., & Steemers, K. (2003). Energy and environment in architecture: a technical design guide. Taylor & Francis.

Baklanov, A. A., & Nuterman, R. B. (2009). Multi-scale atmospheric environment modelling for urban areas. Advances in Science and Research, 3(1), 53-57.

Barriopedro, D., Fischer, E. M., Luterbacher, J., Trigo, R. M., & García-Herrera, R. (2011). The Hot Summer of 2010: Redrawing the Temperature Record Map of Europe. Science, 332(6026), 220-224.

Berardi, U., GhaffarianHoseini, A., & GhaffarianHoseini, A. (2014). State-of-the-art analysis of the environmental benefits of green roofs. Applied energy, 115, 411-428.

Berardi, U., Jandaghian, Z., & Graham, J. (2020). Effects of greenery enhancements for the resilience to heat waves: A comparison of analysis performed through mesoscale (WRF) and microscale (Envi-met) modeling. Science of the Total Environment, 747, 141300.

Berkovic, S., Yezioro, A., & Bitan, A. (2012). Study of thermal comfort in courtyards in a hot arid climate. Solar Energy, 86(5), 1173-1186.

Bosselmann, P., Arens, E., Dunker, K., & Wright, R. (1995). Urban form and climate: case study, Toronto. Journal of the American Planning Association, 61(2), 226-239.

Cheng, C. S., Campbell, M., Li, Q. Et al. (2005). Differential and combined impacts of winter and summer weather and air pollution due to global warming on human mortality in south-central canada. Health policy research program: project number 6795-15-2001/4400011. Retrieved September30, 2009, from www.toronto.ca/health/hphe/pdf/weather_air_pollution_impacts_exec_ summary.pdf.

Chow, W. T., Brennan, D., & Brazel, A. J. (2012). Urban heat island research in Phoenix, Arizona: Theoretical contributions and policy applications. Bulletin of the American Meteorological Society, 93(4), 517-530.

Djongyang, N., Tchinda, R., & Njomo, D. (2010). Thermal comfort: A review paper. Renewable and sustainable energy reviews, 14(9), 2626-2640.

Douglas, I. (2012). Urban ecology and urban ecosystems: understanding the links to human health and well-being. Current Opinion in Environmental Sustainability, 4(4), 385-392.

Environment Canada – Ontario Region. (2010). Historical Heat-Related Events. Environment Canada. Retrieved April 23, 2010, from http://ontario.hazards.ca/historical/Heat_Ontario-e.html.

Fanger, P. O. (1973). Assessment of man's thermal comfort in practice. Occupational and Environmental Medicine, 30(4), 313-324.

Ghaffarianhoseini, A., Berardi, U., & Ghaffarianhoseini, A. (2015). Thermal performance characteristics of unshaded courtyards in hot and humid climates. Building and Environment, 87, 154-168.

Giguere, M. (2009). Urban heat island mitigation strategies. Institut national de santé publique du Québec, Québec.

Grimm, N. B., faeth, S. H., golubiewski, N. E., redman, C. L., Wu, J., Bai, X., & Briggs, J. M. (2008). Global change and the ecology of cities. Science, 319(5864), 756-760.

Höppe, P. (1999). The physiological equivalent temperature–a universal index for the biometeorological assessment of the thermal environment. International journal of Biometeorology, 43(2), 71-75.

Hedquist, B. C., Brazel, A. J., Di Sabatino, S., Carter, W., & Fernando, H. J. S. (2009, January). Phoenix urban heat island experiment: micrometeorological aspects. In Proceedings of the Eighth Symposium on the Urban Environment.

Höppe, P. (1999). The physiological equivalent temperature–a universal index for the biometeorological assessment of the thermal environment. International journal of Biometeorology, 43(2), 71-75.

Huang, Q., & Lu, Y. (2015). The effect of urban heat island on climate warming in the Yangtze River Delta urban agglomeration in China. International journal of environmental research and public health, 12(8), 8773-8789.

Hulley, M. E. (2012). The urban heat Island effect: Causes and potential solutions. In Metropolitan Sustainability (pp. 79-98). Woodhead Publishing.

Huttner, S., Bruse, M., & Dostal, P. (2008, October). Using ENVI-met to simulate the impact of global warming on the microclimate in central European cities. In 5th Japanese-German Meeting on Urban Climatology (Vol. 18, No. 18, pp. 307-312).

IPCC, 2007: Climate Change 2007: The Physical Science Basis. Contribution of Working Group I to the Fourth Assessment Report of the Intergovernmental Panel on Climate Change [Solomon, S., D. Qin, M. Manning, Z. Chen, M. Marquis, K.B. Averyt, M.Tignor and H.L. Miller (eds.)]. Cambridge University Press, Cambridge, United Kingdom and New York, NY, USA.

Krayenhoff, E. S., Broadbent, A. M., Zhao, L., Georgescu, M., Middel, A., Voogt, J. A., ... & Erell, E. (2021). Cooling hot cities: A systematic and critical review of the numerical modelling literature. Environmental Research Letters.

Krayenhoff, E. S., Martilli, A., Bass, B., & Stull, R. (2003, September). Mesoscale simulation of urban heat mitigation strategies in Toronto, Canada. In Fifth International Conference on Urban Climate (Vol. 1, p. 343). University of Łódź.

Lee, H., Mayer, H., & Chen, L. (2016). Contribution of trees and grasslands to the mitigation of human heat stress in a residential district of Freiburg, Southwest Germany. Landscape and Urban Planning, 148, 37-50.

Lima Alves, E. D., & Lopes, A. (2017). The urban heat island effect and the role of vegetation to address the negative impacts of local climate changes in a small Brazilian City. Atmosphere, 8(2), 18.

Lin, Z., & Deng, S. (2008). A study on the thermal comfort in sleeping environments in the subtropics—developing a thermal comfort model for sleeping environments. Building and environment, 43(1), 70-81.

Lindberg, F., & Grimmond, C. S. B. (2011). Nature of vegetation and building morphology characteristics across a city: influence on shadow patterns and mean radiant temperatures in London. Urban Ecosystems, 14(4), 617-634.

Lindberg, F., Holmer, B., Thorsson, S., & Rayner, D. (2014). Characteristics of the mean radiant temperature in high latitude cities—implications for sensitive climate planning applications. International journal of biometeorology, 58(5), 613-627.

Makaremi, N., Salleh, E., Jaafar, M. Z., & GhaffarianHoseini, A. (2012). Thermal comfort conditions of shaded outdoor spaces in hot and humid climate of Malaysia. Building and environment, 48, 7-14.

Makropoulou, M. (2017). Microclimate improvement of Inner-City urban areas in a Mediterranean coastal city. Sustainability, 9(6), 882.

Maleki, A., & Mahdavi, A. (2016). Evaluation of urban heat islands mitigation strategies using 3dimentional urban micro-climate model ENVI-met.

Matzarakis, A., Mayer, H., & Iziomon, M. G. (1999). Applications of a universal thermal index: physiological equivalent temperature. International journal of biometeorology, 43(2), 76-84.

McPherson, E. G., & Muchnick, J. (2005). Effect of street tree shade on asphalt concrete pavement performance. Journal of Arboriculture, 31(6), 303.

Mount, L. E. (1979). Adaptation to thermal environment. Man and his productive animals. Edward Arnold (Publishers) Ltd..

Nik, V. M., Perera, A. T. D., & Chen, D. (2021). Towards climate resilient urban energy systems: a review. National Science Review, 8(3), nwaa134.

Oke, t. R. (1973). City size and the urban heat island. Atmospheric environment (1967), 7(8), 769-779.

Oke, T. R. (1988). Street design and urban canopy layer climate. Energy and buildings, 11(1-3), 103-113.

Oke, T.R. 1982. The Energetic Basis of the Urban Heat Island. Quarterly Journal of the Royal Meteorological Society. 108:1-24.

Oke, T.R. 1997. Urban Climates and Global Environmental Change. In: Thompson, R.D. and A. Perry (eds.) Applied Climatology: Principles & Practices. New York, NY: Routledge. pp. 273-287.

Oke. T.R. 1987. Boundary Layer Climates. New York, Routledge.

Oke, T. R., Mills, G., Christen, A., & Voogt, J. A. (2017). Urban climates. Cambridge University Press.

Olesen, B. W. (1982). Thermal comfort. Technical review, 2, 3-37.

Patz, J. A., Campbell-Lendrum, D., Holloway, T., & Foley, J. A. (2005). Impact of regional climate change on human health. Nature, 438(7066), 310-317.

Pisello, A. L., & Cotana, F. (2014). The thermal effect of an innovative cool roof on residential buildings in Italy: Results from two years of continuous monitoring. Energy and Buildings, 69, 154-164.

Roth, M., & Lim, V. H. (2017). Evaluation of canopy-layer air and mean radiant temperature simulations by a microclimate model over a tropical residential neighbourhood. Building and Environment, 112, 177-189.

Sailor, D. J. (2014). A holistic view of the effects of urban heat island mitigation. In Low Carbon Cities (pp. 308-319). Routledge.

Salata, F., Golasi, I., Petitti, D., de Lieto Vollaro, E., Coppi, M., & de Lieto Vollaro, A. (2017). Relating microclimate, human thermal comfort and health during heat waves: An analysis of heat island mitigation strategies through a case study in an urban outdoor environment. Sustainable Cities and Society, 30, 79-96.

Santamouris, M. (2015). Analyzing the Heat Island Magnitude and Characteristics In One Hundred Asian And Australian Cities And Regions. Science of The Total Environment, 512, 582-598.

Santamouris, M., & Kolokotsa, D. (2016). Urban climate mitigation techniques. Routledge.

Schnall, A., Nakata, N., Talbert, T., Bayleyegn, T., Martinez, D., & Wolkin, A. (2017). Community assessment for public health emergency response (casper): an innovative emergency management tool in the united states. American journal of public health, 107(s2), s186-s192.

Shahidan, M. F., Jones, P. J., Gwilliam, J., & Salleh, E. (2012). An evaluation of outdoor and building environment cooling achieved through combination modification of trees with ground materials. Building and Environment, 58, 245-257.

Skelhorn, C., Lindley, S., & Levermore, G. (2014). The impact of vegetation types on air and surface temperatures in a temperate city: A fine scale assessment in Manchester, UK. Landscape and Urban Planning, 121, 129-140.

Solecki, W. D., Rosenzweig, C., Parshall, L., Pope, G., Clark, M., Cox, J., & Wiencke, M. (2005). Mitigation of the heat island effect in urban New Jersey. Global Environmental Change Part B: Environmental Hazards, 6(1), 39-49.

Synnefa, A., Santamouris, M., & Apostolakis, K. (2007). On the development, optical properties and thermal performance of cool colored coatings for the urban environment. Solar energy, 81(4), 488-497.

Taleb, H., & Taleb, D. (2014). Enhancing the thermal comfort on urban level in a desert area: Case study of Dubai, United Arab Emirates. Urban forestry & urban greening, 13(2), 253-260.

Taleghani, M., & Berardi, U. (2018). The effect of pavement characteristics on pedestrians' thermal comfort in Toronto. Urban climate, 24, 449-459.

Taleghani, M., Kleerekoper, L., Tenpierik, M., & Van Den Dobbelsteen, A. (2015). Outdoor thermal comfort within five different urban forms in the Netherlands. Building and environment, 83, 65-78.

Taleghani, M., Sailor, D., & Ban-Weiss, G. A. (2016). Micrometeorological simulations to predict the impacts of heat mitigation strategies on pedestrian thermal comfort in a Los Angeles neighborhood. Environmental Research Letters, 11(2), 024003.

Thorsson, S., Lindberg, F., Eliasson, I., & Holmer, B. (2007). Different methods for estimating the mean radiant temperature in an outdoor urban setting. International Journal of Climatology: A Journal of the Royal Meteorological Society, 27(14), 1983-1993.

Tian, W., Wang, Y., Xie, Y., Wu, D., Zhu, L., & Ren, J. (2007). Effect of building integrated photovoltaics on microclimate of urban canopy layer. Building and environment, 42(5), 1891-1901.

U.S. Environmental Protection Agency. 2008. "Urban Heat Island Basics." In: Reducing Urban Heat Islands: Compendium of Strategies. Draft. https://www.epa.gov/heat-islands/heat-island-compendium.

United Nations Population Division. World Urbanization Prospects: The 2007 Revision. United Nations Department of Economic and Social Affairs: New York, NY, USA, 2008; Available online: http://www.un.org/esa/population/publications/wup2007/2007WUP_ExecSum_web.pdf

Wang, Y., & Akbari, H. (2014). Development and application of 'thermal radiative power'for urban environmental evaluation. Sustainable Cities and Society, 14, 316-322.

Wang, Y., & Zacharias, J. (2015). Landscape modification for ambient environmental improvement in central business districts–a case from Beijing. Urban forestry & urban greening, 14(1), 8-18.

Wang, Y., Berardi, U., & Akbari, H. (2016). Comparing the effects of urban heat island mitigation strategies for Toronto, Canada. Energy and Buildings, 114, 2-19.

Water, Air, And Climate Change Bureau Healthy Environments and Consumer Safety Branch. (2011). Adapting to Extreme Heat Events: Guidelines for Assessing Health Vulnerability. Retrieved from the Health Canada website: adapt-eng.pdf (canada.ca).

Watts, N., Amann, M., Ayeb-Karlsson, S., Belesova, K., Bouley, T., Boykoff, M., ... & Costello, A. (2018). The lancet countdown on health and climate change: from 25 years of inaction to a global transformation for public health. The lancet, 391(10120), 581-630.

Williamson, T. B., Colombo, S. J., Duinker, P. N., Gray, P. A., Hennessey, R. J., Houle, D., ... & Spittlehouse, D. L. (2009). Natural Resources Canada. Canadian Forest Service, Northern Forestry Centre, Edmonton, Alberta, Sustainable Forest Management Network, University of Alberta, Edmonton, Alberta.

Yang, J., Wang, Z. H., Kaloush, K. E., & Dylla, H. (2016). Effect of pavement thermal properties on mitigating urban heat islands: A multi-scale modeling case study in Phoenix. Building and Environment, 108, 110-121.

Yang, P., Ren, G., & Liu, W. (2013). Spatial and temporal characteristics of Beijing urban heat island intensity. Journal of applied meteorology and climatology, 52(8), 1803-1816.

Chapter 3: ENVI-Met Software

There are various available computational models to simulate urban microclimates (e.g., RayMan, SOLWEIG, TUF-3D, ENVI-met) (Matzarakis et al. 2007; Lindberg et al., 2008; Krayenhoff and Voogt, 2007; Bruse, 2004). The choice of ENVI-met as a simulation tool in this project is motivated by the unique aspects of this software and its ability to simulate the impacts of vegetation, coupling the atmospheric processes with vegetation and soil moisture processes. In addition to the capability of ENVI-met to compute sophisticated study area arrangements, the software is more user-friendly and accessible for users than other similar models (Crank et al., 2018).

3.1 Characteristics of ENVI-met

ENVI-met is a three-dimensional non-hydrostatic model that simulates surface-plant-air interaction and analyzes small-scale interactions between building surfaces and plants. The
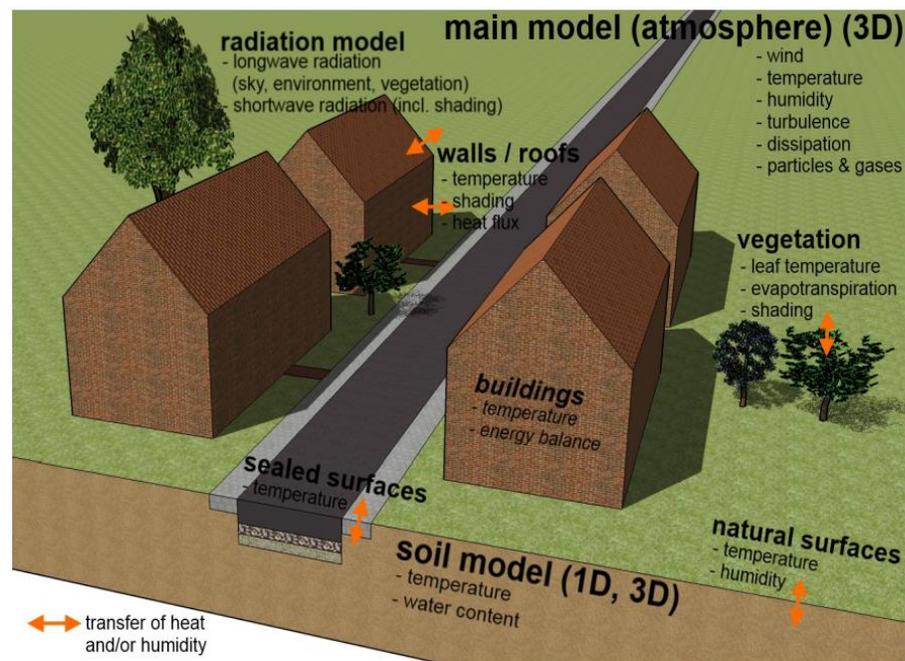
Figure 3-1. Schematic of the sub models of ENVI-met (Huttner, 2012)

release of the first version of the ENVI-met model (version v.3.0) was officially announced in 1998 (Bruse and Fleer, 1998b), and the latest version (version v.4.4.1) was released in 2019. ENVI-met simulates the dynamics of the urban microclimate using atmospheric physics and heat transfer principles (Bruse and Fleer, 1998). Three-dimensional wind flow is calculated using the incompressible, non-hydrostatic Navier-Stokes equations with the Bousinessq approximation of buoyancy effects. Advection-diffusion equations are used to calculate potential temperature and specific humidity distribution, and then distributions are modified by sources and sinks of heat and moisture within the model.

Required input data for the ENVI-met model include latitude and longitude, simulation date and duration, horizontal wind speed, roughness length, air temperature, specific and relative humidity. The significant prognostic variables computed by ENVI-met are (Bruse and Fleer, 1998):

- Wind speed and direction.

- Air and soil temperature.

- Air and soil humidity.

- Radiative fluxes.

- Gas and particle dispersion.

3.2. ENVI-met Model and Sub-models:

The computation of all variables needs to use several sub-models that interact with each other. The ENVI-met model consists of a one-dimensional boundary model that includes vertical profiles of different meteorological parameters up until a height of 2500 meters

and a three-dimensional core model that includes all atmosphere, soil, building, and vegetation processes. Figure 3-2 shows an overview of ENVI-met model.
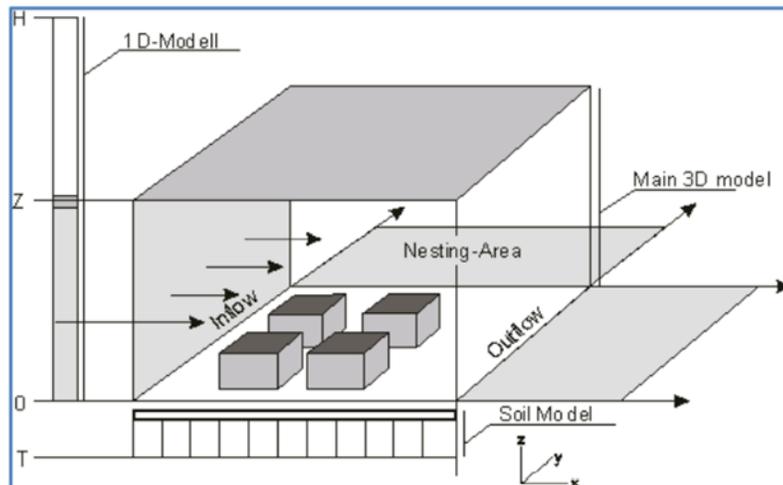
Figure 3-2. Schematic of the ENVI-met model layout (http://www.envi-met.com/).

3.3. One-dimensional Boundary Model

ENVI-met simulates only part of the atmosphere, and for that reason considering boundary conditions are required for the lateral and vertical borders of the 3D model (Bruse, 1999). The 1D boundary model creates one-dimensional profiles for meteorological parameters to provide the boundary conditions of lateral and vertical borders of 3D model (Simons, 2016). The one-dimensional boundary model with its horizontally homogeneous vertical profiles is then used to provide data on the borders of the 3D model (Bruse, 1999).

3.4 The three-dimensional core models

3.4.1 The atmosphere model

The three-dimensional core model consists of three orthogonal orientated axes, which generate a three-dimensional cube. The model area contains several cells representing different objects such as buildings, vegetation, or atmosphere. The number of cells depends on the model area dimensions and its spatial resolution. Each cell is delineated by its physical properties; for instance, a building cell is classified by its material types, and the material type is classified by the specific heat capacity and other parameters. In combination with databases of all the different objects, this structure allows a detailed reconstruction of an urban environment (Simon, 2016). In the atmosphere model the main processes on the urban climate are simulated: wind field, air temperature and humidity distribution, turbulence, gas and particle dispersion, radiation, exchange processes on ground and building surfaces.

3.4.1.1 Wind flow equation

For simplification of wind flow equations, Huttner (2012) used the Boussinesq-approximation to eliminate the fluid density ρ from the Navier-Stokes equations, which can be written as:

$$\frac{\partial u}{\partial t} + u_i \frac{\partial u}{\partial x_i} = -\frac{\partial p'}{\partial x} + K_m \left(\frac{\partial^2 u}{\partial x_i^2}\right) + f\,(v\text{-}v_g) - S_u \tag{3-1}$$

$$\frac{\partial v}{\partial t} + u_i \frac{\partial v}{\partial x_i} = -\frac{\partial p'}{\partial y} + K_m \left(\frac{\partial^2 v}{\partial x_i^2}\right) + f\,(u\text{-}u_g) - S_v \tag{3-2}$$

$$\frac{\partial w}{\partial t} + u_i \frac{\partial w}{\partial x_i} = -\frac{\partial p'}{\partial z} + K_m \left(\frac{\partial^2 w}{\partial x_i^2}\right) + g\,\frac{\theta(z)}{\theta_{ref}(z)} - S_w \tag{3-3}$$

Due to the low speed, air is considered as an incompressible fluid, therefore, the continuity equation reads as:

$$\frac{\partial u}{\partial x} + \frac{\partial v}{\partial y} + \frac{\partial w}{\partial z} = 0 \qquad (3\text{-}4)$$

In the above equations, u, v and w are the wind mean velocities (m/s) in x,y, and z directions, p' is p /ρ where p is the mean local pressure, and K_m is the local eddy viscosity. f is the Coriolis parameter that describes the rotation of the wind near the ground compared to the geostrophic wind components u_g and v_g. S_u, S_v, and S_w are the local source or sink terms that model the wind drag forces from semi-permeable obstacles such as vegetation. In equation (3-3) $\theta(k)$ represents the potential temperature at height z, θ_{ref} represents the average mesoscale conditions (Huttner, 2012).

3.4.1.2 Temperature and humidity

The distribution of the potential temperature θ is calculated from the advection-diffusion equation:

$$\frac{\partial \theta}{\partial t} + u_i \frac{\partial \theta}{\partial x_i} = K_h \left(\frac{\partial^2 \theta}{\partial x_i^2}\right) + Q_h \qquad (3\text{-}5)$$

where, K_h is the turbulent heat diffusivity for air and Q_h is a source term. The distribution of relative humidity is governed by equation (3-6)

$$\frac{\partial q}{\partial t} + u_i \frac{\partial q}{\partial x_i} = K_q \left(\frac{\partial^2 q}{\partial x_i^2}\right) + Q_q \qquad (3\text{-}6)$$

Q_h and Q_q are source terms used to link heat and vapor exchange at the plant surface with the atmospheric mode (Bruse and Fleer, 1998). Q_h is the term that defines the heat exchange between air and vegetation, Q_q defines the exchange of humidity between air and vegetation, and K_q is the turbulent transfer coefficient for humidity.

3.4.1.3 Turbulence and exchange processes

As a result of shearing flow near building walls and vegetation, turbulence is produced. Under windy conditions, the magnitude of local turbulence production normally surpasses its dissipation so that the mean flow transports turbulent eddies. ENVI-met uses a 1.5 order turbulence closure model to simulate these processes. This model is based on the work of Mellor and Yamada (1975) and adds two additional equations for turbulent kinetic energy production (E) and its dissipation (ϵ):

$$\frac{\partial E}{\partial t} + u_i \frac{\partial E}{\partial x_i} = K_E \left(\frac{\partial^2 E}{\partial x_i^2}\right) + P_r - T_h + Q_E - \epsilon \tag{3-7}$$

$$\frac{\partial \epsilon}{\partial t} + u_i \frac{\partial \epsilon}{\partial x_i} = K_\epsilon \left(\frac{\partial^2 \epsilon}{\partial x_i^2}\right) + c_1 \frac{\epsilon}{E} P_r - c_3 \frac{\epsilon}{E} T_h - c_2 \frac{\epsilon^2}{E} + Q_\epsilon \tag{3-8}$$

The terms P_r and T_h represent the production and the dissipation of turbulent energy due to wind and thermal stratification. Q_E and Q_ϵ are the local source terms for turbulent kinetic energy production and its dissipation. The constants c_1, c_2 and c_3 are empirical constants obtained experimentally (Bruse and Fleer, 1998).

3.4.1.4 Radiative fluxes

The absorption and emission coefficients of different atmospheric layers define the atmospheric radiation budget. These coefficients depend on the optical thickness of the atmosphere. Five reduction coefficients are defined to describe the radiation modification inside the model (Bruse and Fleer, 1998; Huttner, 2012):

$$\sigma_{sw,dir}(z) = \exp(F.LAI^*(z)) \tag{3-9}$$

$$\sigma_{sw,dif}(z) = \exp(F.LAI(z, z_p)) \tag{3-10}$$

$$\sigma_{lw}^{\downarrow}(z, z_p) = \exp(F.LAI(z, z_p)) \tag{3-11}$$

$$\sigma_{lw}^{\uparrow}(z, z_p) = \exp(F.LAI(0, z)) \tag{3-12}$$

$$\sigma_{svf}(z) = 1/360 \sum_{\pi=0}^{360} \cos\lambda(\pi) \tag{3-13}$$

LAI is the one-dimensional vertical leaf area index of the plant from level z to the top of the plant at z_p or the ground $z = 0$:

$$LAI(z, z + \Delta z) = \int_{z'}^{z'+\Delta z} LAD(z')dz' \tag{3-15}$$

In Equation (3-13) σ_{svf} describes the local sky obstruction by buildings (sky view factor) which ranges from 1 (completely unobstructed sky) to 0 (no sky visible). λ is the maximum shielding angle found by the ray-tracing module in direction π (Bruse and Fleer, 1998).

The shortwave radiation can be calculated as:

$$Q_{sw}(z) = \sigma_{svf,dir}(z)Q^0_{sw,dir} + \sigma_{sw,dir}(z)\sigma_{svf}(z)Q^0_{sw,dif} + (1 - \sigma_{svf}(z))\, Q^0_{sw,dir}.\bar{a}$$

where, $Q_{sw,dir}^0$ and $Q_{sw,dif}^0$ are the direct and diffuse shortwave radiation and $\bar{a}$ represents the average wall albedo (Bruse and Fleer, 1998).

The longwave radiation can be written as:

$$Q_{lw}^\downarrow (z) = \sigma_{lw}^\downarrow (z, z_p)\, Q_{lw}^{\downarrow,0} + (\,1 - \ \sigma_{lw}^\downarrow 0, z))\, \epsilon_f\, \sigma_B\, \bar{T}_f^4 + (1 - \sigma_{svf}(z))\, Q_{lw}^\leftrightarrow \qquad (3\text{-}17)$$

$$Q_{lw}^\uparrow (z) = \sigma_{lw}^\uparrow (0, z)\, \epsilon_s\, \sigma_B\, T_0^4 + (1 - \ \sigma_{lw}^\uparrow (0, z))\, \epsilon_f \sigma_f \bar{T}_{f-}^4 \qquad (3\text{-}18)$$

where, $\bar{T}_f^4$ and $\bar{T}_{f-}^4$ are the average foliage temperature of the underlying and overlaying of vegetation. ϵ_s and ϵ_f describe the emissivity coefficients of the surface and foliage. T_0 is the surface temperature. $Q_{lw}^\leftrightarrow$ represents the horizontal longwave radiation flux from surrounding walls. σ_B is the Stefan-Boltzmann constant which is equal to $5.67 \cdot 10^{-8}$ $\text{Wm}^{-2}\text{K}^{-4}$.

3.4.2 Soil model

The soil model calculates the temperature and humidity of the soil down to a depth of 1.75m (Huttner, 2012). Each horizontal grid cell has a soil profile with 14 layers with different depths. The depth of the single layers increases from top to bottom; the top layers have a thickness of only 1 cm, the lowest layer has a thickness of 50 cm. In the soil model, only vertical fluxes of temperature and humidity are calculated (1D model) (Huttner, 2012). The equations for calculating the soil temperature T and the volumetric water content η are given below:

$$\frac{\partial T}{\partial t} = k_s \frac{\partial^2 T}{\partial z^2} \qquad (3\text{-}19)$$

$$\frac{\partial \eta}{\partial t} = D_\eta \frac{\partial^2 \eta}{\partial z^2} + \frac{\partial K_\eta}{\partial z} - S_\eta (z) \qquad (3\text{-}20)$$

The thermal diffusivity k_s (m^2/ sec) is a function of the soil moisture for natural soils. η is the volumetric water content of the soil ($m^3 m^{-3}$), K_η is the hydraulic conductivity, and D_η is the hydraulic diffusivity. S_η is the water absorbed by the plant root and is provided by the vegetation model and treated as an internal moisture sink (Bruse and Fleer, 1988).

3.4.3 Vegetation model

Vegetation in ENVI-met is represented by clusters of cells having a leaf area density in the atmosphere model and root area density in the soil model, allowing the remodeling of the distribution and shape of roots and crowns of plants (Simon, 2016). The vegetation model is considered the effects of these cell clusters on the wind field and the radiation. Furthermore, the modeled plants use biological control mechanisms that regulate CO^2 and water vapor exchange with the atmosphere. The direct heat flux $J_{f,h}$, the evaporation flux $J_{f,evap}$ and the transpiration flux $J_{f,trans}$ that define the interactions between vegetation and atmosphere are calculated from the following equations:

$$J_{f,h} = 1.1 \, r_a^{-1} \ (T_f - T_a) \qquad (3\text{-}21)$$

$$J_{f,evap} = r_a^{-1} \ \Delta_q \ \delta_c \, f_w + \ r_a^{-1} \ (1 - \delta_c) \ \Delta q \qquad (3\text{-}22)$$

$$J_{f,trans} = \delta_c (r_a + r_s)^{-1} (1 - f_w) \Delta q \qquad (3\text{-}23)$$

where, T_a is the air temperature, T_f is the foliage temperature, q is the specific humidity of the air, and Δq is the humidity difference. δ_c defines whether the evaporation is possible ($\delta_c = 1$) or not ($\delta_c = 0$). r_a is a function of the leaf diameter and wind speed (Huttner , 2012).

3.5. Simulation with ENVI-met:

The simulation process in ENVI-met usually represents 24-48 hours. To ensure that the simulation follows the atmospheric processes, it is best to initialize the model at night or at sunrise. Typically, 1 hour spin up time is used for ENVI-met (Conry et al., 2015). The spin up time corresponds to the time taken for the model to reach a steady state to create output values. ENVI-met requires an input area which defines the 3D geometry of the target area: the buildings, vegetation, soils, and receptors. The main input information of ENVI-met simulation includes weather conditions, the geometry and materials properties of the urban area, and characteristics of vegetation.

ENVI-met includes a grid-cell structure, with a maximum grid size of (250 x 250 x 30) cells. Horizontal resolution can range from 0.5 m to 10 m, which makes the model suitable for micro-scale to local scale analyses. There are two different types of vertical grid in ENVI-met (http://www.envi-met.com/):

1. An equidistant grid, as depicted in Figure 3-3, splits the first cell closest to the surface into five equally spaced sub-sections with a height equivalent to $0.2\Delta z$, where z is specified grid cell height. Above this, Δz is constant for the rest of model height.

2. A telescoping grid for the vertical resolution. The grid size expands with height, according to a user-specified extension (or telescoping) factor.
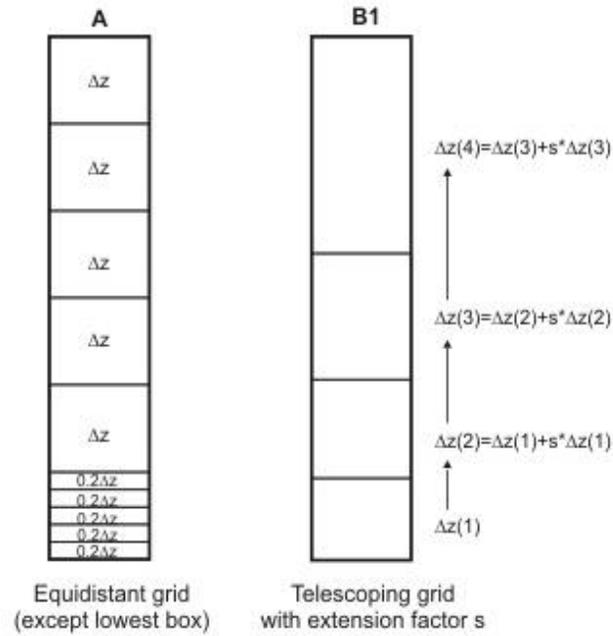
Figure 3-3. Schematic of equidistant vertical grid in ENVI-met(http://www.envi-met.com/)

ENVI-met outputs are binary files (.EDI/.EDT). The results can be visualized by importing

the outputs to the LEONARDO tool, a visualization tool in the ENVI-met software. Figure

3-4 represents a flow diagram of the ENVI-met model and the model inputs and outputs

structure. The outputs of ENVI-met are then used as inputs to a separate model BOTworld,

to calculate the thermal heat stress indices.
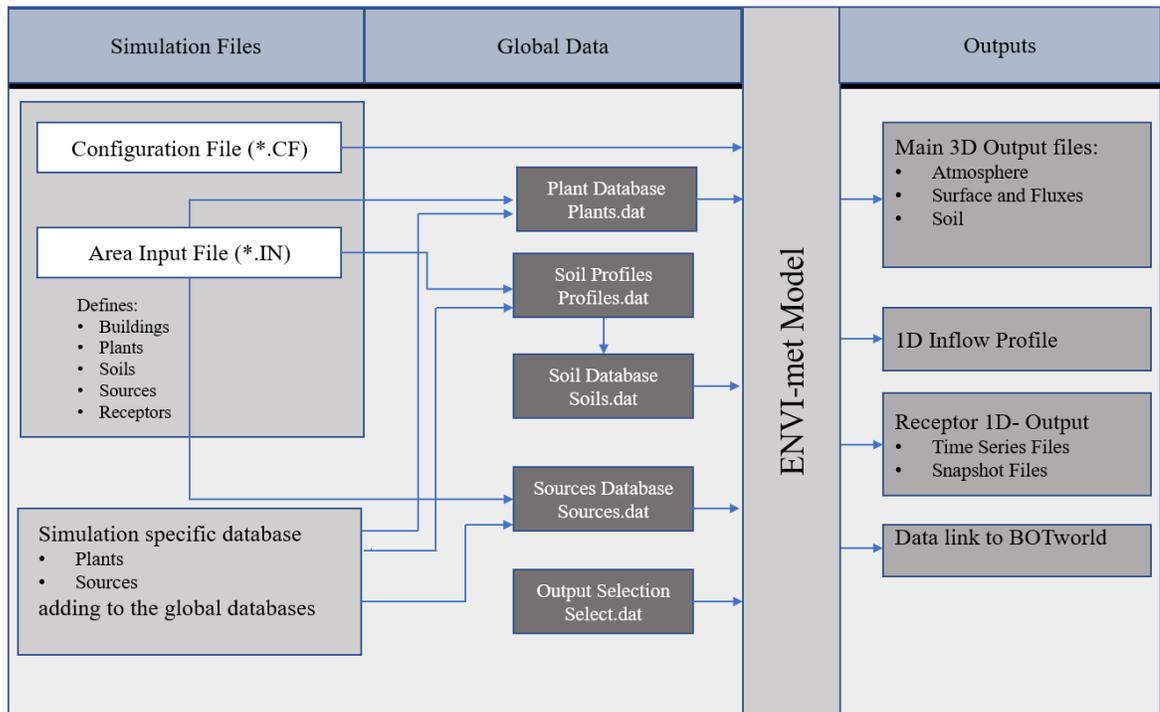
Figure 3-4. Flow diagram and basic data of ENVI-met (www.envi-met.com).

3.6. Reliability of ENVI-met Simulation Results

ENVI-met is the most frequently used software for outdoor microclimate simulation. The

reliability of ENVI-met software for simulating the thermal performance of outdoor spaces

has been frequently demonstrated (Lahme and Bruse, 2002; Johansson, 2005; Krüger et

al., 2011; Chow and Brazel, 2012; Ghaffarianhoseini et al., 2015; Ali-Toudert, 2005; Srivanit and Hokao, 2013). These studies indicated an acceptable agreement between measured values (from field observations or collected data at local meteorological stations) and ENVI-met simulated data patterns.

Lahme and Bruse (2002) compared the measured weather situation data of 25 stations in a park in Essen, Germany, with the results obtained from the ENVI-met model. The study pointed out that even for a non-calibrated model run, ENVI-met reproduces the observed data with sufficient accuracy. Furthermore, it proved that ENVI-met is a reliable tool to simulate the different urban scenarios (Lahme and Bruse, 2002). Yu and Hien (2006) assessed the cooling impacts of parks on their nearby built environment with the ENVI-met model. The agreement between results of simulated air temperature with the field measurements endorsed the reliability of ENVI-met software. Aydin et al. 2020, evaluated the accuracy of ENVI-met and three other urban microclimate tools (RayMan, SOLWEIG, and STEVE). The assessment was based on comparing the simulated results and measured data for a 6-week period in Singapore. They concluded that the accuracy prediction results for ENVI-met are in the acceptable range of error, and the ENVI-met software is the most comprehensive software from capabilities point of view. Ozkeresteci et al. (2003), after an investigation on the impact of urban parks on microclimate conditions in Arizona, concluded that ENVI-met can be successfully used as an integrated part of the city's information system to serve for sustainable environments.

However, ENVI-met has certain limitations and uncertainty in results. Crank et al. (2018) and Krayenhoff et al. (2021) note that microscale models do not account for local-scale advection or boundary- layer scale vertical mixing, and ENVI-met may have additional

41

limitations in terms of accuracy in simulating vertical mixing in the urban canopy layer. Also, Ali-Toudert and Mayer (2006) pointed out excessive nighttime temperature predictions of ENVI-met due to the absence of regional exchange processes. Krayenhoff et al. (2021) recently reviewed the urban heat mitigation modeling literature and their cooling effectiveness. This review shows that the cooling effectiveness values achieved with ENVI-met simulation for increasing the roof albedo, are lower than the lowest median cooling effectiveness of any mesoscale study. Tsoka et al. (2018), in a review article, assessed the ENVI-met model performance and accuracy of microclimate variables. Evaluation of the mean radiant temperature results of 15 studies showed that the model tends to overestimate daytime mean radiant temperature; however, the review concluded that the model can accurately simulate the daytime peak mean radiant temperature values.

Despite the software shortcoming, ENVI-met remains the most comprehensive tool that combines many factors involved in outdoor comfort. With proper input of the initial data and understanding the limitations, the software does represent the pattern of temperature indices in a complex urban environment (Rosheidat, 2014).

3.7. References:

Ali-Toudert, F., & Mayer, H. (2006). Numerical study on the effects of aspect ratio and orientation of an urban street canyon on outdoor thermal comfort in hot and dry climate. Building and environment, 41(2), 94-108.

Aydin, E., Jakubiec, J., & Jusuf, S.K. (2020). A Comparison Study of Simulation-Based Prediction Tools for Air Temperature and Outdoor Thermal Comfort in a Tropical Climate.

Bruse, M. (2004). ENVI-met 3.0: updated model overview. University of Bochum. Retrieved from: www. envi-met. com.

Bruse, M. ENVI-met http://www.envi-met.info/hg2e/doku.php?id=lbc-types (2015b).

Bruse, M., & Fleer, H. (1998). Simulating surface–plant–air interactions inside urban environments with a three dimensional numerical model. Environmental modelling & software, 13(3-4), 373-384.

Chow, W. T., & Brazel, A. J. (2012). Assessing xeriscaping as a sustainable heat island mitigation approach for a desert city. Building and Environment, 47, 170-181.

Conry, P., Sharma, A., Potosnak, M. J., Leo, L. S., Bensman, E., Hellmann, J. J., & Fernando, H. J. (2015). Chicago's heat island and climate change: Bridging the scales via dynamical downscaling. Journal of Applied Meteorology and Climatology, 54(7), 1430-1448.

Crank, P. J., Sailor, D. J., Ban-Weiss, G., & Taleghani, M. (2018). Evaluating the ENVI-met microscale model for suitability in analysis of targeted urban heat mitigation strategies. Urban climate, 26, 188-197.

Ghaffarianhoseini, A., Berardi, U., & Ghaffarianhoseini, A. (2015). Thermal performance characteristics of unshaded courtyards in hot and humid climates. Building and Environment, 87, 154-168.

Huttner, S. (2012). Further development and application of the 3D microclimate simulation ENVI-met (Doctoral dissertation, Universitätsbibliothek Mainz).

Huttner, S., & Bruse, M. (2009, June). Numerical modeling of the urban climate–a preview on ENVI-met 4.0. In 7th international conference on urban climate ICUC-7, Yokohama, Japan (Vol. 29).

Huttner, S., Bruse, M., & Dostal, P. (2008, October). Using ENVI-met to simulate the impact of global warming on the microclimate in central European cities. In 5th Japanese-German Meeting on Urban Climatology (Vol. 18, No. 18, pp. 307-312).

Johansson, E. (2006). Influence of urban geometry on outdoor thermal comfort in a hot dry climate: A study in Fez, Morocco. Building and environment, 41(10), 1326-1338.

Krayenhoff, E. S., & Voogt, J. A. (2007). A microscale three-dimensional urban energy balance model for studying surface temperatures. Boundary-Layer Meteorology, 123(3), 433-461.

Krayenhoff, E. S., Broadbent, A. M., Zhao, L., Georgescu, M., Middel, A., Voogt, J. A., ... & Erell, E. (2021). Cooling hot cities: A systematic and critical review of the numerical modelling literature. Environmental Research Letters.

Krüger, E. L., Minella, F. O., & Rasia, F. (2011). Impact of urban geometry on outdoor thermal comfort and air quality from field measurements in Curitiba, Brazil. Building and Environment, 46(3), 621-634.

Lahme, E., & Bruse, M. (2003). Microclimatic effects of a small urban park in densely built-up areas: measurements and model simulations. ICUC5, Lodz, 5(1).

Lindberg, F., Holmer, B., & Thorsson, S. (2008). SOLWEIG 1.0–Modelling spatial variations of 3D radiant fluxes and mean radiant temperature in complex urban settings. International journal of biometeorology, 52(7), 697-713.

Matzarakis, A., Rutz, F., & Mayer, H. (2007). Modelling radiation fluxes in simple and complex environments—application of the RayMan model. International journal of biometeorology, 51(4), 323-334.

Ozkeresteci, I., Crewe, K., Brazel, A. J., & Bruse, M. (2003, August). Use and evaluation of the ENVI-met model for environmental design and planning: an experiment on linear parks. In Proceedings of the 21st International Cartographic Conference (ICC), Durban, South Africa (pp. 10-16).

Rosheidat, A. (2014). Optimizing the effect of vegetation for pedestrian thermal comfort and urban heat Island mitigation in a hot arid urban environment. Arizona State University.

Simon, H. (2016). Modeling urban microclimate: development, implementation and evaluation of new and improved calculation methods for the urban microclimate model ENVI-met (Doctoral dissertation, Universitätsbibliothek Mainz).

Srivanit, M., & Hokao, K. (2013). Evaluating the cooling effects of greening for improving the outdoor thermal environment at an institutional campus in the summer. Building and environment, 66, 158-172.

Tsoka, S., Tsikaloudaki, A., & Theodosiou, T. (2018). Analyzing the ENVI-met microclimate model's performance and assessing cool materials and urban vegetation applications–A review. Sustainable cities and society, 43, 55-76.

Yu, C., & Hien, W. N. (2006). Thermal benefits of city parks. Energy and buildings, 38(2), 105-120.

Yamada, T., & Mellor, G. (1975). A simulation of the Wangara atmospheric boundary layer data. Journal of Atmospheric Sciences, 32(12), 2309-2329.

Chapter 4: Microclimate Simulation of the Urban Heat Mitigation Scenarios

4.1. Introduction:

The main objective of this study is to assess appropriate possible configurations to the existing urban setting and to evaluate the spatial thermal perception that pedestrian experiences in the outdoor spaces in downtown London, Ontario. First, the existing urban conditions of the site were evaluated and simulated with ENVI-met software. After that, the different heat mitigation strategies were designed and tested to find the most effective strategy. In order to evaluate the impacts of heat mitigation scenarios on other seasons, the heat mitigation strategies were applied for four-time scopes; current summer conditions, current winter conditions, future summer conditions and, future winter conditions. The evaluation of scenarios was carried out through simulation by ENVI-met. The list of scenarios that were tested with the software and compared with the current condition of the site include:

- "Base" scenario: The initial case study of downtown London. Figure 4-6 represents the 3D configuration simulated by ENVI-met.

- "Green" Scenarios: Vegetation coverage was increased on the site. Specifically, on the two parking lots, without any shading facility and capable of creating uncomfortable thermal conditions for pedestrians, an area similar to a park with trees and grass was designed.

- "Cool road" scenario: Asphalt roads are replaced with concrete pavement with higher surface albedo and lower heat capacity. The surface albedo in the cool pavement model is 0.5, which is 0.3 points higher than that of asphalt road.

4.2. Study Location

London is a city in southwestern Ontario, Canada, along the Quebec City–Windsor Corridor. London is located at 42.98° N, -81.24° E summers are warm and partly cloudy, and winters are freezing, dry, windy, and mostly cloudy. Over the course of the year, the temperature typically varies from -9 °C to 26 °C and is rarely below -18 °C or above 31 °C. Annual average relative humidity for afternoon is 64% and for morning is 85% (Environment Canada, 2020).
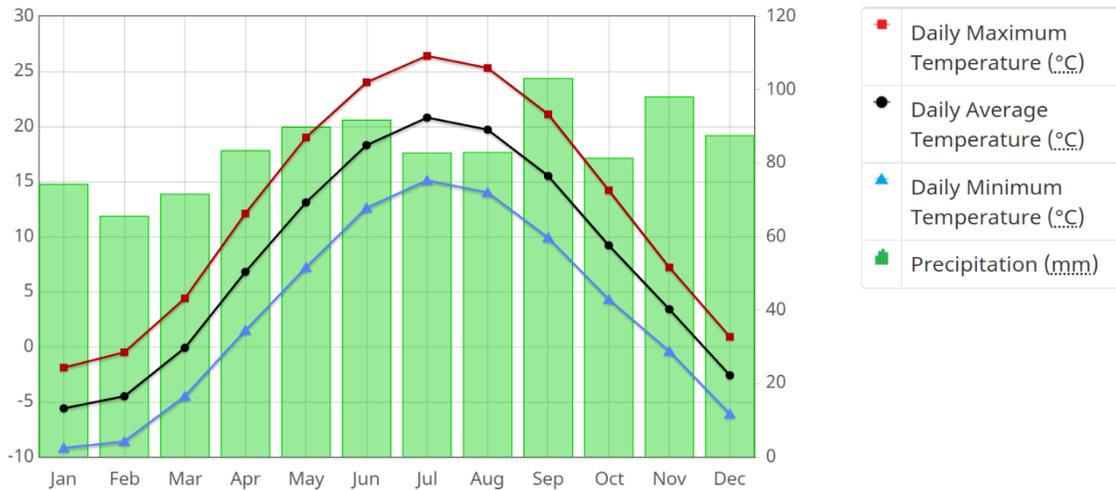
Figure 4-1. Temperature and Precipitation Graph for 1981 to 2010 Canadian Climate Normals at London International airport station (Environment & Climate Change Canada, 2021)

Figure 4-1 presents the London normalized temperature and precipitation graph for 1981 to 2010 for Canadian climate. *(Environment & Climate Change Canada, 2021).*

Figure 4-2. Location of London Ontario and inset
Google Earth satellite image of the city.
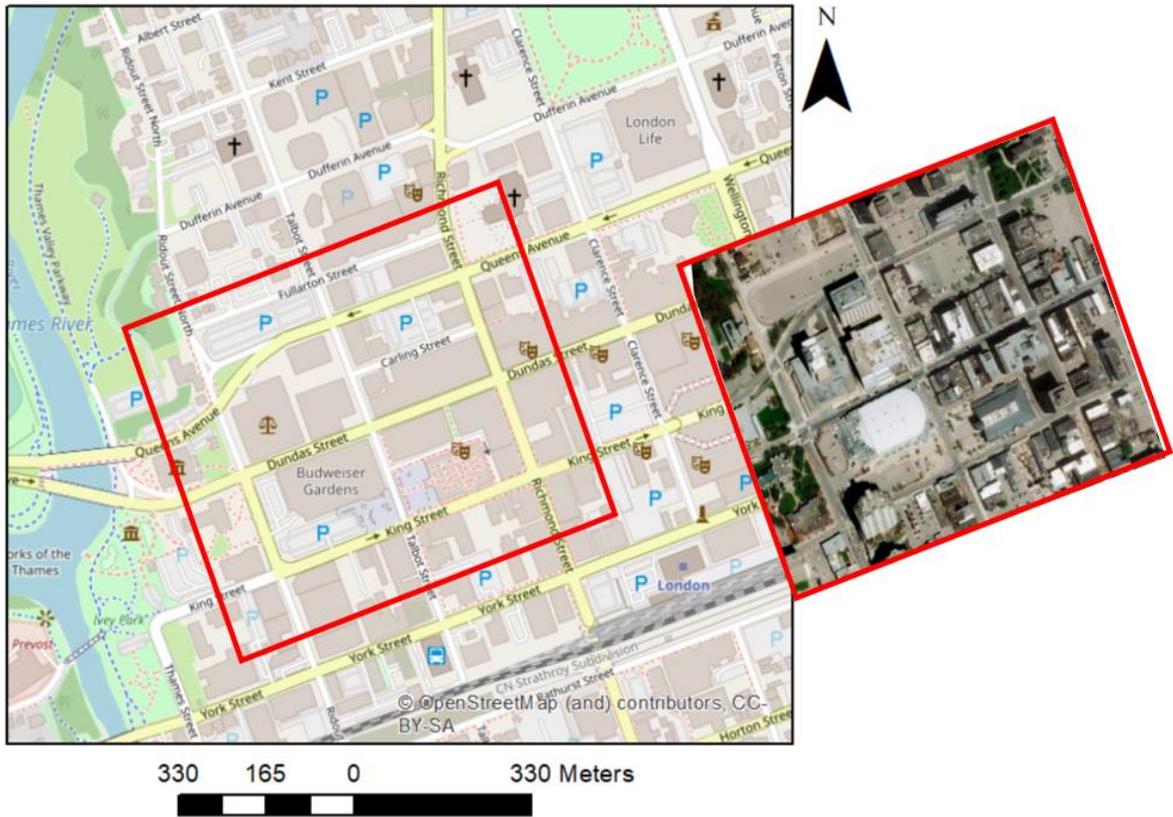
Figure 4-3. Map of study area with inset satellite visible image (Google Earth)
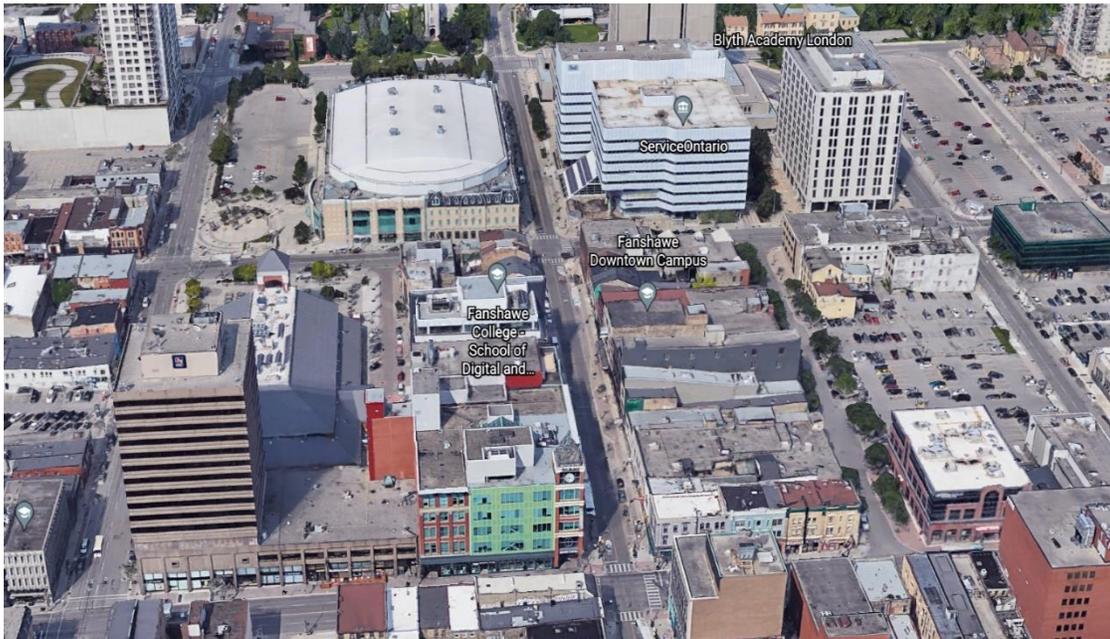
Figure 4-4. Oblique image of study area (Google Earth)

The present study area is located in a downtown neighbourhood of London, a high-density neighbourhood. High-rise residential communities are composed of densely built tall buildings and homing a large number of people; they have significant impacts on an urban climate and human health. A 500m×500m area constitutes the model domain (Figure 4-7a), which is characterized by densely placed high-rise buildings, parking lots. The local climate zone (LCZ) is a system for urban surface classification developed by Stewart and Oke (2012). According to this classification, the four climatically relevant controls on urban climates (fabric, land cover, structure, and metabolism) tend to cluster together in a city (Oke et al., 2017) (Figure4-5). Using this classification system, the study area is classified as a compact high-rise area with a dense mix of tall buildings, a mean height of greater than 25m, few trees, and most of the land cover is paved. Construction materials mainly include concrete, glass, brick, and tile (Stewart and Oke, 2012). The main streets are Dundas and Talbot street which respectively have a NE-SE and SE-NW directions. Secondary streets connected to the main streets are oriented similar to the main streets. The study area is dominated by impervious surfaces, with buildings covering 36.6%, pavements 43.4%, and roads 15% of the surface. Vegetation covers less than 5% of the area, where 2.7% and 2.3% are grass and trees, respectively.
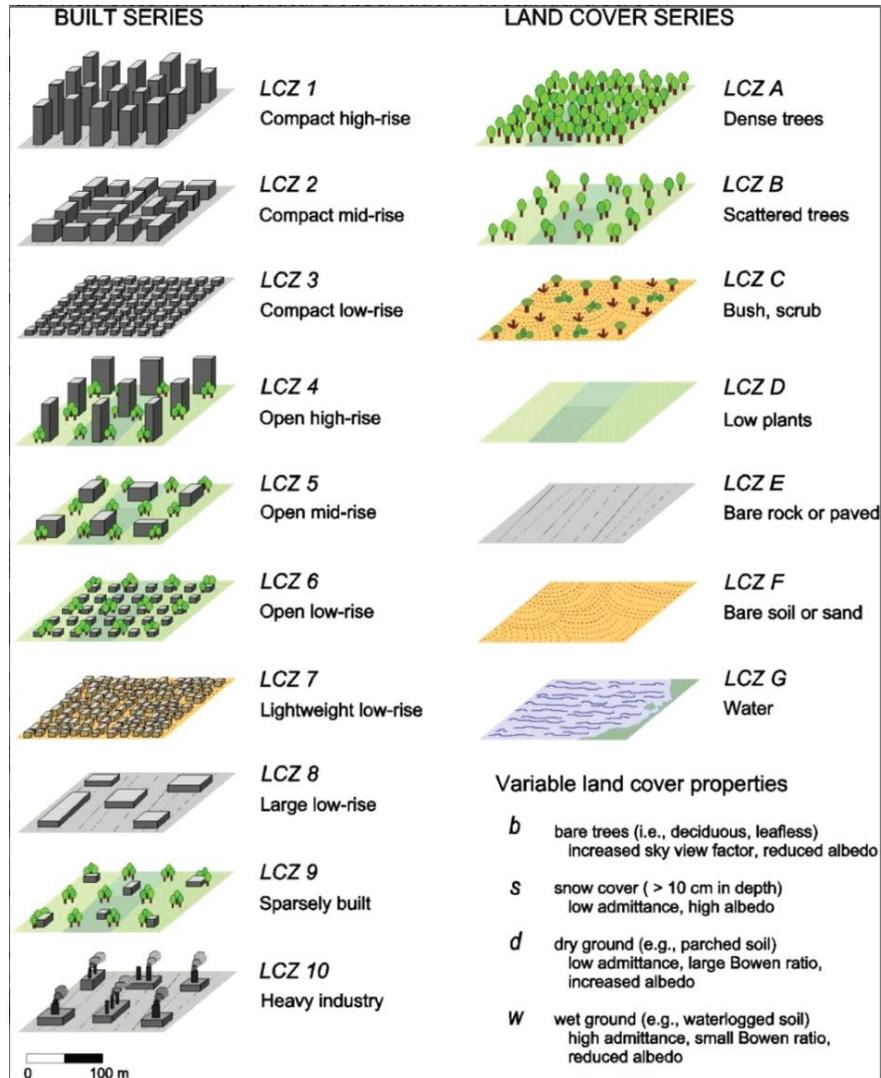
Figure 4-5. Classification of Local Climate Zones (LCZ) according to their perceived ability to modify local climate (Stewart and Oke, 2012; Oke et al., 2017; Stewart et al., 2014)

4.3. Modeling with ENVI-Met

ENVI-met model inputs include a vegetation database, physical soil structure, and profile information. A 3D area input file (*.in) representing the modeled arrangement of built structures, surface characteristics, and vegetation. A configuration file (*.cf) contains meteorological data to initialize the model parameters for the simulation date. The model required data include air and soil temperature, soil moisture, wind speed and direction, and relative humidity. In addition, ENVI-met calculates incoming solar radiation based on latitude/longitude, date, time, and cloud cover (Middel et al., 2014).

The model's user-selectable high spatial (0.5-10 m) and temporal (1-10 s) resolution make it useful for evaluating canopy-layer temperature and thermal comfort. The resolution can vary substantially over short distances and periods of time (Roth and Lim, 2017). The building layouts in the area input file (Figure 4-6) are based on a realistic design, and the GoogleEarth™ satellite image was used as a reference map while designing the study area.
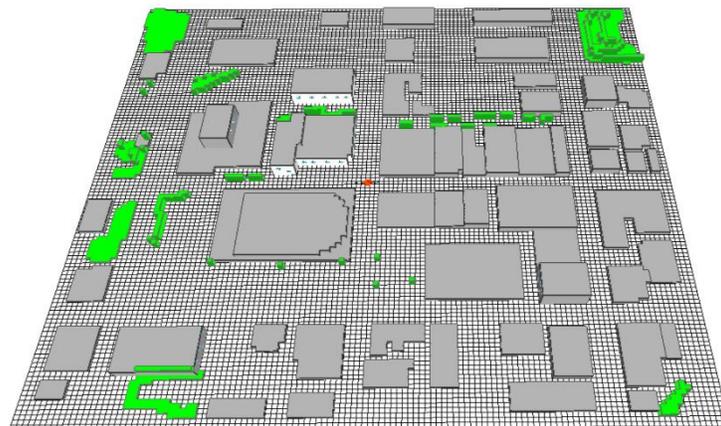
Figure 4-6. Perspective view of current condition of site
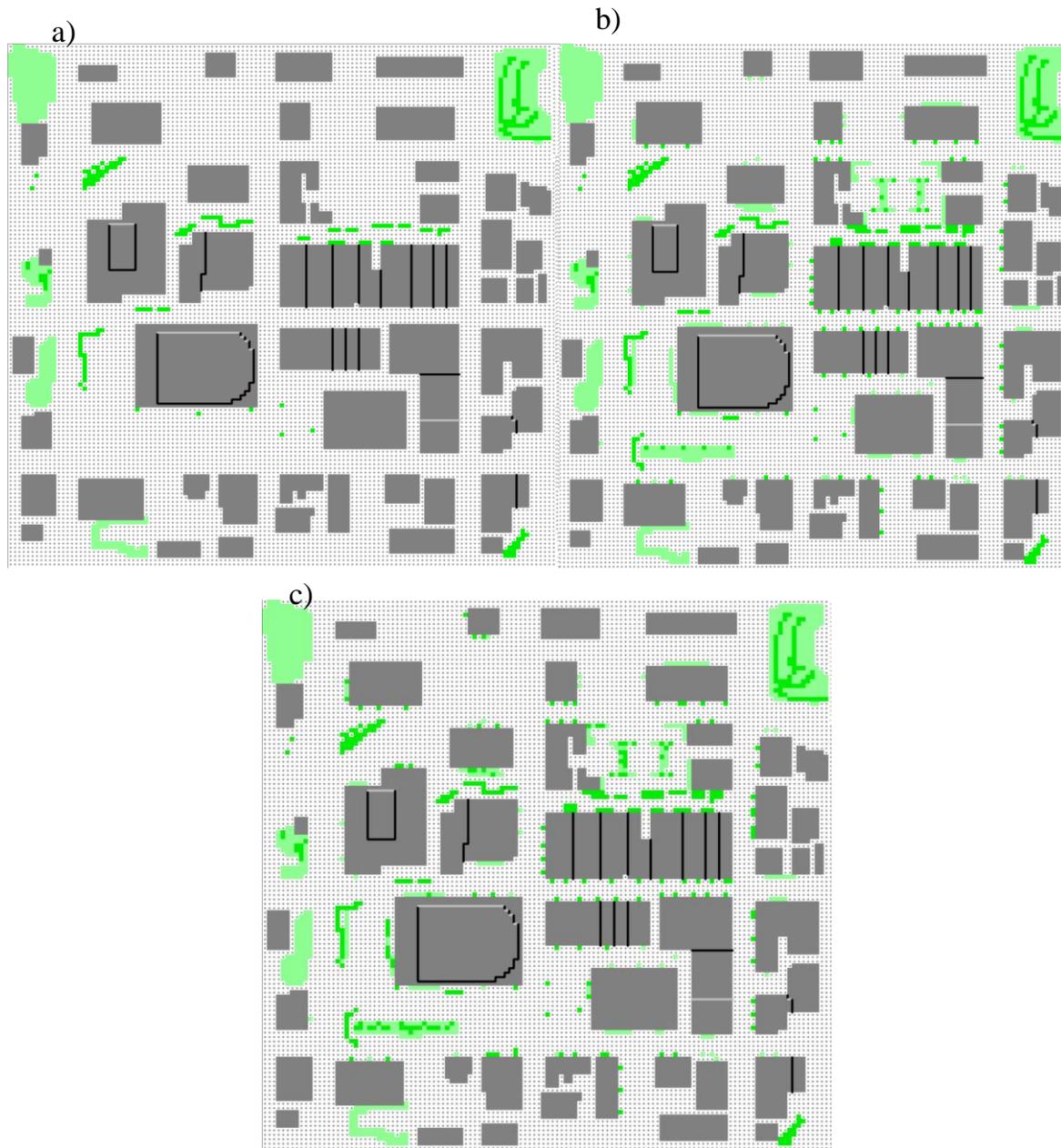
Figure 4-7. ENVI-Met 2D model screenshot a) "Base" scenario (current condition of the site), b) "Green1" scenario c) "Green2" scenario

The grid cell size for the model environment was defined as 4m×4m×3m (W x L x H) with a total of 125×125×45 cells, covering a horizontal area of 500m×500m extending 125m above the surface. The model is run for 24 hours starting at 3 am. The "Base" scenario was

modeled without any mitigation solutions applied. The natural ground was represented with loamy soil, and the street cover was represented with the asphalt road. Exact location of local vegetation, including trees and grass was modeled according to the "Trees" map from the City of London map database (City of London, 2020).

After modeling the current condition of the site, three additional mitigation scenarios were simulated. The impacts of scenarios were assessed for different time scopes to first, evaluate the most impactful mitigation solution on the site, and assess the impact of these solutions on other seasons and time scopes.

Three different building and vegetation layouts were designed according to three scenarios (Figure 4-7). Figure 4-7a illustrates the designed layout for the Base scenario. Figure 4-7b is the designed layout for the Green1 scenario with a 10% increase in vegetation fraction and mostly grass and low-height vegetation. Finally, Figure 4-7c presents the designed layout for the Green2 scenario with a 10% increase in greenery and mostly taller trees and vegetation.

Base scenario Representing the current condition of the site. Table 4-1 presents the plan area cover types for Base scenario. The values determined according to the site's current condition and for the horizontal area in the plan.

Table 4-1. Plan area cover type details for the "Base" scenario

Coverage (%)	Building	Pavements	Roads	Vegetation	
				Trees	Grass
Base Scenario	36.6	43.4	15	2.7	2.3

Green scenarios include increasing the vegetation (trees and grass) coverage on the site. In order to compare the different combinations of trees and grass, two proposed models for the site are simulated. Table 4-2 shows the plan area vegetation coverage in the "Green" Scenarios and "Base" scenario. The detailed parameters of vegetation types designed with Albero tools of ENVI-met and added to the Green scenarios models are presented in Table 4-3.

Table 4-2. Plan area vegetation coverage in the "Green" Scenarios and "Base" scenario

Coverage (%)	Trees	Grass	Total
Green1	6.1	8.9	15
Green2	10.7	5.3	16
Base	2.7	2.3	5

Table 4-3.Detailed parameters for vegetation in "Green" Scenarios (Albero tools of ENVI-met)

	Heigh(m)	Width(m)	Leaf Area Density (m^2/m^3)	Root Depth(m)
Grass	0.63	0.05	0.3	0.5
Dense Hedge	2	1	2.5	1
Tree 1	5	3	0.7	3
Tree 2	15	11	0.95	5

Cool scenario: the solar reflectance of road materials was increased. In the "Cool" scenario asphalt roads are replaced with concrete pavement; The concrete pavement albedo is 0.5, which is 0.3 points higher than asphalt pavement albedo. Table 4-4 presents the pavement characteristics for the "Cool" and "Base" Scenarios.

Table 4-4.Pavement characteristics for "Cool" Scenario and "Base" Scenario

	Surface albedo	**Thickness(m)**
Base model	0.2	0.3
Cool model	0.5	0.3

4.3.1 Forcing file:

The weather data used to initiate the simulation models were provided by Environment and Climate Change Canada, from historical data recorded at London International Airport station. A full forcing file is created with the ENVI-met forcing manager. Further required inputs to prepare a forcing file are direct and diffuse shortwave radiation and longwave radiation. Direct and diffuse radiation for 24 June 2016 forcing file is achieved from the measured global radiation data of green roof lab on top of Talbot College, Western University. Diffuse and direct radiation for the other simulation days is calculated with the Bird and Hulstrom model that calculates the direct and diffuse radiation on a clear sky (Bird and Hulstrom, 1981). The longwave radiation that is used for the forcing files is

calculated with the Prata model, a formula for estimating the longwave radiation from clear sky (Prata, 1996).

In selecting the simulation days for summer conditions, two parameters were considered:

Days were selected with clear sky condition only; ENVI-met cannot account for dynamic changes in cloud cover and rainfall. Furthermore, the impact of altered surface conditions is maximized under clear sky conditions. And days were chosen among the 10% of the days with the highest average temperature in the season.

A similar procedure was applied for selecting the future summer forcing file. Future weather data for simulation were prepared from the climatedata.ca datasets, a collaboration between Environment and Climate Change Canada (ECCC), the Computer Research Institute of Montréal (CRIM), Ouranos, the Pacific Climate Impacts Consortium (PCIC), the Prairie Climate Centre (PCC), and HabitatSeven. In this dataset, the daily minimum and maximum temperatures are obtained from the ensemble of global climate models for three RCPs (2.6, 4.5, and 8.5). The values for each climate model were re-gridded to a common 1° x 1° grid. Available projection weather data based on the RCP8.5 scenario for a grid point closest to London was employed to collect the future forcing file. Maximum and minimum temperatures for future forcing files selected and averaged among a window of three years 2048, 2049, ad 2050. Two other forcing files for current and future winter conditions were created to assess the impact of mitigation scenarios on the local microclimate in different seasons. Overall, 13 simulations were carried out with ENVI-met to evaluate the microclimate condition of the base scenario and mitigation scenarios during the simulation days.

Table 4-5. List of simulation dates and summary of forcing files data

Date	Max T (°C)	Min T (°C)	Max Wind speed(m/s)	Min wind speed(m/s)	Relative humidity (%)
24/06/2016	27.7	12.4	3.44	0	50
08/06/2049	31.12	24.8	3.36	0	62
03/03/2018	3.4	-4.7	5.25	2.7	70
05/02/2049	10	3	4.02	2	65

4.4. Results:

The following sections describe the most significant calculated parameters for the base scenario and heat mitigation scenarios. Furthermore, the cooling effectiveness of heat mitigation scenarios is presented in the last section. The simulation results were extracted at pedestrian height, 1m and 1.5m above ground. The outputs were analyzed in terms of air temperature (° C), relative humidity (%), wind speed (m/s), and mean radiant temperature (°C). Regarding temporal variation of microclimatic conditions, plots were created based on the average values of all grid cells inside the domains except the building. The hourly average air temperatures during the simulation period were prepared for the entire domain and two sub-domains. Sub-domains locations and characteristics are presented in Figure 4-

8 and Table 4-6. Furthermore, the values that correspond to the grid cells of the edge of the study area, which show very low values, were not considered for the calculation. Discarded values are those from the first five rows of grid cells of all edges, equal to the first 20m of each side of the site.

Table 4-6.Characteristics of sub-domains selected for hourly average air temperature profile.

Location	Characteristics
Carling Street	Low-rise and dense urban area, a parking lot is located on the north side of the street.
Dundas Street	Medium-rise and dense urban area, densely frequented
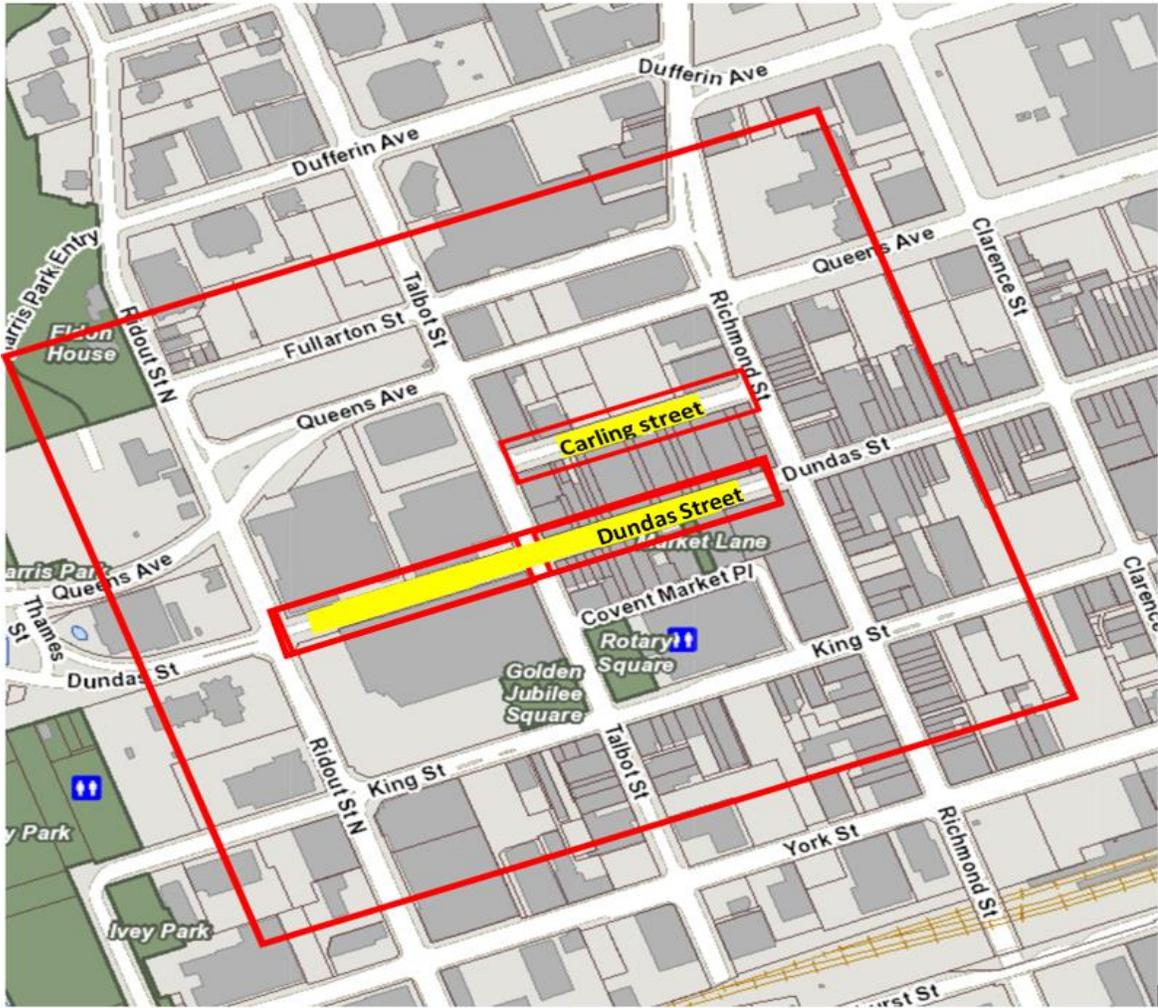
Figure 4-8. Location of selected sub-domains for hourly average air temperature profile-Map from the London City Map gallery (City of London.ca)

4.4.1. Microclimate Simulations of the Reference Scenario:

This section presents the results of 24h microclimate simulations of the base scenario, without application of any mitigation strategy, for current years summer and winter, and 2050, future.

Figure 4-9 is visualized with Leonardo tools of ENVI-met software. Figures 4-9,10, and 11 represent the air temperature distribution map of the "base" scenario at 1.5m above ground and on 24 June 2016. The maps are provided for 2h, 14h, and 17h warmest hour of the day. Air temperature distribution at 17h (Figure 4-11) shows that the hottest zones correspond to less dense areas without vegetation. The maximum temperature is 31.33 °C, while the minimum temperature is 27.6 °C at this time and is reported in densely vegetated areas. The warm air plumes generated by the east-west streets are influenced by the easterly wind direction at this time. According to the air temperature distribution of other simulated dates (Figure 4-14,15,16,17) it appears that these plumes of warm air exist in those locations during the day and is originated from the geometry of the area. The area corresponding to these plums are parking lots, large flat areas without any obstacle to block the wind or create shading in these sections. Furthermore, the shaded areas with buildings and close to vegetation have a lower temperature at this time.

Figure 4-12 shows the distribution of other microclimate parameters; wind speed and direction, relative humidity, and mean radiant temperature at 17h (when the air temperature is highest during the day). At 17h, relative humidity ranges between 36 % to 54%. According to the relative humidity distribution map, warmer areas have lower relative humidity, while the colder areas and near vegetation have higher relative humidity values.

The mean radiant temperature ranges between 52°C to 58°C. Areas of vegetation and with greater shading provide zones of lower mean radiant temperature and more thermal comfort climates. While areas that solar radiation directly reaches the ground have higher mean radian temperature. The northwest of the site corresponding to Victoria Park and Carling Street with trees in two rows, have the lowest mean radiant temperature and have

more comfortable thermal climates. At the same time, the wind speed differs from 0 m/s to

2.3 m/s. Urban geometry has a great influence on wind distribution; near obstacles and in

narrow areas, the wind velocity is low, whereas open spaces have greater wind velocity

(Ambrosini et al., 2014). Figure 4-12 shows the wind speed values calculated at 17h and

illustrates the wind direction at this time. Flat areas, parking spaces without barriers to

block wind speed have the highest wind speed value of 2.1m/s.
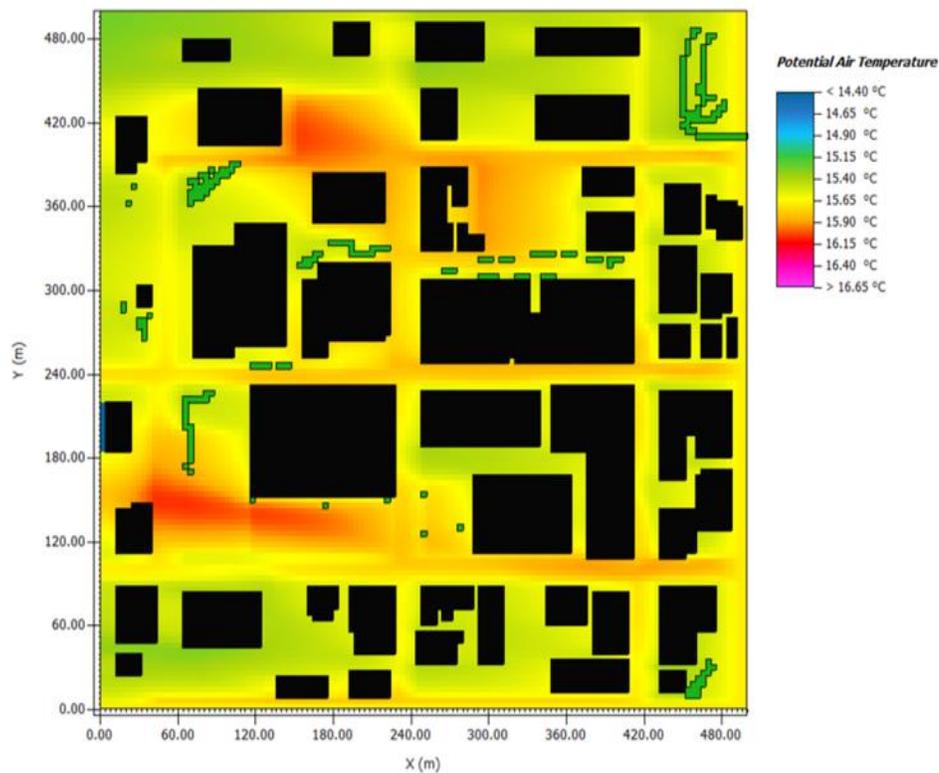
Figure 4-9. Summer air temperature map and distribution - 24 June 2016- 2h
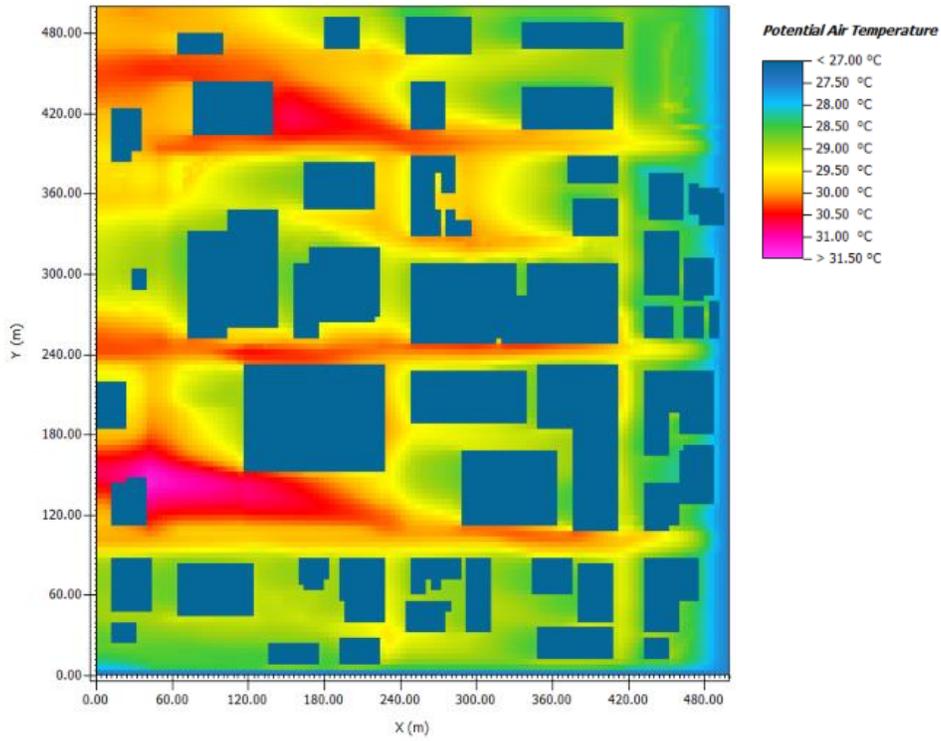
Figure 4-10. Summer air temperature map and distribution - 24 June 2016- 17h
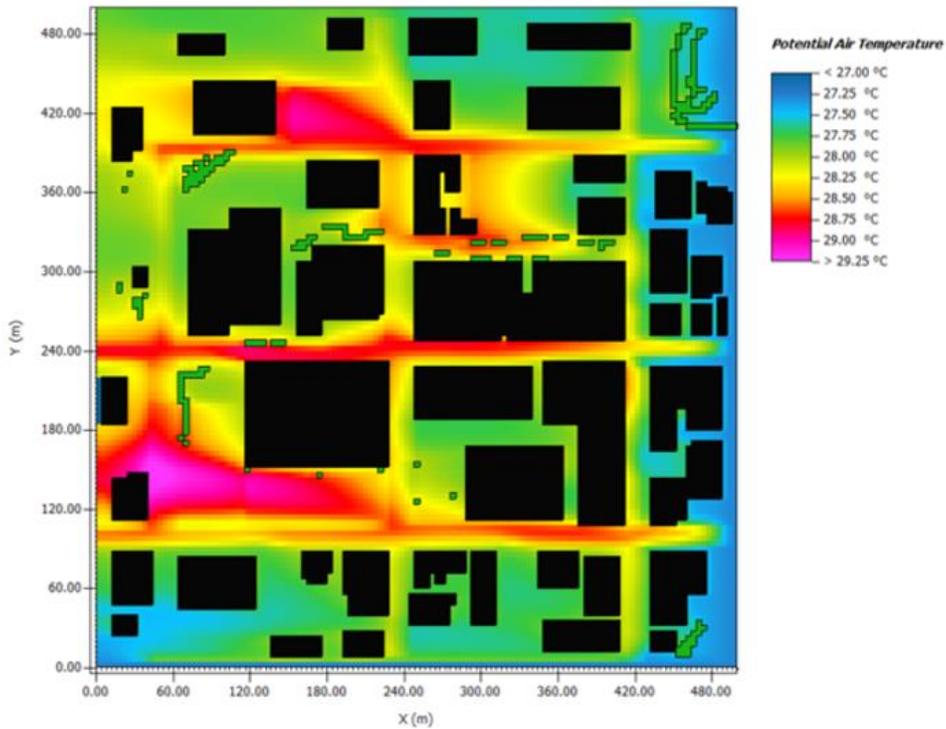
Figure 4-11. Summer air temperature map and distribution - 24 June 2016- 14h

Wind speed (m/s) and Wind Direction – 17h

Mean radiant temperature (°C) – 17h

Relative Humidity (%) – 17h
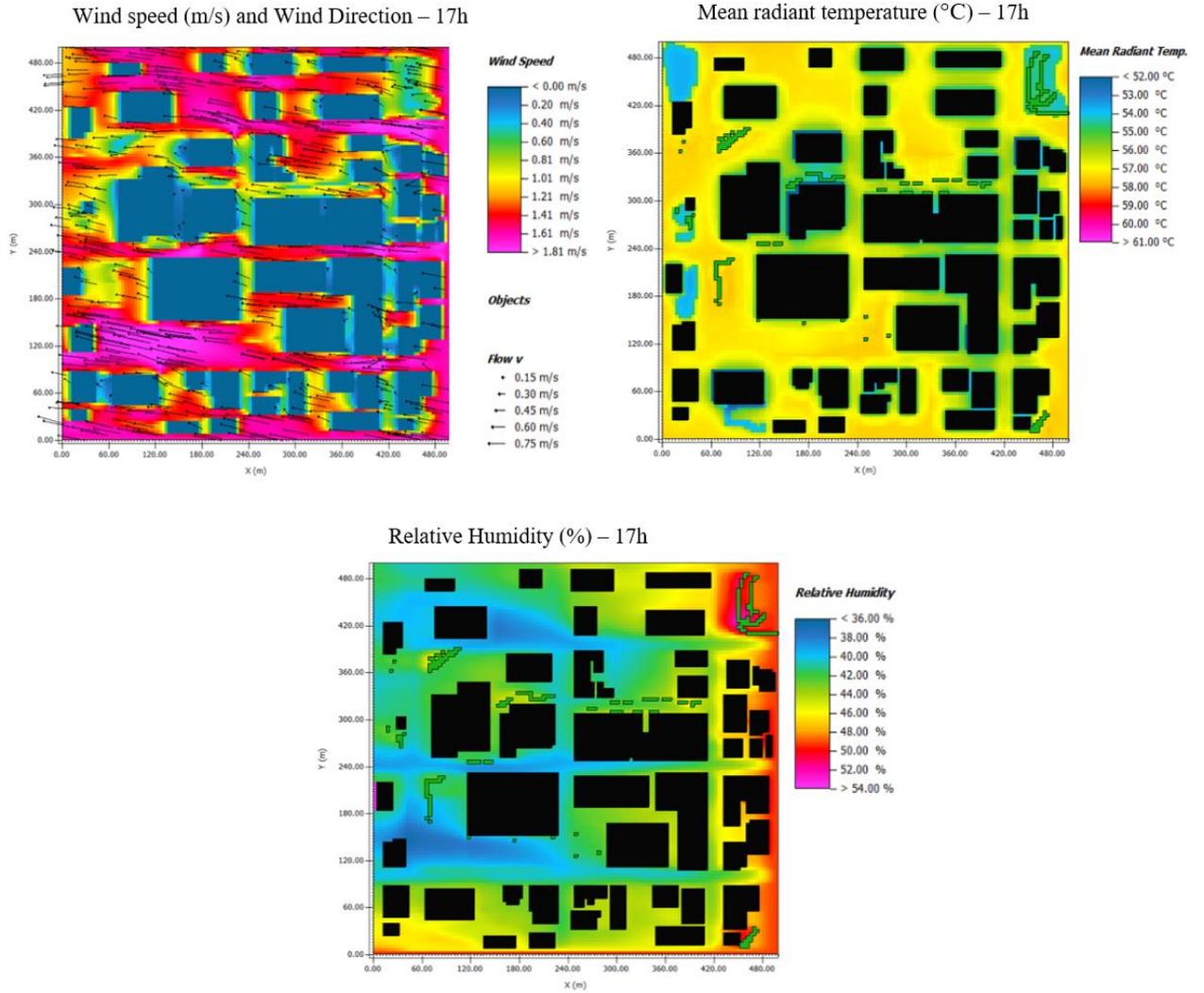
Figure 4-12. Spatial distribution of mean radiant temperature, wind speed , wind direction and relative humidity at 17h-Base Scenario- 24 June 2016

To better understand the temporal variation of simulated temperature by the software, the outdoor average air temperature at different areas of the site was calculated (Figure 4-13). The outdoor average air temperature ranges between 11.5°C and 30.1 °C. The average air temperature at Dundas street is higher than Carling street and the entire domain. This difference varies from 0.1°C to 0.5°C at 17h, the warmest hour of the day. This is likely driven by the difference in greenery coverage percentage of both domains; the Carling Street domain is inherently vegetated with trees in two rows.
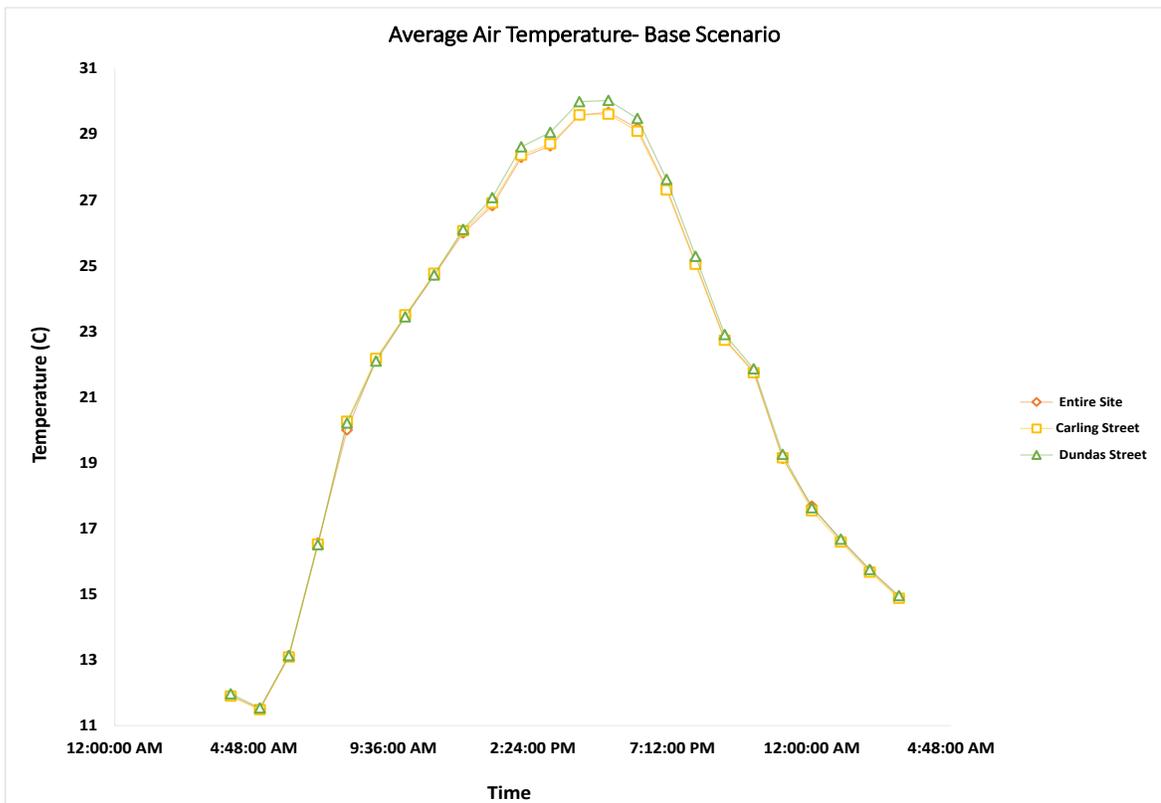
Figure 4-13. Air temperature variation plots, for entire site, Carling Street and Dundas Street- at 1 m above ground-Base scenario on 24 June 2016
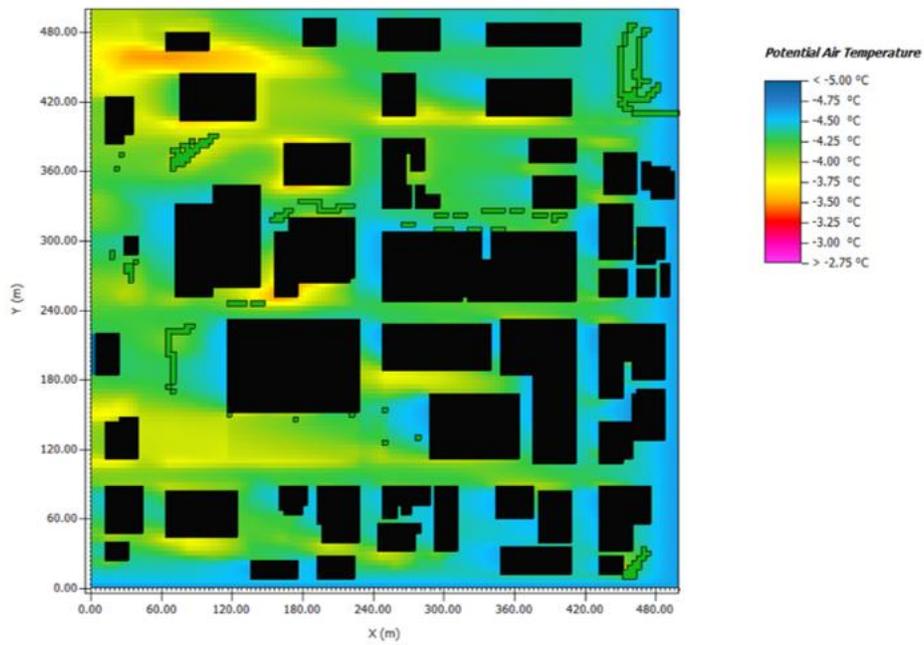
Figure 4-15. Winter air temperature map at 1.5m above ground- 3 March 2018- 2h
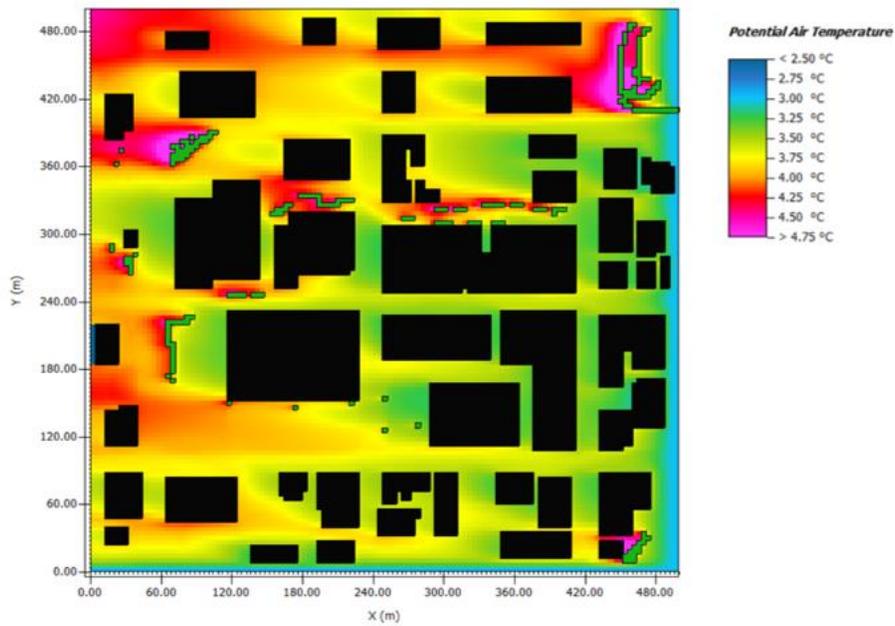
Figure 4-14. Winter air temperature map at 1.5m above ground- 3 March 2018- 14h
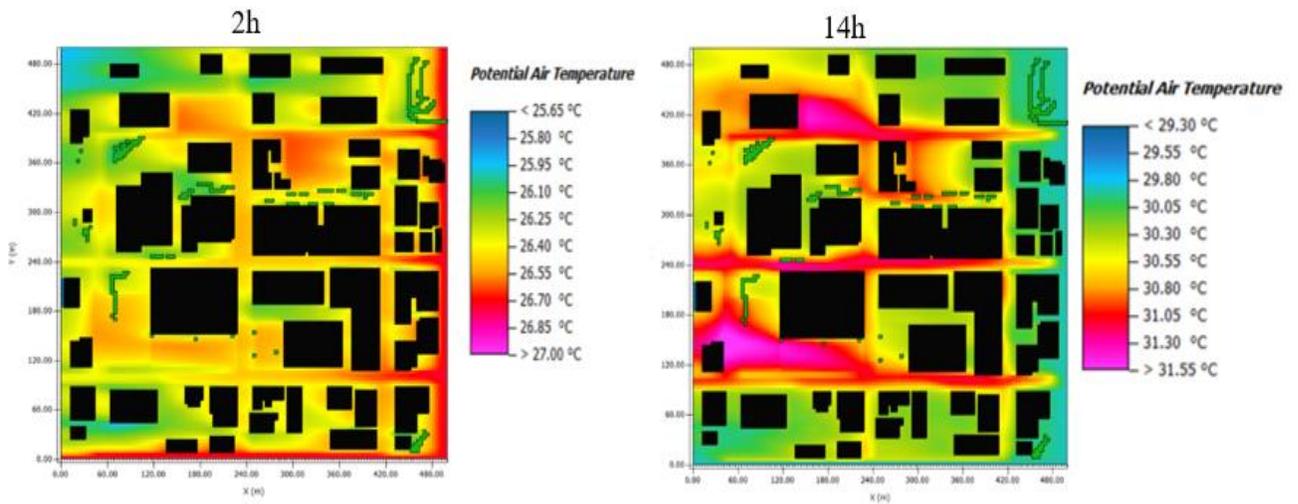
Figure 4-16. Future summer air temperature map and distribution at 2h and 14h- 8 June 2050
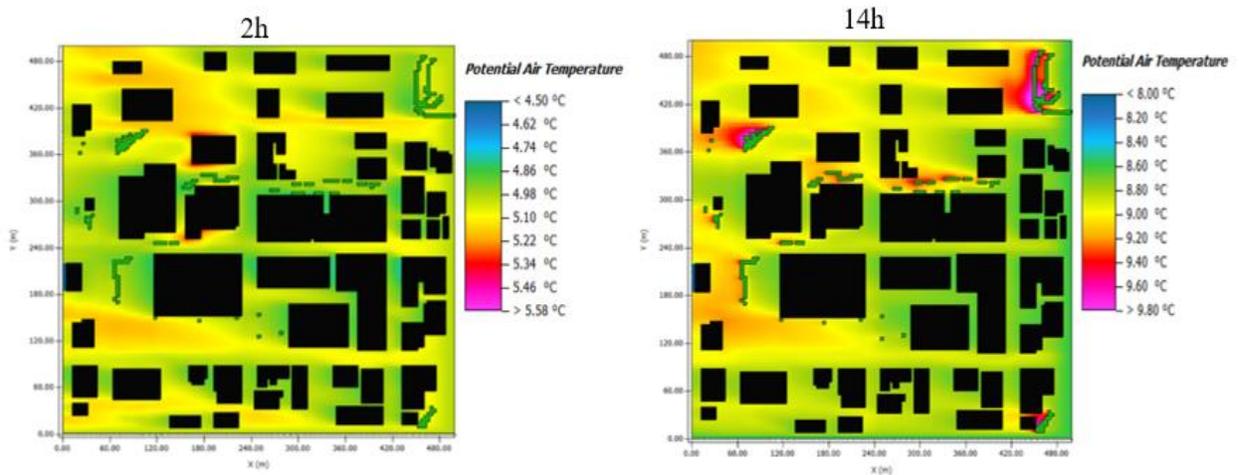
Figure 4-17. Future winter air temperature map and distribution at at 2h and 14h- 6 February 2049

Figures 4-14 and 4-15 show the spatial distribution of air temperature at 2h and 14h in winter condition on 3 March 2018.

Figures 4-16, 4-17 represent the spatial distribution of air temperature at 2h and 14h in future weather conditions, summer, and winter. For the future summer condition, the maximum air temperature is detected at 33.5°C and a minimum of 30°C during the site at 14h in Figure 4-16. The maximum air temperature at 14h for the future winter condition is 10 °C, and the minimum is 8.4 °C at the same time. Zones with vegetation coverages have higher air temperatures in winter, providing a more comfortable thermal condition for the pedestrian.

In conclusion, microclimate simulations for the future and current summer conditions indicate that the zones with higher air temperature during the day correspond to the area with low vegetation coverage, low building plan area (low shading), and areas paved with asphalt. For instance, the high air temperature values at the southwest part of the site are related to the parking space characterized by paved areas and without shading facilities. Furthermore, Microclimate simulations for winter conditions reveal that the higher mean radiant temperature that improves thermal comfort corresponds to the area near the vegetation. The simulation results of "Base" scenario guide the choice of how to construct the mitigation scenarios. Mitigation scenarios are concentrated in areas with high potential outdoor thermal discomfort and consist of, adding vegetation coverage, increasing shading, and increasing the albedo of pavement for these areas.

4.4.2. Microclimate simulation of mitigation scenarios

The following section presents the results of 24 hours microclimate simulations of the different mitigation scenarios in summer and winter conditions. There are several heat mitigation strategies; increasing tree and vegetative coverage, installing green roofs, using cool pavements (high albedo material) and, installing cool roofs. In this study, according to the geometry of the site and a high percentage of pavement coverage, two heat mitigation strategies, increasing the green coverage of the study area and applying high albedo material, are evaluated. We first describe the impact of increasing vegetation on the outdoor air temperature and then present the result of increasing the albedo of road material in the site under study.

4.4.2.1. Green scenario (increasing vegetation):

This section presents and evaluates the impact of adding trees and increasing vegetation coverage on the average air temperature. Two different green scenarios were simulated. As mentioned in Table 4-2, in both green scenarios, the vegetation increased 10%; the "Green1" model focused on increasing grass and green areas, while the "Green2" model was concentrated on increasing trees in the study area.

 The reduction impact is assessed for three domains, the entire site, Carling Street and Dundas Street. The intention of assessing the mitigation impact on the Carling and Dundas Street domain is that there is a parking lot on one side of each street. According to the results of the previous section, under the current conditions of the site, the highest outdoor

air temperature corresponds to parking spaces and paved areas without vegetation. These parking spaces are partially replaced with a designed park, grass, trees, and soil by applying the green scenario. The results of Dundas street domain show the impact of increasing vegetation on the medium-rise neighborhood. Moreover, Carling street domain results show the microclimate impact of trees on the average air temperature in a dense low-rise neighborhood. Figures 4-18, 4-19, 4-20 show the variation of hourly average air temperature on a summer day by increasing the vegetation coverage for the entire site, Carling Street and Dundas Street. The maximum reduction is observed for the entire site at 17h with a value of 0.36°C for the "Green1" model and 0.56°C at 16h for the "Green2" model.
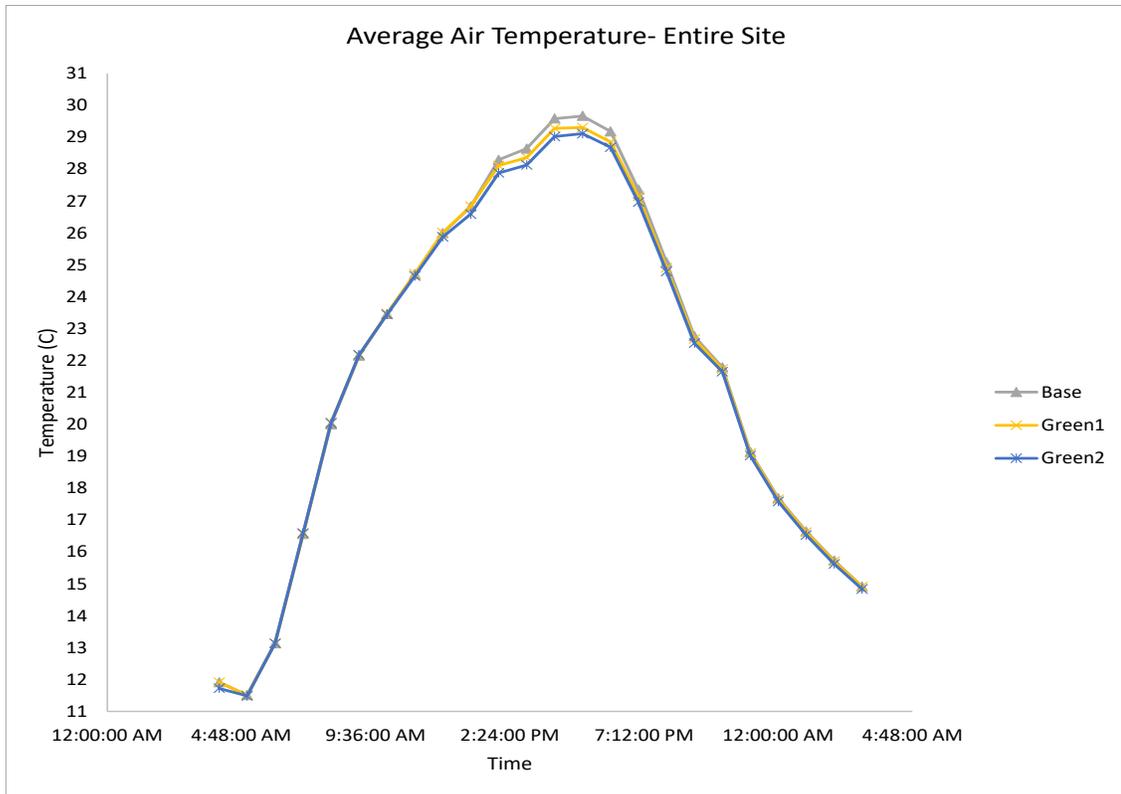
Figure 4-18. Average air temperature for the entire domain at 1 m above ground, Base scenario,"
Green1" and "Green2" scenarios- 24 June 2016
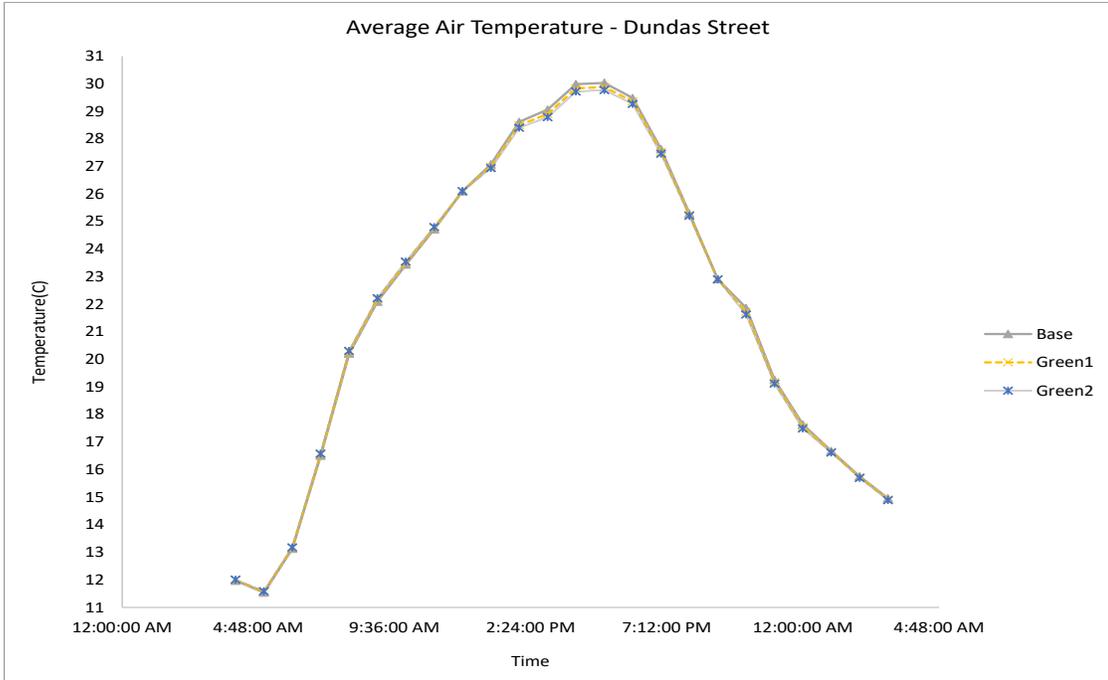
Figure 4-19. Average air temperature for the Dundas Street domain at 1 m above ground, Base scenario," Green1" and "Green2" scenarios- 24 June 2016
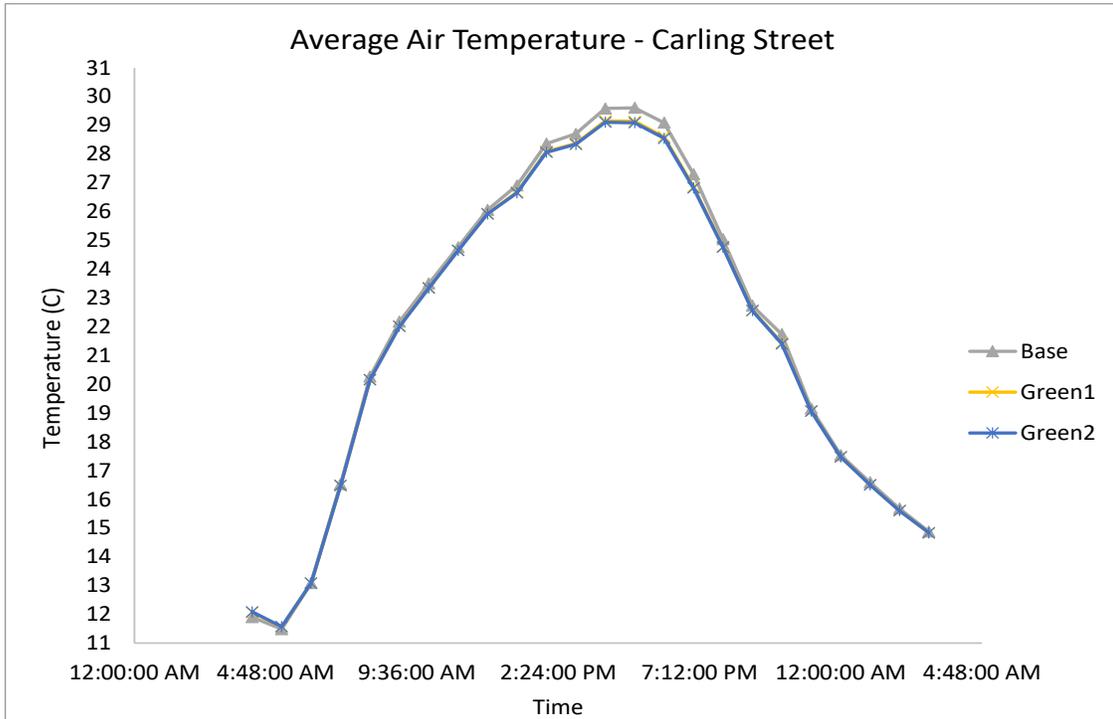
Figure 4-20. Average air temperature for the Carling Street domain at 1 m above ground, Base scenario," Green1" and "Green2" scenarios- 24 June 2016
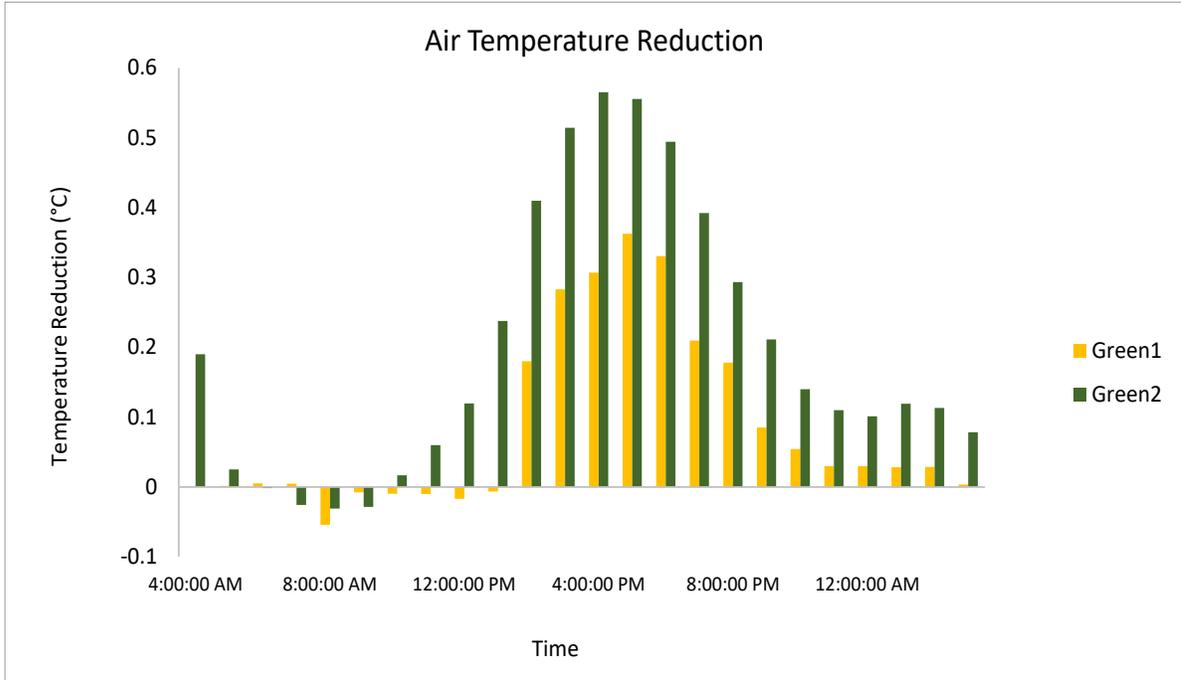
Figure 4-21. The average hourly air temperature reduction (°C) of two green scenarios for Entire site– 24 June 2016

Carling Street's maximum air temperature reduction at 17h is 0.47°c and 0.51°c, respectively, for the "Green1" and "Green2" models. For Dundas Street, the reduction for "Green1" and "Green2" is 0.15°C and 0.27°C at 16h. The difference in air temperature reduction between Carling Street and Dundas Street is due to the fact that Carling Street is inherently vegetated with two rows of trees. Moreover, the area is more compact in comparison to Dundas Street and therefor provides more shading.

In overall, the observed reduction that with the "Green2" model is higher than the reduction achieved with the "Green1" scenario in the daytime. While the vegetation fraction in the two models is similar, "Green2", with more trees, provides larger shaded zones. Figure 4-21 presents the averaged air temperature reduction in the two "Green" scenarios.

By applying the green scenario similar reduction trends in air temperature are detected for future summer, 8 June 2050.
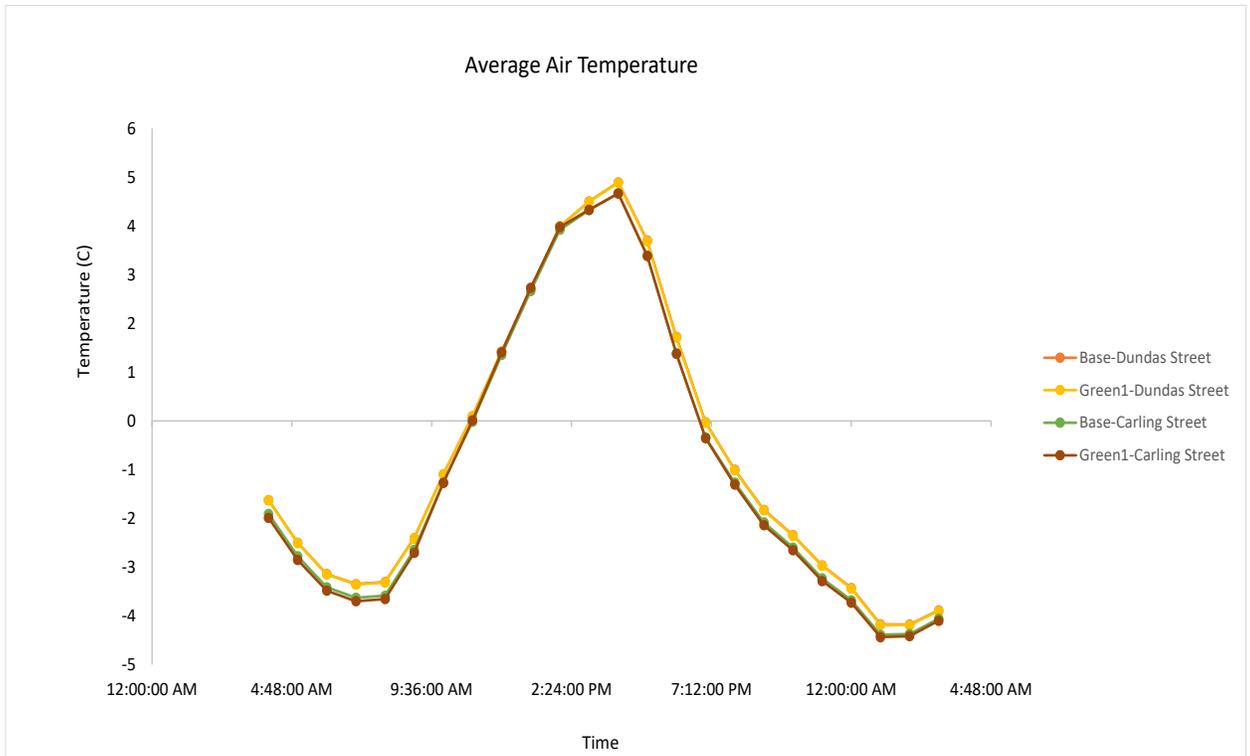
Figure 4-22. Hourly average air temperature of "Base" and "Green1" scenario for winter conditions- 8 March 2018- Carling Street domain and Dundas Street domain- 1 m above ground

Figure 4-22 shows the average air temperature results of the "Green1" scenario simulation for winter conditions. In winter, a globally lower effect is detected in terms of air temperature variation. The "Green1" scenario shows the air temperature ranges for Carling Street and Dundas Street are respectively -3.70°C to 4.66°C and -2.35°C to 4.88°C.

The average air temperature plots for Carling and Dundas Street domains show a negligible reduction during the simulation day. There is a maximum 0.05°C reduction detected for Carling Street, while Dundas Street values remain without any reduction.

4.4.2.2. Cool Road scenario:

The mitigation effect of the "Cool road" scenario is reported in this section. In the "Cool road" scenario, the albedo of road material was increased. Therefore, more shortwave radiation was reflected, and less heat could be stored in the ground surface of the cool pavement model (Wang et al., 2016). Figure 4-23 shows the spatial distribution of air temperature at 17h and 1 m above ground level for summer conditions. The air temperature curves at the left side of the plot correspond to all the

points from a transect along Talbot Street (x = 238 for y = 0 - 500). The maximum air temperature reduction detected is 1.57°C at 17h.
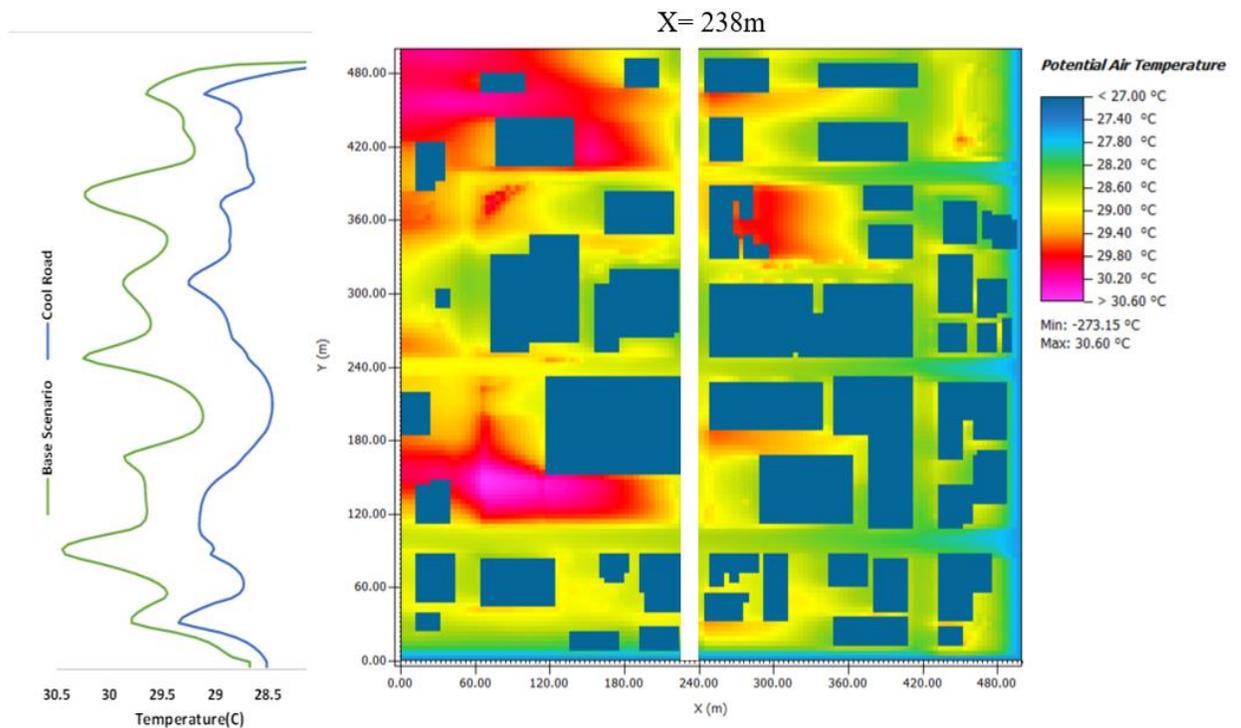
Figure 4-23. Air temperature distribution, at 17h 24 June 2016, 1 m above ground

White line = transect along Talbot Street
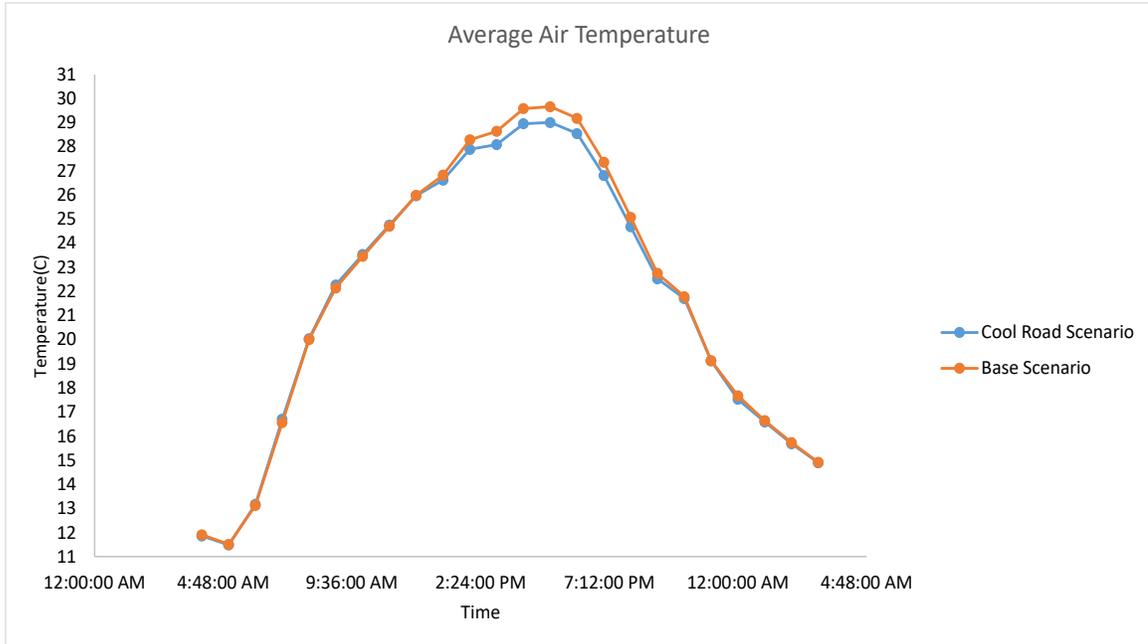
Figure 4-24. Hourly average air temperature of "Base" and "Cool road" scenario for summer condition- 24 June 2016- 1 m above ground

Figure 4-24 presents the comparison of hourly average air temperature of "Base" and "Cool road" scenarios for summer conditions. It can be seen that the application of cool materials with the higher albedo values generates a cooling effect during the day over the entire site. Increasing the albedo of road material by 0.3 points contributed to air temperature reduction of 0.66°C at 17h, the warmest hour of the day. During the night time "Cool road" scenario contributes to a negligible reduction of air temperature, as it could be expected.
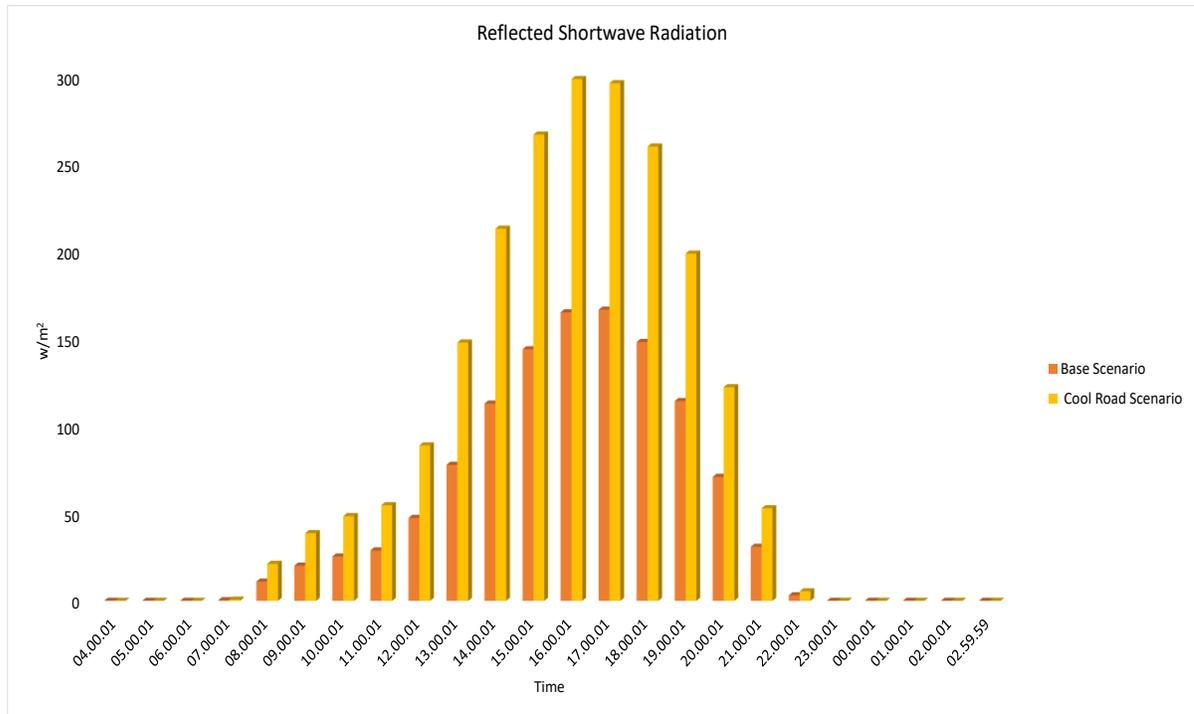
Figure 4-25. Hourly reflected shortwave radiation of "Base" and "Cool road" scenario for summer condition- 24 June 2016- 1 m above ground

The achieved temperature cooling potential in "Cool road" scenario is attributed to the significantly higher amounts of reflected solar radiation and the consequent lower absorption by high albedo material (tsoka et al., 2018). Increasing the road albedo material resulted an increase in the reflected shortwave radiation by 45% (133 w m-2), compared to the "Base" scenario (Figure 4-25).

4.4.3. Thermal comfort evaluation of mitigation scenarios:

After the analysis of the local microclimate in the "Base" model and mitigation scenarios "Green1", "Green2" and "Cool road," a thermal comfort analysis was carried out to investigate the outdoor environmental quality for pedestrians. The predicted mean vote (PMV) and mean radiant temperature (MRT) indexes were calculated for all the assessed configurations in summer conditions. PMV predicts the mean value of the votes given by

a large group of people exposed to the same thermal environment (Salata et al., 2016). Figure 4-27 shows the spatial distribution of PMV values at 17h for the four models. According to the PMV maps, the thermal condition of the site at 17h is classified as "Hot". Increasing the albedo of pavement materials causes a slight reduction in PMV values for road areas. Furthermore, the Green2 scenario, that creates more shading, was able to reduce PMV values for larger areas compared to the Green1 scenario. Figure 2-2 summarizes PMV values for different levels of thermal sensation and physiological stress in standard conditions. The following assumption was considered for calculation of PMV with ENVI-met; 35 years old man, 1.75m tall, weighing 75 kg, total metabolism of 164.49 W, and with a clothing resistance of 0.5 clo (thermal insulation of clothing).
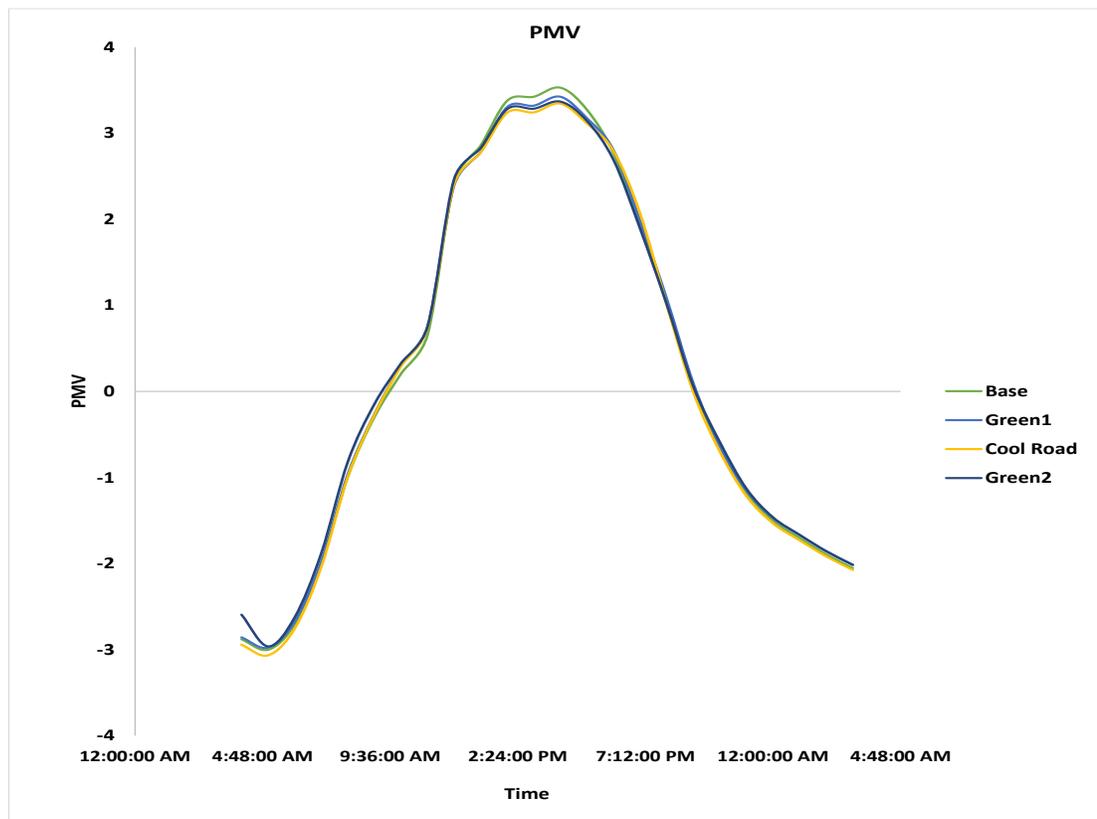
Figure 4-26. Hourly predicted mean vote values for the "Base", "Green1", "Green2" and, "Cool road" scenarios - 24 June2016 at 1.5 m above ground

According to the hourly PMV plots (Figure 4-26), the minimum PMV for all models occurred at 6h and the maximum PMV for all scenarios is detected at 17h. PMV values for all the mitigation scenarios are lower than the "Base" scenario. Green1 and Green2 had close PMV values, however, Green2 shows a higher reduction in PMV values.
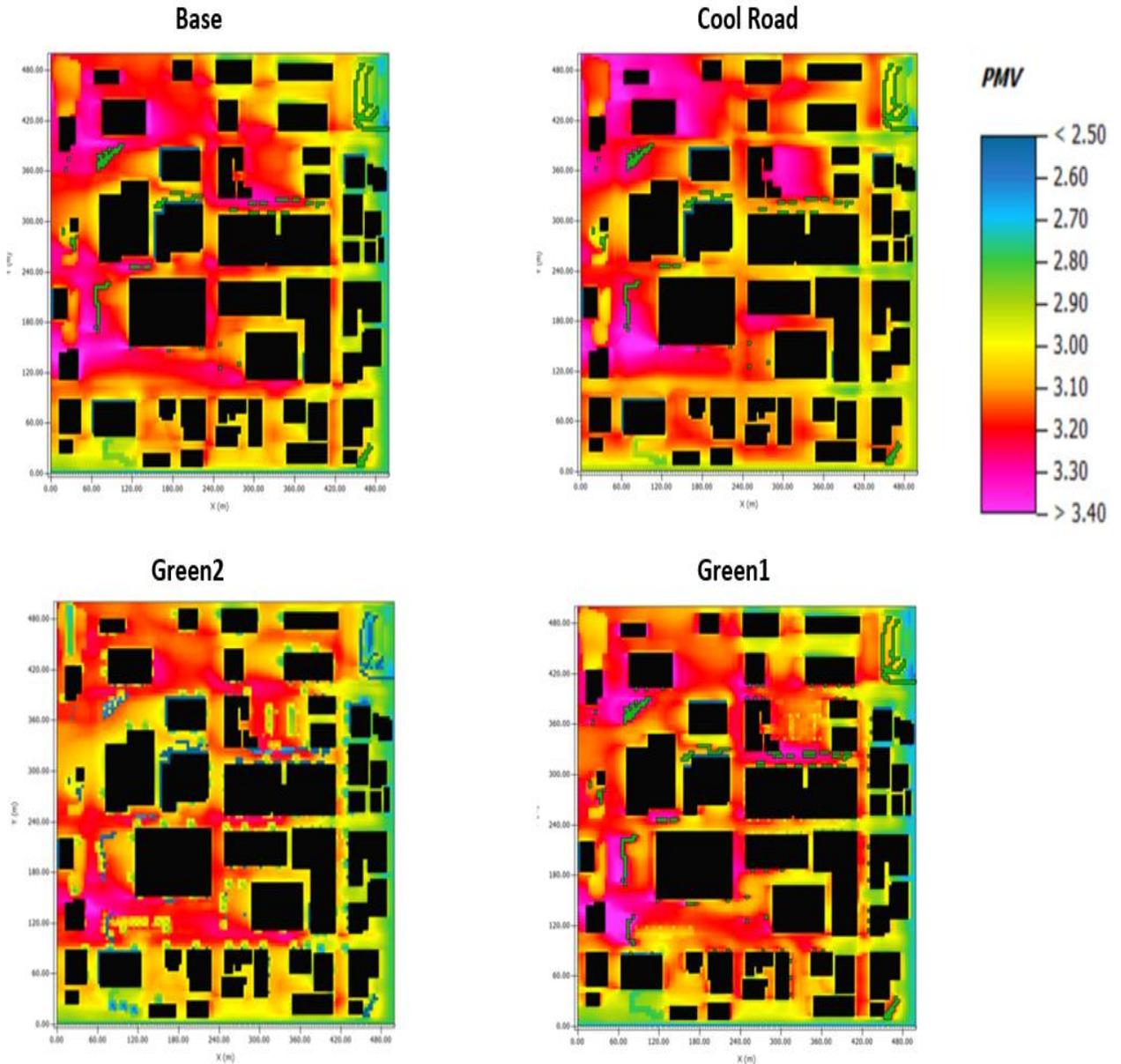
Figure 4-27. PMV distribution maps of "Base", "Green1", "Green2" and, "Cool road" scenarios on 24 June 2016, 1.5 m above ground at 17h
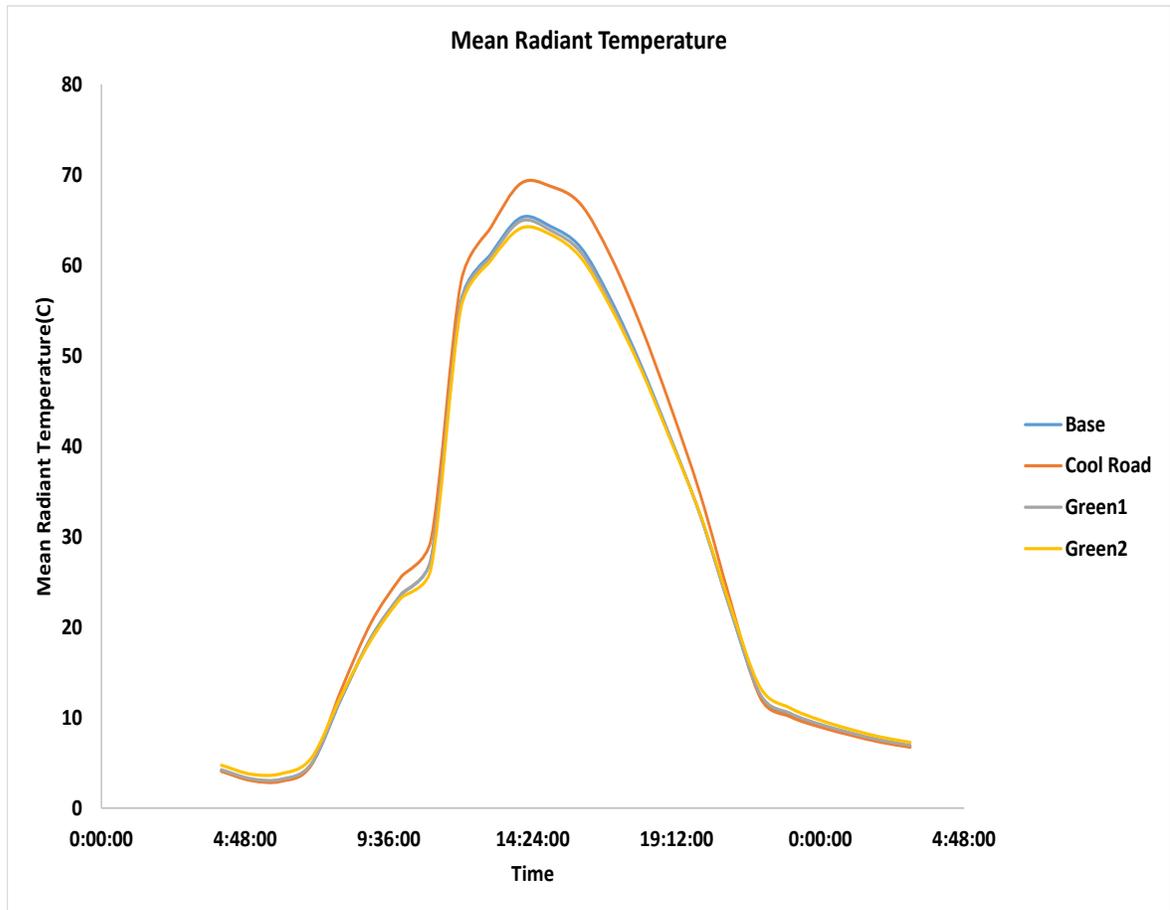
Figure 4-28. Hourly mean radiant temperature values for the "Base", "Green1", "Green2" and, "Cool road" scenarios - 24 June2016 at 1.5 m above ground

Green2 scenario has the maximum mean radiant temperature reduction. This scenario was based on increasing the number of trees in the study area; the trees elevated the canopy layer and providing shade during the hottest part of the day. Consequently, by reducing the solar radiation access, the pedestrian thermal comfort would improve, and the mean radiant temperature reduces.

The MRT values related to the "Cool road" scenario are higher than the base case (Figure 4-28). The results of the outdoor thermal comfort show that the higher albedo of road material increases the mean radiant temperature. This increase of MRT may enhance heat stress despite the air temperature reduction (Taleghani et al., 2016; Karakounos et al., 2018).

4.4.4. Cooling effectiveness of heat mitigation strategies:

This section describes the cooling effectiveness of heat mitigation strategies assessed in this study. Krayenhoff et al. 2021, in an article on heat reduction strategies in cities, reviewed 146 studies that applied numerical modeling to assess air temperature reduction. For comparison purposes among studies, they introduced two metrics; the albedo cooling effectiveness (ACE) and the vegetation cooling effectiveness (VCE) (Krayenhoff et al., 2021).

The authors defined cooling effectiveness (CE) as:

$$CE = -\frac{\Delta T}{\Delta a} \qquad (4\text{-}1)$$

In the cooling effectiveness (CE) equation, T is air temperature, and a is a plan area-averaged non-dimensional variable that quantifies the principal change associated with the heat mitigation implementation. Following this definition, albedo cooling effectiveness (ACE) is defined as

$$ACE = -\frac{\Delta T}{\Delta \alpha_s . \lambda_s} \qquad (4\text{-}2)$$

where $\Delta\alpha_s$ represents the change in albedo of the modified surface, and λ_s is the modified surface area divided by the overall horizontal plan area. Albedo cooling effectiveness shows the cooling achieved from a neighborhood albedo increase, and it assumes temperature responses to albedo changes are linear (Krayenhoff et al., 2021). The vegetative cooling effectiveness is defined as

$$VCE = -\frac{\Delta T}{\lambda_s} \tag{4-3}$$

where λ_s is the added surface area of vegetation divided by the associated plan area.

The cooling effectiveness (CE) metrics for heat mitigation scenarios are calculated under summer conditions. Figure 4-29 represents the calculated ACE and VCE for the simulated scenarios; ACE values represent the cooling achieved from a 0.3 increase in road material albedo ("Cool road" scenario) and VCE values represent the cooling obtained by a 10% increase in the vegetated area of the entire domain (green scenario).

Cooling effectiveness values were calculated for 12 hours, from 9h to 20h. ACE values range between 0.16°C to 5.03°C, with mean value of 2.73°C. The maximum value is obtained at 17h and corresponds to maximum air temperature reduction. VCE values for the "Green1" scenario vary from 0°C to 3.6°C, with a mean of 1.58°C. Likewise, the cooling effectiveness of "Green2" ranges from 0°C to 5.6°C with a mean of 3°C.
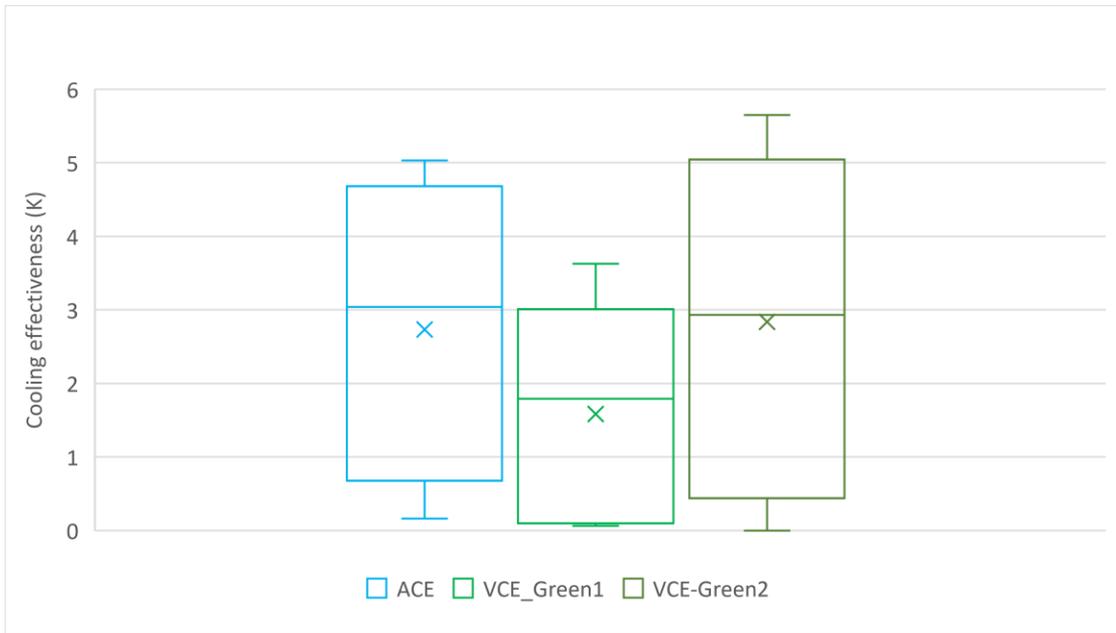
Figure 4-29. Albedo Cooling Effectiveness (ACE) of "Cool road' scenario and Vegetation Cooling Effectiveness (VCE) of green scenarios, on 24 June 2016, from 9h to 20h

4.5. Discussion and Conclusion

Previous studies had indicated the impact of increasing green area and high albedo materials on outdoor thermal climate. However, the impacts of these heat mitigation strategies generally have been assessed in cities with hot and dry climates; few studies investigated the impacts of these strategies on cold climates. This study evaluated the outdoor thermal climate of a domain in downtown London, Ontario. The impact of increasing vegetation on the site and increasing the albedo of road material on microclimate conditions of the site, for present summer and winter and future summer and winter was assessed.

ENVI-met v4.4.5 software was used for simulating the study area. The software has many abilities and advantages, namely, it allows to simulate the ground plane and building materials thermal properties, the ability to simulate vegetations, trees/ plants with specification of all plants physical parameters (evaporation, transpiration). However, despite these advantages, the software has limitations. The accuracy of ENVI-met outputs highly relies on the input parameters. The anthropogenic heat, the heat related to transportation and building heating/cooling, is not taken into consideration in ENVI-met (Ohashi et al., 2007; Tsoka et al., 2018).

The analysis of the results of this study has indicated that increasing trees and grassland in a neighborhood in downtown London can reduce the average air temperature. The average air temperature was reduced by 0.36 °C with the "Green1" scenario and 0.56 °C with the "Green2" scenario, at the warmest hour of the day in summer conditions. These results correlate to those found in other studies (Middel et al.,2015; Wang et al., 2016; Ziaul and Pal, 2020; Lee et al., 2016; Morakinyo et al., 2018; Morakinyo et al., 2020). For instance,

in Phoenix, Arizona, increasing the tree coverage from 10% to 25% resulted in a 2°C air temperature reduction at the local scale in summer (Middel et al., 2015), while in Toronto, the air temperature was found to be reduced by 0.6 °C at 16h after adding 10% of urban vegetation coverage in a middle-rise area (Wang et al., 2016). The air temperature reductions obtained from these studies are slightly larger in comparison to the "Green1" scenario, and this might be due to the existence of two parking spaces and lower building density in the present study. The reason is that in parking spaces the geometry is more open; given the high amount of impervious surfaces, the solar radiation heating these surfaces, and air temperature is becoming higher, especially by day. In a neighbourhood where buildings are taller, there would be more ground-level shade that could reduce the warming, through the first part of the day. "Green2" scenario with more trees compensates the lack of shaded zones in the study area and led to a more comfortable thermal condition. Similar results were detected for the green scenario on future summer conditions. However, the air temperature difference between the "Base" and green scenarios in winter was insignificant.

The results of increasing the albedo of road material, the "Cool road" scenario, indicated an average air temperature reduction up to 0.66 °C at 17h and 1 m above ground. A transect along Talbot Street in the study domain indicated a decrease of air temperature of up to 1.57°C at 17h and 1m above the ground (Figure 4-23). Similar air temperature reductions were found for the "Cool road" scenario for future summer conditions. The effect of increasing the albedo of road material is not significant at night in comparison to daytime. Taleghani et al. (2016) have simulated the impact of increasing the albedo of road materials by 0.3 in Los Angeles with ENVI-met software. Their results showed up to 2°C air

temperature reduction under hot summer conditions (Taleghani et al., 2016). Wang et al. assessed the impact of replacing road materials with higher albedo material by 0.2 and 21% lower heat capacity on the different neighborhoods in Toronto. Results indicated 7.9 °C reduction in surface ground temperature and up to 0.4 °C air temperature reduction at noon for summer conditions (Wang et al., 2016). Results of the present study are similar to the latter assessment, and it might be because of the similar climate conditions of Toronto and London city.

Further results indicated the impact of the mitigation scenarios on pedestrian thermal comfort. Results of the "Cool road" scenario were shown to increase the mean radiant temperature during the daytime by up to 6°C at a height of 1 m above ground. This increase corresponds to the impact of high albedo material on the radiative balance of the ground surface and, consequently, the radiative exchange of the pedestrian with the surrounding environment will change (Tsoka et al., 2020). These results are comparable to those found in other studies (Taleghani and Berardi, 2018; Wang et al., 2016). For example, the results of Taleghani and Berardi study on increasing the pavement albedo by 0.3 in downtown Toronto resulted in a 10.53°C increase in mean radiant temperature at 1m height. Furthermore, in the present study, increasing the vegetation and grasslands ("Green1" scenario) reduced the mean radiant temperature at daytime by 0.52°C at 17h. The obtained mean radiant temperature reduction from the "Green1" is lower than the similar studies on the impact of urban vegetation on thermal comfort (Wang et al., 2016; Morakinyo et al., 2018). This lower reduction in mean radiant temperature compared to the mentioned studies corresponds to the lower building density and the fact that grasslands and low height vegetations provide low shading in the present study. The influence of increasing

vegetation on the mean radiant temperature varies between shaded areas and open areas (Yang and Lin, 2016). The highest mean radiant temperature reduction is achieved with the "Green2" scenario, because trees with shading reduce the solar irradiance in the daytime.

In a systematic review of previous works, Krayenhoff et al. (2021) defined new metrics to assess the cooling effectiveness of different heat mitigation scenarios. These metrics are practical tools for city planners and policymakers. We applied these metrics to evaluate the cooling effectiveness of the simulated heat mitigation scenarios in the present study. For the present study, by increasing the albedo from 0.2 to 0.5, the ACE values in simulation date range between a minimum of 0.94°C to a maximum of 5°C over the period of 9h to 20h. The median ACE value is 3.02°C, generating 0.90°C cooling per 0.3 neighborhood-scale albedo increase. The VCE for the Green1 scenario shows that by increasing 10% vegetation coverage and mostly ground-level vegetation, the mean cooling on the simulation date (summer) varies from 0°C to 3°C and with a median of 1.75°C with 10% increase in ground-level vegetation. At the same time, the median VCE value of the Green2 scenario on the simulation date is 3.45°C with 10% increase in tree canopy cover. These results are compatible with the calculated ACE and VCE value of other studies with ENVI-met in the Krayenhoff et al. article. For example, a median VCE of 3.3 °C was yielded for a summer afternoon for studies that evaluated the application of street-level trees with ENVI-met. The article reported that for a ground-level albedo variation, studied with ENVI-met, there is a large variation between studies, but an ACE of approximately 5.7 °C was derived during a summer afternoon.

Chapter 4 has assessed the ENVI-met modeling results for a neighbourhood in downtown London with respect to microclimate conditions, especially air temperature and thermal comfort, including MRT and PMV. Urban microclimate and large scale climate change also impact building energy demand, and heat mitigation scenarios modulate this demand. Assessment of building energy demand is considered next in Chapter 5.

4.6. References

Ambrosini, D., Galli, G., Mancini, B., Nardi, I., & Sfarra, S. (2014). Evaluating mitigation effects of urban heat islands in a historical small center with the ENVI-Met® climate model. Sustainability, 6(10), 7013-7029.

Berardi, U. (2016). The outdoor microclimate benefits and energy saving resulting from green roofs retrofits. Energy and Buildings, 121, 217-229.

Bird, R. E., & Hulstrom, R. L. (1981). Simplified clear sky model for direct and diffuse insolation on horizontal surfaces (No. SERI/TR-642-761). Solar Energy Research Inst., Golden, CO (USA).

Karakounos, I., Dimoudi, A., & Zoras, S. (2018). The influence of bioclimatic urban redevelopment on outdoor thermal comfort. Energy and Buildings, 158, 1266-1274.

Krayenhoff, E. S., Broadbent, A. M., Zhao, L., Georgescu, M., Middel, A., Voogt, J. A., ... & Erell, E. (2021). Cooling hot cities: A systematic and critical review of the numerical modelling literature. Environmental Research Letters.

Lee, H., Mayer, H., & Chen, L. (2016). Contribution of trees and grasslands to the mitigation of human heat stress in a residential district of Freiburg, Southwest Germany. Landscape and Urban Planning, 148, 37-50.

Middel, A., Häb, K., Brazel, A. J., Martin, C. A., & Guhathakurta, S. (2014). Impact of urban form and design on mid-afternoon microclimate in Phoenix Local Climate Zones. Landscape and urban planning, 122, 16-28.

Middel, A., Chhetri, N., & Quay, R. (2015). Urban forestry and cool roofs: Assessment of heat mitigation strategies in Phoenix residential neighborhoods. Urban Forestry & Urban Greening, 14(1), 178-186.

Morakinyo, T. E., Ouyang, W., Lau, K. K. L., Ren, C., & Ng, E. (2020). Right tree, right place (urban canyon): Tree species selection approach for optimum urban heat mitigation-development and evaluation. Science of the Total Environment, 719, 137461.

Ohashi, Y., Genchi, Y., Kondo, H., Kikegawa, Y., Yoshikado, H., & Hirano, Y. (2007). Influence of air-conditioning waste heat on air temperature in Tokyo during summer: Numerical experiments using an urban canopy model coupled with a building energy model. Journal of Applied Meteorology and climatology, 46(1), 66-81.

Oke, T. R., Mills, G., Christen, A., & Voogt, J. A. (2017). Urban climates. Cambridge University Press.

Prata, A. J. (1996). A new long-wave formula for estimating downward clear-sky radiation at the surface. Quarterly Journal of the Royal Meteorological Society, 122(533), 1127-1151.

Roth, M., & Lim, V. H. (2017). Evaluation of canopy-layer air and mean radiant temperature simulations by a microclimate model over a tropical residential neighbourhood. Building and Environment, 112, 177-189.

Salata, F., Golasi, I., de Lieto Vollaro, R., & de Lieto Vollaro, A. (2016). Urban microclimate and outdoor thermal comfort. A proper procedure to fit ENVI-met simulation outputs to experimental data. Sustainable Cities and Society, 26, 318-343.

Stewart, I. D., & Oke, T. R. (2012). Local climate zones for urban temperature studies. Bulletin of the American Meteorological Society, 93(12), 1879-1900.

Stewart, I. D., Oke, T. R., & Krayenhoff, E. S. (2014). Evaluation of the 'local climate zone'scheme using temperature observations and model simulations. International journal of climatology, 34(4), 1062-1080.

Taleghani, M., Sailor, D., & Ban-Weiss, G. A. (2016). Micrometeorological simulations to predict the impacts of heat mitigation strategies on pedestrian thermal comfort in a Los Angeles neighborhood. Environmental Research Letters, 11(2), 024003.

Tsoka, S., Theodosiou, T., Tsikaloudaki, K., & Flourentzou, F. (2018). Modeling the performance of cool pavements and the effect of their aging on outdoor surface and air temperatures. Sustainable Cities and Society, 42, 276-288.

Tsoka, S., Tsikaloudaki, K., Theodosiou, T., & Bikas, D. (2020). Urban Warming and Cities' Microclimates: Investigation Methods and Mitigation Strategies—A Review. Energies, 13(6), 1414.

Wang, Y., Berardi, U., & Akbari, H. (2016). Comparing the effects of urban heat island mitigation strategies for Toronto, Canada. Energy and Buildings, 114, 2-19.

Yang, S. R., & Lin, T. P. (2016). An integrated outdoor spaces design procedure to relieve heat stress in hot and humid regions. Building and Environment, 99, 149-160.

Ziaul, S., & Pal, S. (2020). Modeling the effects of green alternative on heat island mitigation of a meso level town, West Bengal, India. Advances in Space Research, 65(7), 1789-1802.

Chapter 5: Impact of Urban Heat Mitigation Techniques on Building Energy Performance

5.1. Introduction

In Chapter 4, the effects of heat mitigation scenarios on microclimate and thermal comfort were assessed. The current chapter aims to evaluate, via simulation, the role of different heat mitigation techniques on the improvement of the energy performance of a multi-story building located in downtown London, Ontario. Three simulations were carried out with HAP Carrier software: a reference scenario representative of the current microclimate condition of the site, another scenario using mitigated microclimate weather files that corresponds to results of the Green2 scenario in Chapter4 for the present weather condition, and finally, a scenario of the building with green walls were simulated. Characteristics of the building energy simulator are described, and the results are discussed in the following sections.

5.2. Microclimate mitigation solutions and building energy performance:

More than 30% of global energy consumption can be attributed to building energy use for maintaining indoor comfort conditions (i.e., heating and cooling services) (Edenhofer et al., 2011). According to the IPCC AR5 Synthesis Report published in 2014, temperature will increase in all future scenarios, resulting in more frequent and longer heat waves (IPCC, 2014). Consequently, increasing the difference between outdoor and indoor temperature will cause higher energy demand for cooling purposes. Akbari et al. indicated

that the peak urban electric demand in six American cities rises by 2-4% for each 1˚C rise in daily maximum temperature above a threshold of 15 to 20˚C (Akbari et al., 1992). Analysis of fifteen studies examining the impact of ambient temperature on the total electricity consumption indicated that the electricity demand increased varies between 0.5% and 8.5% per degree of the outdoor temperature increase (Santamouris et al., 2015). According to the results of a study on the impact of the London (UK) urban heat island on the building energy usage, there is a dependency between the rate of urbanization and building cooling and heating load (Kolokotroni et al., 2007). An investigation was carried out in Athens to estimate the effect of high temperature on the annual cooling energy and peak demand. Both were found to be significantly increased as a result of the urban heat island effect, highlighting the need to reduce cooling energy by natural means (Hassid et al, 2000; Priyadarsini, 2011).

The heat reduction and increasing thermal comfort aspect of urban greenery on a neighborhood microclimate was assessed in previous chapters; additionally, this heat reduction technique has been proposed as an effective strategy to reduce the building energy demand. To date, there are a large number of studies assessing the role of street trees and plants on the improvement of the outdoor thermal environment under hot summer conditions and the consequent reduction of the buildings' cooling energy needs, either by empirical or by simulation means (Ko, 2018). Akbari reported that urban shade trees can reduce building air conditioning, decrease air temperature, and thus improving urban air quality by reducing smog. Urban trees reduce energy use from air conditioning by 20% and save over $10 billion per year (Akbari, 2001). In terms of vegetation's positive effect on the buildings' energy needs, the results of a monitoring campaign of Parker et al. in

Florida (USA) has suggested that planting trees and shrubs around a building can reduce the daily air-conditioning electricity use by 50 % as a result of the solar radiation interception and the evapotranspiration effect (Parker, 1983). Recently a literature review by Ko (2018) summarized the results of studies that assessed the effect of trees on the buildings cooling energy needs. The review indicated wide variations of the reported energy savings, varying from 2.3 % to 90 %. The author pointed out that the magnitude of reductions widely depends on the climate, method of approach, data, and assumptions for buildings and trees.

Green walls can be defined as climbing plants grown directly on support structures integrated into external building walls (Cuce, 2017). Several benefits are accrued from the application of green walls, such as reducing internal building temperatures, mitigating building energy consumption, and facilitating urban adaptation to a warming climate (Cuce, 2017). Results of an experimental study on thermal impacts of green walls on buildings in La Rochelle city (France) underlined the positive effect of green walls in summer and moderate reduction of heat losses in winter (Djedjiga et al., 2017). An experimental and numerical investigation on the impact of green walls revealed that an average of 2.5 °C reduction in internal wall temperature could be achieved via green walls with about 10 cm thick climbing vegetation (Cuce, 2017). Another experimental study on the impact of green walls and green facades indicated a high potential for energy savings during cooling season for the green wall (58.9%) and double-skin green facade (33.8%) compared to the reference system (Coma et al., 2017). The energy-saving potential of green walls and street trees strongly depends on the climate and building characteristics. Most of the studies that have assessed the energy-saving potential of heat mitigation techniques

were carried out for warm climates. Akbari and Konopacki calculated the effect of heat island reduction strategies on annual energy saving of the building sector for the Greater Toronto Area. Results of the study indicated a significant saving potential of over $11M from the effect of urban heat mitigation strategies, such as adding trees for Toronto as a city with a cold climate. The present study aims to assess the benefits of adding trees and green walls on building cooling and heating load for the climate of London, Ontario (Latitude of 42.98° N).

5.3. Methodology and HAP Carrier software

The estimated load demand in this study is according to a building module simulation under specific weather conditions. The effect of adding trees and greenery on the street and also green walls on energy demand is assessed. In order to assess the thermal-energy performance of the case study buildings with various microclimate boundary conditions, Carrier (HAP 4.5) Hourly Analysis Program was applied to calculate a building's cooling, heating, and electrical loads. The Carrier HAP program aids in the day-to-day work of estimating loads, designing systems, and evaluating the energy performance of HVAC and non-HVAC systems used in buildings. Simulation with software includes two stages; first, it designs a system by estimating the building loads and then determining the energy consumption to calculate the energy costs.

HAP estimates the design of cooling and heating loads for different types of buildings to determine the required sizes of HVAC system components. The program provides the necessary information for the selection and identification of equipment. Users can either

modify the climate and environmental data from an external resource or use the HAP weather and climate condition database, including nearly 500 cities around the world.

Service Ontario building in Dundas Street is selected as a case study for simulation. The building is representative of other buildings in the study area in several aspects; the size, geometry, thermal insulation of the building's construction material, and the density of surrounding buildings categorized the building as an appropriate choice for simulation. A 7-story office building was defined with a 3600 m^2 area, representing the Service Ontario building. The required input data file for HAP includes data relevant to the characteristics that directly impact the thermal loads on the building. These characteristics have included the orientation, geometrical shape, weather data, the internal loads including sensible heat, HVAC system, and the construction materials of the building.

In order to assess the impact of increasing vegetation on the building neighborhood and green walls on the thermal performance of the case study building, three simulations were carried out with HAP Carrier software. A reference scenario with the current characteristics of the building and local microclimate conditions were simulated with the software. According to the results of the previous chapter, adding trees and increasing vegetation to the site can reduce the air temperature up to 0.6°C in hot months of the year. The second set of simulations was carried out by using the output of the Green2 scenario microclimate simulation for current conditions. The third set of simulations was carried out by replacing the existing building walls with green walls.

5.3.1. Weather data:

Weather data has a significant effect on the building heating and cooling loads (Wan et al., 2011). HVAC systems of the building and the portions of the building exposed to the external environment are strongly influenced by temperature, humidity, and solar radiation. Also, the geographical location, soil properties, local time, clear sky index albedo are used under the "Weather" section in the software (Carrier Corporation, 2006).

HAP deals with two different kinds of weather data: design weather data and simulation weather data. Design weather data is used to perform cooling and heating design load estimates. It consists of 24-hour profiles of temperature and humidity representing maximum conditions for summer and winter design-day conditions according to standard industry practices. Simulation weather data are used to perform hourly energy simulations. It refers to an 8760-hour sequence of actual weather data to simulate building loads. These results can be used to estimate annual energy use and costs (Carrier Corporation, 2006).

The simulations with HAP carrier were carried out with two sets of weather data. These weather files represent the microclimate condition of the site under the following site configuration; current condition of the site ("Base" scenario), and "Green2" scenario for present years. To couple the outputs of ENVI-met simulation with HAP Carrier software, a similar procedure to (Castaldo et al., 2018) was adopted to generate the new weather files. With interpolation of available hourly values of ENVI-met microclimate simulation outputs, temperature, direct and diffuse solar radiation, and wind speed for a day in summer

and winter, the hourly values of the same parameters for an entire year were generated for each configuration (Castaldo et a., 2018).

First, the hourly ratio between Base scenario parameters and two Green scenarios for summer and winter was calculated. A sinusoidal interpolation was assumed to obtain hourly ratio values of annual mitigation effect in terms of air temperature and solar radiation, and linear interpolation was assumed for wind speed. Same sinusoidal interpolation was applied to obtain the parameters values in the whole year:

$$P_{ik} = p_{i\ winter} + (p_{i\ summer} - p_{i\ winter})\ \sin\frac{\pi k}{365} \qquad 5\text{-}1)$$

for i=1,24 (hours) and for k=1, 365(days)

Further details on the equations can be found in the Appendices and Castaldo et al., 2018.

Finally, by completing the input file to be imported into Meteonorm, the complete annual weather files for two configurations were generated. By means of Meteonorm software, the complete weather files (.epw format) were created for two "Base" and "Green2" simulated configurations. These .epw weather files were imported to HAP Carrier for building energy simulations.

Meteonorm is a global climatological database. The basic input for the software is monthly mean values of the Linke turbidity factor and global radiation. The software outputs are hourly values of global radiation on inclined planes, monthly temperature, and precipitation. The stochastic process leads to an hourly dataset of a statistically average year with average mean, minimum and maximum values (Badescu,2008).

The weather properties and monthly values for maximum and minimum temperature are according to Figure 5-1, and the values of solar gain for different building directions were considered according to Figure 5-2.
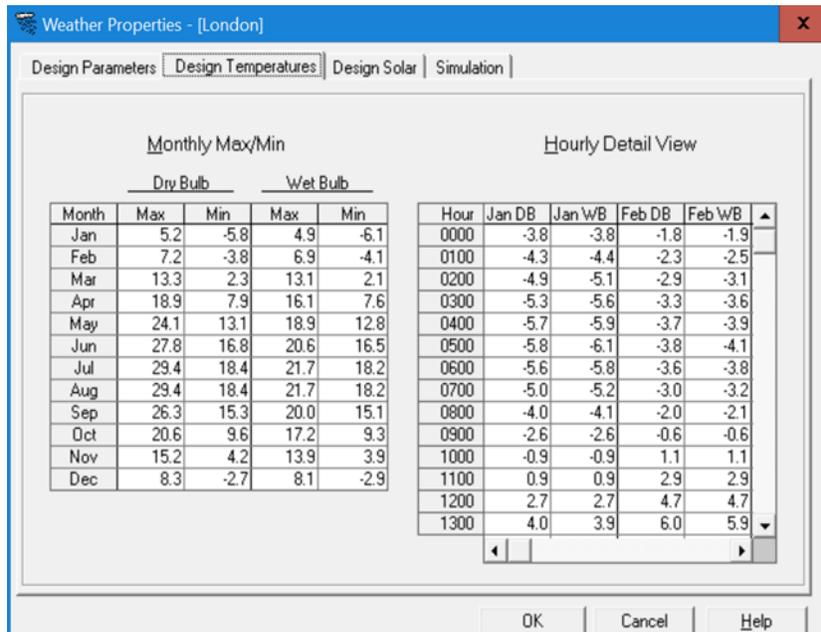
Figure 5-1. Weather properties input data for the Carrier HAP software

Design Day Maximum Solar Heat Gains W/m²

Month	Multiplier	N	NNE	NE	ENE	E	ESE	SE	SSE	S
Jan	1.00	56.6	56.6	56.6	219.1	447.4	612.2	738.9	788.7	798
Feb	1.00	71.2	71.2	149.2	366.4	577.2	719.2	781.3	783.6	774
Mar	1.00	87.5	87.5	274.1	517.6	670.4	748.8	748.5	700.9	679
Apr	1.00	103.8	204.8	435.8	588.1	698.4	710.3	657.2	569.9	526
May	1.00	115.1	308.2	511.1	642.0	687.1	665.4	571.4	457.2	401
Jun	1.00	150.5	343.6	534.9	648.6	677.5	637.1	530.5	405.1	347
Jul	1.00	118.0	308.7	505.7	623.0	679.4	647.5	558.2	443.2	390
Aug	1.00	109.1	209.8	419.8	568.9	675.6	680.6	634.0	549.8	509
Sept	1.00	90.9	90.9	275.2	478.9	638.1	704.0	722.2	681.7	656
Oct	1.00	73.5	73.5	117.5	365.3	549.8	687.5	749.9	758.0	747
Nov	1.00	57.4	57.4	57.4	214.7	435.4	611.5	722.4	767.1	782
Dec	1.00	50.1	50.1	50.1	156.9	385.2	558.6	701.3	766.4	783

Month	Multiplier	SSW	SW	WSW	W	WNW	NW	NNW	Horiz
Jan	1.00	786.0	739.5	613.7	449.7	200.7	56.6	56.6	363.7
Feb	1.00	779.0	770.9	720.3	561.4	383.7	131.0	71.2	519.2
Mar	1.00	703.5	751.2	745.1	673.7	514.8	285.5	87.5	663.3
Apr	1.00	565.7	654.9	702.1	701.0	594.1	428.6	216.6	765.3
May	1.00	453.1	571.1	658.9	695.8	628.0	511.6	315.2	816.7
Jun	1.00	403.6	530.8	635.1	681.6	644.1	536.2	345.6	828.3
Jul	1.00	443.6	558.2	648.2	678.6	624.5	505.8	307.1	808.2
Aug	1.00	548.1	632.9	676.5	676.0	573.5	416.2	213.5	752.7
Sept	1.00	680.5	716.8	717.8	620.1	485.3	274.5	90.9	639.9
Oct	1.00	760.6	755.7	677.8	558.5	348.7	143.5	73.5	507.7
Nov	1.00	774.4	718.6	611.0	424.3	226.4	57.4	57.4	360.3
Dec	1.00	766.9	695.4	568.5	371.9	168.6	50.1	50.1	298.4

Figure 5-2. Solar gain data for the London, Ontario, according to Carrier HAP default value

5.3.2. Building data:

The building envelope is defined as the separation of the controlled indoor environment and the uncontrolled outdoor environment. It typically includes the foundation, floors, walls, fenestration (windows and doors), and roof. In order to present building energy simulation for the tested building, required building envelope data were collected from the available architectural and summarized in Table 5-1. The floor plan was a 65m by 55.4 m

layout with a total air-conditioned floor area of 3600 m^2. The building operated from 6 a.m. to 10 p.m. on weekdays.

Table 5-1. Building Parameters

Total Floor Area	3600 m^2
No. of Floors	7
Wall Construction U-Value	1.37 W/m^2.k
Roof Construction U-Value	0.557 W/m^2.k
Lighting Intensity	15 w/m^2
Indoor design temp. cooling / heating	24 °C /21 °C
Electrical Equipment intensity	16 w/m^2
Number of Occupants	50

5.3.3. HVAC system data:

Air is typically treated in air handling units (AHUs) to control moisture content and temperature in centrally cooled or heated buildings. Once the air is treated, it is transported and distributed to various parts of the building. Air distribution systems are classified into single and dual duct categories as well as constant and variable volume categories. In variable air volume systems (VAV), thermal comfort in the conditioned space is maintained by having a constant temperature and varying supply air quantities. The air distribution system used in the simulation for this project was a dual-duct system single zone with constant air volume (CAV) system.

The heating and cooling load of the air system of the base case building model depends on the actual schedules of all types of functions.

   1. Occupancy activity schedule

   2. Lighting schedule

   3. Equipment schedule

   4. Fan/thermostat

   5. Ventilation

The Carrier HAP uses two types of schedule-fractional and fan/thermostat. Fractional schedules are used to describe the variation of internal heat load (ie., lighting, equipment, control of outside ventilation in an HVAC system, and hot water in a domestic water heating system). Fan/thermostat schedules are used to match the hours of use of HVAC equipment with tenant occupancy schedules. The occupied and unoccupied thermostat set points are assigned to each hour in the HVAC system (Carrier, 2006).

5.4. Results:

This section presents the results of an assessment of the effects of increasing trees around the building neighborhood and green walls, on the building heating and cooling loads for a simulated building in downtown London, Ontario. The cooling and heating load were calculated for the defined building using HAP Carrier software. The local commercial electricity and natural gas rates were applied to the energy simulation results. Average commercial rates for electricity and natural gas consumption were assumed 0.17 \$/kwh and 0.115 \$/m^3.

The system design simulation outputs estimated the annual cooling and heating loads of the system. Values normalized per 100 m^2 of area. Table 5-2 represents the annual system design cooling and heating load for the Base scenario and load saving for two other scenarios. System design simulations show that the maximum cooling load reduction corresponds to the increasing trees and vegetation in the building neighborhood. By increasing 10% trees and vegetation in the building neighborhood, the central cooling load is reduced (saved) by up to 11.79 kWh/100m^2 this scenario caused an increase of 0.74 kWh/100m^2 in the heating load of the building. Trees with shading and reducing the outdoor air temperature saved the building cooling load in the hot season. In contrast, this reduction in air temperature and shading in cold seasons is resulted a penalty for the heating load.

Table 5-2. System Design Annual Heating and Cooling load for Base scenario and saving loads for mitigated scenarios

Scenario	Central Cooling Coil Load (kWh/100m^2)	Central Heating Coil Load (kWh/100m^2)
Base	434.23	5533.1
Green Walls	-1.84	44.54
Increasing trees	11.79	-0.74

For the green walls scenario, the cooling load is increased by 1.84 kWh/100m^2, and installing green walls reduced the heating load of the building system by up to 44.54 kWh/100m^2. According to the hourly analysis of the cooling/heating load, vegetation on

the green walls reduced the ability of the building to cool at night and increased the cooling load of the building at night.

Table 5-3 shows the results of the building energy usage simulation. Building energy simulation is calculated for two types of energy supply for heating purpose, electricity and natural gas. The annual total cost of energy consumption of the building, the annual total cost per floor area, and the annual actual energy consumption are presented. Values correspond to the Base scenario and the difference (Δ) value for two mitigated scenarios with the Base scenario.

Table 5-3. Building Simulation Report of Annual Cost Summary, and Annual Actual Energy Consumed for the Base scenario and the Δ value of the two green walls and Green2(Increasing trees) scenarios for two types of heating supply

Scenario	Natural Gas Heat			Electric Heat		
	Total Annual cost ($)	Total Annual Cost per Unit Floor Area ($)	Annual Actual Energy Consumed (kwh)	Total Annual cost ($)	Total Annual Cost per Unit Floor Area ($)	Actual Energy Consumed (kwh)
Base	16,585	4.493	812,399	57,927	15.692	714,733
Green Walls	42	0.012	4243	374	0.11	4,459
Increasing trees	161	0.04	1588	147	0.04	1428

For both mitigated scenarios, a reduction in the annual cost and consumption of energy is estimated. The difference between natural gas and electricity price has driven the difference between cost reduction of the two types of energy supply. The differences between natural

gas and electricity supply values are insignificant for the Green2 (increasing trees) scenario; the reason is that most of the reduction with this scenario is calculated for cooling purposes, which does not affect the heating load and heating supply demand.

5.5. Discussion and Conclusions

This chapter described an investigation of the impact of urban heat mitigation scenarios on the thermal energy performance of buildings. There is a direct connection between outdoor microclimate conditions and indoor cooling and heating loads. Increasing natural area and vegetation covers on urban areas was introduced as an effective solution to mitigate the impact of urban heating arising due to urban microclimate and larger scale climate change. In this chapter my study focused on an office building, and the impact of two different mitigated scenarios is assessed.

In reviewing the results of this chapter, the following should be considered:

1. increasing trees (Green2) reduces the summer cooling load of the building and increases the winter heating load. But the total annual cost savings and the annual energy consumption for this scenario are positive. Tree shading, evapotranspiration and wind shielding affect the outdoor air temperature and building energy consumption. In this study, by interpolation of the ENVI-Met simulation results for two days in summer and winter, these impacts are taken in to account in the weather input file of the HAP Carrier model. Future studies to

investigate further impact of increasing trees and more accurate weather files with more simulated days would improve the current estimate.

2. Simulations in this study were performed for an office building with a rectangular shape in downtown London, Ontario. These results can be different for other building prototypes, material thermal properties, and different cooling and heating systems. The shape, orientation, and compactness of buildings significantly impact the building energy consumption in cooling and heating (Tibermacine and Zemmouri, 2016).

3. This study was carried out for current weather conditions. The future weather and climate change will affect building energy consumption. According to the results of a projection on building energy consumption in 2050 and 2080 in Florida (USA), gas and electricity demand for heating are predicted to decrease, and electricity demand for cooling to increase. According to the differences in base and mitigation scenarios in the present, the other beneficial aspect of increasing trees is reducing the building cooling load for future weather.

4. The price of energy affects the total annual energy cost of buildings and cost-saving with different scenarios. Moreover, simulations with natural gas for heating supplies will be subject to an increasing carbon tax.

5.6. References:

Akbari, H., & Konopacki, S. (2004). Energy effects of heat-island reduction strategies in Toronto, Canada. Energy, 29(2), 191-210.

Akbari, H., & Matthews, H. D. (2012). Global cooling updates: Reflective roofs and pavements. Energy and Buildings, 55, 2-6.

Badescu, V. (2014). Modeling solar radiation at the earth's surface (Vol. 1). Berlin Heidelberg: Springer.

Castaldo, V. L., Pisello, A. L., Piselli, C., Fabiani, C., Cotana, F., & Santamouris, M. (2018). How outdoor microclimate mitigation affects building thermal-energy performance: A new design-stage method for energy saving in residential near-zero energy settlements in Italy. Renewable Energy, 127, 920-935.

Coma, J., Pérez, G., de Gracia, A., Burés, S., Urrestarazu, M., & Cabeza, L. F. (2017). Vertical greenery systems for energy savings in buildings: A comparative study between green walls and green facades. Building and environment, 111, 228-237.

Cuce, E. (2017). Thermal regulation impact of green walls: An experimental and numerical investigation. Applied Energy, 194, 247-254.

Dahanayake, K. K. C., & Chow, C. L. (2017). Studying the potential of energy saving through vertical greenery systems: Using EnergyPlus simulation program. Energy and Buildings, 138, 47-59.

Djedjig, R., Belarbi, R., & Bozonnet, E. (2017). Green wall impacts inside and outside buildings: experimental study. Energy Procedia, 139, 578-583.

Edenhofer, O., Pichs-Madruga, R., Sokona, Y., Seyboth, K., Matschoss, P., Kadner, S., ... & von Stechow, C. (2011). IPCC special report on renewable energy sources and climate change mitigation. Prepared By Working Group III of the Intergovernmental Panel on Climate Change, Cambridge University Press, Cambridge, UK.

Hassid, S., Santamouris, M. N. A. N. C., Papanikolaou, N., Linardi, A., Klitsikas, N., Georgakis, C., & Assimakopoulos, D. N. (2000). The effect of the Athens heat island on air conditioning load. Energy and Buildings, 32(2), 131-141.

Jiang, A., Zhu, Y., Elsafty, A., & Tumeo, M. (2018). Effects of global climate change on building energy consumption and its implications in Florida. International Journal of Construction Education and Research, 14(1), 22-45.

Ko, Y. (2018). Trees and vegetation for residential energy conservation: A critical review for evidence-based urban greening in North America. Urban Forestry & Urban Greening, 34, 318-335.

Kolokotroni, M., Zhang, Y., & Watkins, R. (2007). The London Heat Island and building cooling design. Solar Energy, 81(1), 102-110.

Parker, J. H. (1983). Landscaping to reduce the energy used in cooling buildings. Journal of Forestry, 81(2), 82-105.

Priyadarsini, R. (2009). Urban heat island and its impact on building energy consumption. Advances in building energy research, 3(1), 261-270.

Santamouris, M., Cartalis, C., Synnefa, A., & Kolokotsa, D. (2015). On the impact of urban heat island and global warming on the power demand and electricity consumption of buildings—A review. Energy and Buildings, 98, 119-124.

Santamouris, M., Ding, L., Fiorito, F., Oldfield, P., Osmond, P., Paolini, R., ... & Synnefa, A. J. S. E. (2017). Passive and active cooling for the outdoor built environment–Analysis and assessment of the cooling potential of mitigation technologies using performance data from 220 large scale projects. Solar Energy, 154, 14-33.

Tibermacine, I., & Zemmouri, N. (2017). Effects of building typology on energy consumption in hot and arid regions. Energy Procedia, 139, 664-669.

Wan, K. K., Li, D. H., Liu, D., & Lam, J. C. (2011). Future trends of building heating and cooling loads and energy consumption in different climates. Building and Environment, 46(1), 223-234.

Chapter 6: Concluding Remarks and Future Work

The objective of this study was to evaluate heat mitigation solutions on the existing urban form for a study site in downtown London, Ontario. There are several heat mitigation strategies. Due to the geometry of the site and the high percentage of pavement coverage in the study area, two heat mitigation strategies, increasing the green coverage of the study area and applying high albedo material, were evaluated. A computational fluid dynamics ENVI-Met model simulated the site's existing and mitigation conditions for evaluation and comparison. Furthermore, the impact of heat mitigation solutions on the building energy performance was evaluated.

Comparing the results of heat mitigation scenarios with the base scenario revealed that increasing the albedo of road material or adding vegetation coverage could decrease the near-ground air temperature in the study domain. The air temperature reduction is greater for the green scenario with a higher coverage of trees. The cool pavement scenario increased the mean radiant temperature at the pedestrian (1.5m) level during the daytime. This increase arises from the increase in reflected shortwave radiation. Increasing greenery showed a slight reduction in the average air temperature, mean radiant temperature, and PMV. Furthermore, increasing street-level trees demonstrates higher VCE and cooling effectiveness comparing to increasing ground-level vegetation with the same fraction. Calculated ACE for Cool road scenario shows 1.5°C cooling per 0.3 increase in albedo.

Similar reduction potential on air temperature and thermal comfort was detected for increasing greenery and cool road scenarios for future summer conditions. Impacts of these

mitigation scenarios were also assessed for winter weather conditions. Results did not reveal a significant impact on the air temperature for both scenarios.

The energy performance of a building in downtown London, Ontario, was simulated using HAP Carrier software. The impact of two different heat mitigation solutions, increasing greenery and green walls, on building heating/cooling load for the current climate were assessed. Comparing the results of the two scenarios with the base scenario indicated a decrease in the buildings' cooling load for the Green2(increasing trees) configuration. However, the simulation predicted an increase in building heating load for the Green2(increasing trees) model, but the net saving was positive. A significant reduction in the building heating load was calculated for the green walls model. It was found that the capability of the software to simulate the insulation effect of green walls was more refined than simulating the cooling effect of vegetation on walls.

Urban climate simulations, coupled with detailed thermal energy performance of a building in the studied domain in downtown London, Ontario, revealed that the above-mentioned mitigation solutions contribute to energy saving.

The following section highlights suggestions for policy makers in the City of London to consider:

- The results of this study indicated that there is a correlation between unshaded and paved areas with thermal comfort. The more uncomfortable thermal areas correspond to the areas without shading facility and with the paved ground. Increasing shading on the flat areas and replacing part of these flat areas and parking spaces with grass and vegetations are options to improve thermal comfort and

reduce air temperature. For future research identifying other sensitive domains with high heat risks is suggested for practical shading with trees and live plants.

- Reducing the maximum size for parking spaces in downtown London and replacing parts of these areas with green areas or trees can be beneficial in several aspects; increase shading, reduce pollutants in the downtown district with high traffic, and improve pedestrian thermal comfort.

- It is proven with previous studies that increasing vegetation improves thermal comfort. This study indicates a correlation between the percentage of trees and temperature reduction and pedestrian thermal comfort. Adding more trees instead of low-height vegetation with the same vegetation fraction revealed more temperature reduction. Therefore, increasing taller trees is another suggestion to improve the pedestrian thermal experience on the streets of downtown.

It should be recalled however, that this study has some limitations related to the ENVI-met software. For instance, the software does not represent the internal structure of walls, and the simulation does not consider heat emission from the building. In hot summer conditions these emissions contribute a positive feedback to outdoor air temperature that is maximized under conditions of most concern to human thermal comfort. Furthermore, the software does not consider the impacts of heat emission from transportation. High traffic volume in the downtown area can strongly affect the amount of heat emission from vehicles.

This study investigated the thermal comfort improvements and energy-saving potentials of adopted heat mitigation strategies. Results of the study demonstrated the increasing trees in the downtown district improves the thermal comfort of pedestrians in hot summer conditions. Furthermore, microclimate simulation results of this scenario coupled with a

single building energy analysis showed a reduction in building energy demand in the downtown area.

Appendices

Appendices 1: ENVI-Met Weather Forcing Files

Table 7-1. ENVI-Met Weather Forcing File- Current summer Condition

Date	Time	SW DIR / low clouds	SW DIF / med clouds	LW / high clouds	Abs. Temperature[K]	Rel. Humidity	Windspeed	WindDir	Percipitation
24.06.2016	3:00:00	0	0	303.5350883	285.65	82.1	0.214	30.36	0
24.06.2016	3:30:00	0	0	301.8202604	285	80.7	0	0	0
24.06.2016	4:00:00	0	0	302.5367985	284.75	83.1	0	0	0
24.06.2016	4:30:00	0	0	298.3137707	284.75	80	0	0	0
24.06.2016	5:00:00	0	0	298.4289766	284.55	79	0	0	0
24.06.2016	5:30:00	0	0	296.8887197	285.5	81	0.125	74	0
24.06.2016	6:00:00	0	0	297.3528906	286.55	83	0.484	63.07	0
24.06.2016	6:30:00	0	0	296.4337671	288	77	0.544	43.77	0
24.06.2016	7:00:00	0.26	3.29	307.8542577	290.45	67.68	2.68224	45	0
24.06.2016	7:30:00	11.39	41.85	311.6250224	292.45	60.6	2.3356	74.8	0
24.06.2016	8:00:00	47.63	80.95	321.5200362	294.35	56.09	2.2352	63.07	0
24.06.2016	8:30:00	103.08	108.81	336.1362724	295	52.79	3.3678	43.77	0
24.06.2016	9:00:00	169.87	128.8	353.910893	296.05	47.79	4.02336	54.74	0
24.06.2016	9:30:00	242.51	143.74	370.82345	296.55	40.83	3.4432	65.11	0
24.06.2016	10:00:00	317.11	155.32	382.6747242	297.15	36.69	2.68224	50	0
24.06.2016	10:30:00	390.65	164.5	394.6898366	297.8	35.58	3.0065	16.03	0
24.06.2016	11:00:00	460.7	171.89	412.6579954	298.25	34.75	3.12928	71.99	0
24.06.2016	11:30:00	525.24	177.85	419.1432768	298.8	34.12	2.5692	99.4	0
24.06.2016	12:00:00	582.55	182.61	418.3880927	299.25	31.29	2.2352	74.57	0
24.06.2016	12:30:00	631.2	186.35	431.599271	299.35	29.65	1.8542	68.22	0
24.06.2016	13:00:00	670.02	189.15	420.065492	299.55	29.72	1.34112	110	0
24.06.2016	13:30:00	698.1	191.09	453.183673	300	29.68	1.05442	130	0
24.06.2016	14:00:00	714.82	192.22	446.1933467	300.45	27.09	0.89408	150	0
24.06.2016	14:30:00	719.79	192.55	437.0175265	300.35	27.78	1.78922	190	0
24.06.2016	15:00:00	712.89	192.09	431.2637716	300.25	27.9	2.68224	200	0
24.06.2016	15:30:00	694.29	190.83	436.7512688	300.55	27.74	2.35002	240	0
24.06.2016	16:00:00	664.41	188.75	437.3623349	300.85	26.53	2.2352	280	0
24.06.2016	16:30:00	623.92	185.8	421.5203779	300.8	27.56	2.2352	300	0
24.06.2016	17:00:00	573.77	181.91	420.1842971	300.75	25.76	2.2352	336.9	0
24.06.2016	17:30:00	515.18	176.96	413.6220647	300.55	25.26	1.7645	300	0
24.06.2016	18:00:00	449.61	170.79	396.9376288	300.35	28.78	0.89408	11.08	0
24.06.2016	18:30:00	378.83	163.14	376.0043734	299.35	33.52	2.2325	316	0
24.06.2016	19:00:00	304.94	153.61	365.7293494	298.85	34.02	3.12928	322.7	0
24.06.2016	19:30:00	230.43	141.56	356.8582784	298	35.5	3.12928	348	0
24.06.2016	20:00:00	158.43	125.93	351.0642575	297.05	36.85	3.12928	350	0
24.06.2016	20:30:00	93.06	104.89	349.8503754	296	38.46	2.95823	360	0
24.06.2016	21:00:00	40.14	75.37	343.7792494	295.25	41.61	2.68224	14	0
24.06.2016	21:30:00	7.87	34.51	339.4902265	295	44.82	2.3532	10	0
24.06.2016	22:00:00	0	0	337.3023111	294.85	47.75	2.2352	11	0
24.06.2016	22:30:00	0	0	334.7048949	293.25	50.65	2.45711	65	0
24.06.2016	23:00:00	0	0	333.5869153	292.25	60.02	2.68224	70	0
24.06.2016	23:30:00	0	0	332.9890212	291.25	58.96	2.3572	65	0
25.06.2016	0:00:00	0	0	330.6696939	290.65	62.8	2.2352	40	0
25.06.2016	0:30:00	0	0	329.3279939	290	68.88	1.6548	5	0
25.06.2016	1:00:00	0	0	327.6381281	289.75	71.39	0.89408	330	0
25.06.2016	1:30:00	0	0	326.5607012	289	73.7	1.65782	345	0
25.06.2016	2:00:00	0	0	324.7326042	288.85	74.56	2.2352	360	0
25.06.2016	2:30:00	0	0	323.6493295	288.45	81.3	1.6528	15	0
25.06.2016	3:00:00	0	0	321.783503	288.05	81.2	0.89408	30	0

Table 7-2. ENVI-Met Weather Forcing File- Current winter Condition

Date	Time	SW DIR / low clouds	SW DIF / med clouds	LW / high clouds	Abs. Temperature	Rel. Humidity	Windspeed	WindDir	Percipitation
03.03.2018	03:00:00	0	0	216.7693301	269.85	80	2.68224	335	0
03.03.2018	03:30:00	0	0	216.437729	269.85	78	2.7	335	0
03.03.2018	04:00:00	0	0	214.6321674	269.45	77	3.12928	335	0
03.03.2018	04:30:00	0	0	214.3063354	269.45	75	3.129	335	0
03.03.2018	05:00:00	0	0	212.9340229	269.15	74	3.12928	325	0
03.03.2018	05:30:00	0	0	212.9340229	269.15	74	3.129	325	0
03.03.2018	06:00:00	0	0	211.8030343	268.75	77	3.12928	325	0
03.03.2018	06:30:00	0	0	211.8030343	268.75	77	3	325	0
03.03.2018	07:00:00	0	0	211.9575705	268.75	78	2.68224	320	0
03.03.2018	07:30:00	0	0	212.2041914	268.85	77	3	320	0
03.03.2018	08:00:00	0	0	212.4491637	268.95	76	4.02336	325	0
03.03.2018	08:30:00	0	0	211.9744809	268.95	73	4.023	325	0
03.03.2018	09:00:00	0	0	216.479048	270.15	71	4.02336	320	0
03.03.2018	09:30:00	7.550995692	34.5361916	215.6021609	270.15	66	4.023	320	0
03.03.2018	10:00:00	43.21778826	80.03823193	220.7170455	271.45	65	4.4704	325	0
03.03.2018	10:30:00	98.48408802	110.5331317	220.3275407	271.45	63	4.5	325	0
03.03.2018	11:00:00	161.4674918	131.0564591	224.067165	272.45	61	5.7056	330	0
03.03.2018	11:30:00	225.0515439	145.5429307	223.002179	272.45	56	5.7	330	0
03.03.2018	12:00:00	284.7957137	156.0971682	228.1947821	273.75	55	5.25856	330	0
03.03.2018	12:30:00	337.6805243	163.8660575	227.4824573	273.75	52	5.25	330	0
03.03.2018	13:00:00	381.5446822	169.5048341	232.474237	275.05	50	5.7056	340	0
03.03.2018	13:30:00	414.827245	173.4000927	231.1418431	275.05	45	5.7	345	0
03.03.2018	14:00:00	436.4444672	175.7796463	235.5150103	276.15	44	5.25856	350	0
03.03.2018	14:30:00	445.7297214	176.7681885	235.2223881	276.15	43	5.25	350	0
03.03.2018	15:00:00	442.4052284	176.4145878	234.3340721	276.15	40	6.59968	350	0
03.03.2018	15:30:00	426.5719465	174.7019307	236.3267716	276.55	41	5.79	345	0
03.03.2018	16:00:00	398.7129309	171.5440845	235.3522528	276.25	42	5.7056	335	0
03.03.2018	16:30:00	359.7117416	166.7675123	238.6334028	276.15	55	5.36448	325	0
03.03.2018	17:00:00	310.8946244	160.0712792	234.4506313	274.75	63	4.4704	325	0
03.03.2018	17:30:00	254.1175803	150.9479048	232.2624225	274.15	65	4.47	315	0
03.03.2018	18:00:00	191.9461483	138.5254574	227.0197023	272.75	69	4.4704	305	0
03.03.2018	18:30:00	128.0396281	121.2410071	225.436486	272.15	74	4.47	315	0
03.03.2018	19:00:00	68.00562301	96.17085306	222.1960212	271.35	75	4.4704	315	0
03.03.2018	19:30:00	21.19962483	58.23077972	221.3476586	271.15	75	4.47	315	0
03.03.2018	20:00:00	0.953974257	9.506613386	220.7425904	271.05	74	4.4704	315	0
03.03.2018	20:30:00	0	0	220.3223096	270.95	74	4.47	315	0
03.03.2018	21:00:00	0	0	218.6517042	270.55	74	4.4704	325	0
03.03.2018	21:30:00	0	0	217.1694608	270.15	75	4.47	325	0
03.03.2018	22:00:00	0	0	217.1694608	270.15	75	4.02336	325	0
03.03.2018	22:30:00	0	0	215.2847157	269.65	76	3.7	325	0
03.03.2018	23:00:00	0	0	214.87661	269.55	76	3.12928	325	0
03.03.2018	23:30:00	0	0	213.254302	269.15	76	3.12	325	0
04.03.2018	00:00:00	0	0	213.4136493	269.15	77	3.12928	325	0
04.3.2018	00:30:00	0	0	211.4028688	268.65	77	3.12	330	0
04.3.2018	01:00:00	0	0	210.7568807	268.45	78	2.2352	335	0
04.3.2018	01:30:00	0	0	210.7568807	268.45	78	2.23	340	0
04.03.2018	02:00:00	0	0	211.0036911	268.55	77	2.2352	345	0
04.3.2018	02:30:00	0	0	211.0036911	268.55	77	3	350	0
04.03.2018	03:00:00	0	0	212.6063437	268.95	77	3.57632	355	0

Table 7-3. ENVI-Met Weather Forcing File- Future Summer Condition

Date	Time	SW DIR / low clouds	SW DIF / med clouds	LW / high clouds	Abs. Temperature	Rel. Humidity	Windspeed	WindDir	Percipitation
08-06-2049	3:00:00	0	0	394.4637177	299.45	73.57	0.214	30.36	0
08-06-2049	3:30:00	0	0	392.0317586	299.15	73.57	0	0	0
08-06-2049	4:00:00	0	0	392.3610567	299.01	75.71	0	0	0
08-06-2049	4:30:00	0	0	389.4535635	298.65	75.71	0	0	0
08-06-2049	5:00:00	0	0	390.2278382	298.57	77.86	0	0	0
08-06-2049	5:30:00	0	0	386.8486668	298.15	77.86	0.125	74	0
08-06-2049	6:00:00	0	0	388.0537562	298.13	80	0.484	63.07	0
08-06-2049	6:30:00	0	0	389.8254735	298.35	80	0.544	60	0
08-06-2049	7:00:00	0.32	4	391.036954	298.74	77	2.68224	62	0
08-06-2049	7:30:00	12.4	43.76	394.3589256	299.15	77	2.3356	74.8	0
08-06-2049	8:00:00	49.97	82.69	394.0314471	299.36	74	2.2352	63.07	0
08-06-2049	8:30:00	106.53	110.29	396.3903929	299.65	74	3.3678	60	0
08-06-2049	9:00:00	174.15	130.08	396.8668093	299.97	71	4.02336	54.74	0
08-06-2049	9:30:00	247.36	144.88	398.3363445	300.15	71	3.4432	65.11	0
08-06-2049	10:00:00	322.28	156.35	399.6962585	300.59	68	2.68224	50	0
08-06-2049	10:30:00	395.91	165.45	404.3000687	301.15	68	3.0065	45	0
08-06-2049	11:00:00	465.82	172.75	402.3456808	301.2	65	3.12928	50	0
08-06-2049	11:30:00	530.01	178.64	406.0570007	301.65	65	2.5692	60	0
08-06-2049	12:00:00	586.76	183.34	404.8845696	301.81	62	2.2352	65	0
08-06-2049	12:30:00	634.66	187	407.6967459	302.15	62	1.8542	68.22	0
08-06-2049	13:00:00	672.57	189.74	407.382051	302.43	59	1.34112	70	0
08-06-2049	13:30:00	699.59	191.6	409.2063744	302.65	59	1.05442	80	0
08-06-2049	14:00:00	715.13	192.65	409.6572588	303.04	56	0.89408	90	0
08-06-2049	14:30:00	718.82	192.9	412.2369813	303.35	56	1.78922	100	0
08-06-2049	15:00:00	710.58	192.34	411.8582101	303.66	53	2.68224	100	0
08-06-2049	15:30:00	690.6	190.99	415.951681	304.15	53	2.35002	80	0
08-06-2049	16:00:00	659.34	188.79	413.7983091	304.27	50	2.2352	70	0
08-06-2049	16:30:00	617.5	185.71	412.7987182	304.15	50	2.2352	50	0
08-06-2049	17:00:00	566.09	181.67	412.3929864	303.83	52.14	2.2352	40	0
08-06-2049	17:30:00	506.34	176.54	410.3981088	303.59	52.14	1.7645	40	0
08-06-2049	18:00:00	439.77	170.15	410.9040221	303.39	54.29	0.89408	30	0
08-06-2049	18:30:00	368.21	162.21	408.9121664	303.15	54.29	2.2325	30	0
08-06-2049	19:00:00	293.82	152.3	409.319072	302.95	56.43	3.12928	30	0
08-06-2049	19:30:00	219.2	139.72	406.8349096	302.65	56.43	3.12928	20	0
08-06-2049	20:00:00	147.63	123.28	407.7383931	302.52	58.57	3.12928	10	0
08-06-2049	20:30:00	83.48	100.97	404.6820593	302.15	58.57	2.95823	0	0
08-06-2049	21:00:00	33.07	69.45	406.0025981	302.08	60.71	2.68224	14	0
08-06-2049	21:30:00	4.96	26.8	402.4603153	301.65	60.71	2.3532	10	0
08-06-2049	22:00:00	0	0	404.2089371	301.64	62.86	2.2352	11	0
08-06-2049	22:30:00	0	0	402.6448548	301.45	62.86	2.45711	20	0
08-06-2049	23:00:00	0	0	402.3456808	301.2	65	2.68224	25	0
08-06-2049	23:30:00	0	0	400.2940454	300.95	65	2.3572	30	0
09-06-2049	0:00:00	0	0	400.4264312	300.76	67.14	2.2352	30	0
09-06-2049	0:30:00	0	0	398.7074182	300.55	67.14	1.6548	20	0
09-06-2049	1:00:00	0	0	398.4631342	300.32	69.29	0.89408	10	0
09-06-2049	1:30:00	0	0	397.0752524	300.15	69.29	1.65782	0	0
09-06-2049	2:00:00	0	0	396.444649	299.88	71.43	2.2352	360	0
09-06-2049	2:30:00	0	0	393.7618686	299.55	71.43	1.6528	10	0
09-06-2049	3:00:00	0	0	389.4980468	299.15	70	0.89408	15	0

Table 7-4. ENVI-Met Weather Forcing File- Future winter Condition

Date	Time	SW DIR / low clouds	SW DIF / med clouds	LW / high clouds	Abs. Temperature	Rel. Humidity	Windspeed	WindDir	Percipitation
05-02-2049	3:00:00	0	0	250.8961502	277.65	73.57	0.98224	335	0
05-02-2049	3:30:00	0	0	250.8961502	277.65	73.57	1	335	0
05-02-2049	4:00:00	0	0	248.9991445	277.15	75.71	1.42928	335	0
05-02-2049	4:30:00	0	0	248.9991445	277.15	75.71	1.429	335	0
05-02-2049	5:00:00	0	0	247.0971296	276.65	77.86	1.42928	325	0
05-02-2049	5:30:00	0	0	247.0971296	276.65	77.86	1.429	325	0
05-02-2049	6:00:00	0	0	245.1862425	276.15	80	1.42928	325	0
05-02-2049	6:30:00	0	0	245.1862425	276.15	80	1.3	325	0
05-02-2049	7:00:00	0	0	247.8587793	276.85	77	0.98224	320	0
05-02-2049	7:30:00	0	0	247.8587793	276.85	77	1.3	320	0
05-02-2049	8:00:00	0	0	250.5179869	277.55	74	2.32336	325	0
05-02-2049	8:30:00	0	0	250.5179869	277.55	74	2.323	325	0
05-02-2049	9:00:00	0	0	253.1597752	278.25	71	2.32336	320	0
05-02-2049	9:30:00	0	0	253.1597752	278.25	71	2.323	320	0
05-02-2049	10:00:00	2.84	19.73	255.7796845	278.95	68	2.7704	325	0
05-02-2049	10:30:00	26.8	65.3	256.7941273	279.15	68	2.8	325	0
05-02-2049	11:00:00	70.36	98.11	258.3728468	279.65	65	4.0056	330	0
05-02-2049	11:30:00	121.83	120.04	260.9362502	280.15	65	4	330	0
05-02-2049	12:00:00	173.68	135.19	260.9339408	280.35	62	3.55856	330	0
05-02-2049	12:30:00	221.33	145.9	262.4774173	280.65	62	3.55	330	0
05-02-2049	13:00:00	261.8	153.47	263.457141	281.05	59	4.0056	340	0
05-02-2049	13:30:00	293.08	158.62	263.9731188	281.15	59	4	345	0
05-02-2049	14:00:00	313.85	161.77	265.9360577	281.75	56	3.55856	350	0
05-02-2049	14:30:00	323.27	163.13	268.0177955	282.15	56	3.55	350	0
05-02-2049	15:00:00	321.01	162.81	268.3636678	282.45	53	4.89968	350	0
05-02-2049	15:30:00	307.15	160.77	270.979412	282.95	53	4.09	345	0
05-02-2049	16:00:00	282.21	156.88	270.732233	283.15	50	4.0056	335	0
05-02-2049	16:30:00	247.19	150.86	269.6919852	282.95	50	3.66448	325	0
05-02-2049	17:00:00	203.68	142.19	268.9867562	282.65	52	2.7704	325	0
05-02-2049	17:30:00	154	129.97	267.4327527	282.35	52	2.77	315	0
05-02-2049	18:00:00	101.65	112.58	267.2147958	282.15	54	2.7704	305	0
05-02-2049	18:30:00	52.12	87.06	266.1808225	281.95	54	2.77	315	0
05-02-2049	19:00:00	14.58	48.85	265.4189503	281.65	56	2.7704	315	0
05-02-2049	19:30:00	0.42	5.06	264.9031662	281.55	56	2.77	315	0
05-02-2049	20:00:00	0	0	263.601648	281.15	58	2.7704	315	0
05-02-2049	20:30:00	0	0	262.5754804	280.95	58	2.77	315	0
05-02-2049	21:00:00	0	0	261.7651607	280.65	60	2.7704	325	0
05-02-2049	21:30:00	0	0	260.2345048	280.35	60	2.77	325	0
05-02-2049	22:00:00	0	0	259.9116159	280.15	62	2.32336	325	0
05-02-2049	22:30:00	0	0	258.8945833	279.95	62	2	325	0
05-02-2049	23:00:00	0	0	258.3728468	279.65	65	1.42928	325	0
05-02-2049	23:30:00	0	0	257.3568231	279.45	65	1.42	325	0
06-02-2049	0:00:00	0	0	256.5226375	279.15	67.14	1.42928	325	0
06-02-2049	0:30:00	0	0	255.5114924	278.95	67.14	1.42	330	0
06-02-2049	1:00:00	0	0	254.6611504	278.65	69.29	0.5352	335	0
06-02-2049	1:30:00	0	0	253.1540978	278.35	69.29	0.53	340	0
06-02-2049	2:00:00	0	0	252.7840256	278.15	71.43	0.5352	345	0
06-02-2049	2:30:00	0	0	251.7834253	277.95	71.43	1.3	350	0
06-02-2049	3:00:00	0	0	249.2483575	277.35	73	1.87632	355	0

Appendices 2: Generation Weather File for Mitigated Weather Scenario

Steps that followed to create the new weather file from mitigation scenarios (Castaldo et al., 2018):

1. Sinusoidal interpolation for temperature, direct and diffuse solar radiation parameters:

$$P_{ik} = p_{i,\text{winter}} + (p_{i,\text{summer}} - p_{i,\text{winter}}) \sin\frac{\pi k}{365} \qquad \text{for } i= (1,24) \text{ hours and } k= (1, 365) \text{ days}$$

2. Linear interpolation for wind speed parameter:

$$V_{ik} = v_{i,\text{winter}} \left(\frac{k - k_{\text{summer}}}{k_{\text{winter}} - k_{\text{summer}}}\right) - v_{i,\text{summer}} \left(\frac{k - k_{\text{winter}}}{k_{\text{winter}} - k_{\text{summer}}}\right) \text{ for } i=1 \div 24 \text{ hours and }, k=$$

1÷200 days

$$V_{ik} = v_{i,\text{summer}} \left(\frac{k - k_{\text{winter}}}{k_{\text{summer}} - k_{\text{winter}}}\right) - v_{i,\text{winter}} \left(\frac{k - k_{\text{summer}}}{k_{\text{summer}} - k_{\text{winter}}}\right) \text{ for } i=1 \div 24 \text{ hours and }, k=$$

201÷365 days

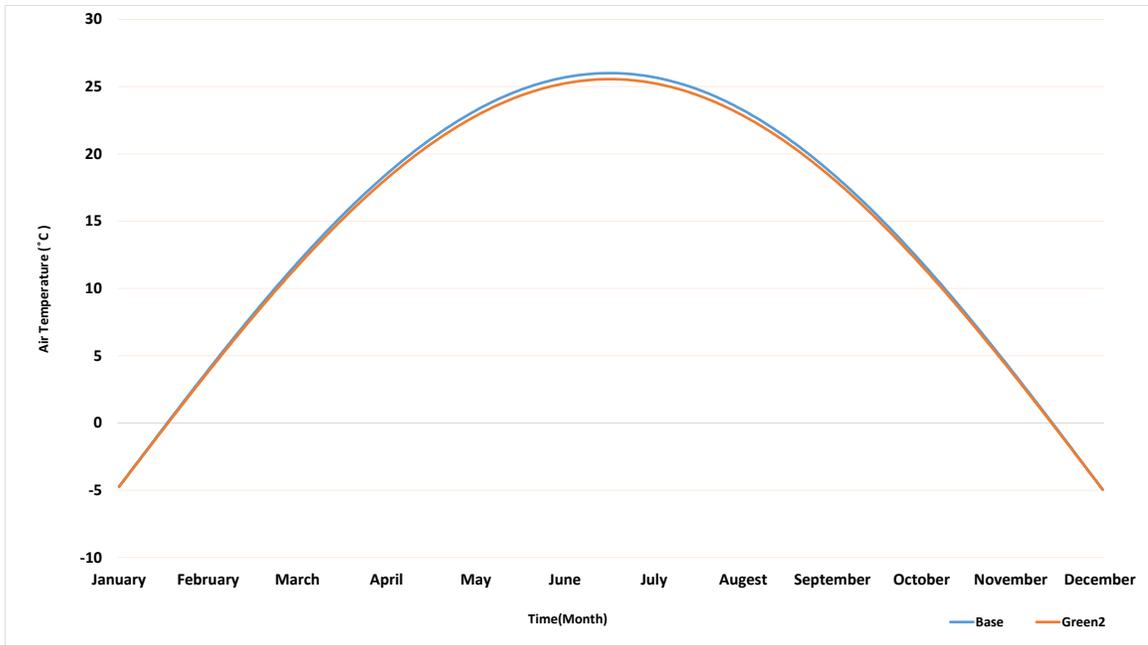Figure 7.1 shows the calculated temperature for the Base and Green2 scenarios for the entire year.

Figure 7-1. Generated air temperature for the entire year

Curriculum Vitae

Name: Maryam Shams

Post-secondary   University of Shahid Chamran

Education and   Ahwaz, Iran

Degrees: 2012-2016 B.A.

        The University of Western Ontario

        London, Ontario, Canada

        2019-2021 M.E.Sc.

Honours and   Scholarship for Excellent Student Awards

Awards: 2013-2014-2015-2016

Related Work   Teaching Assistant

Experience   The University of Western Ontario

        2020

        Research Assistant

        The University of Western Ontario

        2020-present